Chem Soc Rev

Metal-Free Photocatalysts for Hydrogen Evolution

Journal:	*Chemical Society Reviews*
Manuscript ID	CS-SYN-04-2019-000313.R3
Article Type:	Review Article
Date Submitted by the Author:	14-Feb-2020
Complete List of Authors:	Rahman, Mohammad; University of Texas at Austin, Department of Chemical Engineering Kibria, Md ; University of Calgary, Chemical and Petroleum Engineering Mullins, Charles; University of Texas at Austin, Department of Chemical Engineering

Chem Soc Rev

ARTICLE

Metal-Free Photocatalysts for Hydrogen Evolution

Mohammad Ziaur Rahman, *[a] Golam Kibria,[b] and Charles Buddie Mullins*[a]

+Received 00th January 20xx,
Accepted 00th January 20xx

DOI: 10.1039/x0xx00000x

www.rsc.org/

This review focuses on the discussion of the latest progress and remaining challenges in selected metal-free photocatalysts for hydrogen production. The scope of this review is limited to the metal-free elemental photocatalysts (i.e. B, C, P, S, Si, Se etc.), binary photocatalysts (i.e. BC_3, B_4C, C_xN_y, h-BN etc.) and their heterojunction, ternary photocatalysts (i.e. BCN) and their heterojunction, and different types of organic photocatalysts (i.e. linear, covalent organic frameworks, microporous polymer, covalent triazine frameworks etc.) and their heterostructures. Following a succinct depiction of the latest progress in hydrogen evolution on these photocatalysts, discussion has been extended to the potential strategies that are deemed necessary to attain high quantum efficiency and high solar-to-hydrogen (STH) conversion efficiency. Issues with reproducibility and the disputes in reporting the hydrogen evolution rate have been also discussed with recommendations to overcome them. A few key factors are highlighted that may facilitate the scalability of the photocatalyst from microscale to macroscale production in meeting the targeted 10% STH. This review is concluded with additional perspectives regarding future research in fundamental materials aspects of high efficiency photocatalysts followed by six open questions that may need to be resolved by forming a global hydrogen taskforce in order to translate bench-top research into large-scale production of hydrogen.

1. Introduction

The transformation and ongoing progress of civilization depends on our ability to harness energy beyond human and animal power, and our ability to find, extract and use energy with ever increasing dexterity. Among the available energy sources, fossil-fuels (i.e., oil, gas and coal) contribute to >85% of the world's energy production.[1] To meet the global average rate of consumption of 17.2 TW, a sustainable supply of 1066 barrels of oil, 108,000 cubic meters of natural gas and 250 tonnes of coal per second need to be produced.[2] With the increasing world population growth rate (1.12 %/year) and industrialization, the world energy demand is expected to be tripled by 2050.[3] Even if the current rate of global primary energy consumption (2.1 % p.a.) holds constant, it would lead to an 'energy crisis' situation because of faster depletion of limited fossil fuel reserves.

Additionally, emissions of toxic effluents from burning fossil fuels create anthropogenic and environmental threats, for which all living creatures and plants are affected.[4] According to the United Nations Framework Convention on Climate Change (UNFCCC), climate change represents an irreversible threat to human societies. Therefore, the Paris Agreement calls for the development of alternative net CO_2 removal strategies beyond the typical options of bioenergy with carbon capture and storage (BECCS) and afforestation.

The response to this situation drives the research for renewable energy sources. It is agreed that a transition from non-renewable fossil fuels to renewable fuels is a must to minimize (or further prevent) the anthropogenic damages caused by burning fossil fuels, and to tackle the security of energy supply in a post-fossil fuels era. The production of hydrogen from H_2O using solar energy is considered a viable option, provided that catalysts with the requisite activity, selectivity and durability are developed.[5] Notably, hydrogen fuel burns cleanly without any CO_2 or NO_x release. It can also be stored, and used as, and when, required.

Two third of earth constitutes water, while the sun is an inexhaustible source of energy with an expected lifetime of 4 billion years. The earth surface receives solar energy equivalent to 90 PW which is four orders of magnitude greater than the current rate of human energy consumption.[2] Therefore, producing hydrogen from water using solar energy would seemingly provide a potential low-cost option to meet the current and future energy demands.

From a consumer perspective, hydrogen is a gas much like natural gas that can be used to heat buildings and power vehicles. From an environmental perspective, hydrogen is unique among liquid and gaseous fuels in that it emits absolutely no CO_2 emissions when burned. From an energy perspective, each kilogram of hydrogen contain about 2.4 times as much energy as natural gas, while it is equivalent to the energy that would be produced from burning 4L of petrol.[6] At a global level, replacing fossil fuels with carbon-free hydrogen will significantly reduce greenhouse gas emissions, with estimated potential annual reductions of up to 6 billion tonnes of CO_2 by

[a] John J. Mcketta Department of Chemical Engineering and Department of Chemistry, The University of Texas at Austin, Austin, TX 78712-1589, USA
[b] Department of Chemical and Petroleum Engineering, University of Calgary, 2500 University Drive, NW Calgary, Alberta, Canada
*corresponding e-mail: mullins@che.utexas.edu

2050. Considering the benefits of hydrogen fuel, the hydrogen economy will be worth an estimated US$2.5 trillion by 2050. [7] Using hydrogen in place of fossil fuels therefore offers a viable pathway to decarbonise our energy systems.

Because water and sunlight are abundant and practically inexhaustible, photocatalytic hydrogen production via water-splitting offers a truly viable alternative for green fuel production. The corner stone of photocatalytic hydrogen production is semiconductor photocatalysts that absorb solar photons and create electron–hole pairs for water redox reactions. Over four decades of research, some hundreds of photocatalyst materials have been catalogued that can be categorised into mainly two types – metal-based and metal-free. Metal-based photocatalysts have been extensively researched since 1972.[8] However, a new generation of metal-free photocatalysts (MFP) is slowly but steadily emerging in parallel to widely accepted metal-based photocatalysts for water-splitting.

Metal-free photocatalysts are made out of earth abundant inexpensive materials, for example, carbon (C), nitrogen (N), oxygen (O), phosphorus (P), and sulphur (S). These elements are light weight and corrosive resistant. Therefore, appropriate combinations of these elements may result in a highly robust compounds with tuneable photophysical properties suitable for light harvesting and catalytic application. While scalable and stable performance is yet elusive with metal-based photocatalysts; metal-free photocatalysts (MFP), in this regards, hold true promise provided that they can overcome poor solar-to-hydrogen (STH) conversion efficiency. Among MFP, carbon nitrides have made significant progress,[9-12] while other MFP (i.e. P, C, S, B, covalent organic frameworks etc.) are further behind.[13-15] It is therefore very timely to assess the current progress and determine the outstanding challenges with various MFP's to devise future design strategies for achieving benchmark efficiency. This review article, in this regard, is a collaborative endeavor with leading researchers in the field, all over the world, to fill this gap.

Photocatalytic water-splitting is a blend of both fundamental and applied research. Development of a catalyst material is a cascaded process of synthesis and characterization, optimization, and understanding of charge transport and electrodynamics. This knowledge can also compatibly be exploited to develop other materials for diverse applications. Similarly, the design of a reactor and evaluation of the evolved H_2 and O_2 is transferrable to other catalytic processes, for example, CO_2 reduction, N_2 reduction etc.[16] Clearly, a review on metal-free photocatalysts will provide an important knowledge-base to foster research on different materials development and understanding of the fundamental physicochemical processes for other applications, such as, solar cells, batteries, supercapacitors, sensors, and optoelectronic devices, etc.[17-19]

Photocatalytic water-splitting is a multidisciplinary research avenue that includes chemistry, chemical engineering, materials science, physics, nanoscience and nanotechnology. Therefore, an authoritative review would provide a wealth of knowledge for students, scientist, and engineers to learn about the current status of the field with an understanding of the issues to be resolved to create a path forward.

To the best of our knowledge, a review that has treated the large collection of metal-free photocatalysts has not yet been reported. Considering the pace of research progress, such a review is therefore very timely. We hope that a comparative study of the various metal-free photocatalysts will offer knowledge to judge, scrutinize and screen the best combination of metal-free photocatalysts for high solar-to-hydrogen conversion efficiency.

2. Basic Concepts in Photocatalysis and Photocatalysts

The general field of catalysis can be divided into thermal catalysis (usually simply known as catalysis, which is not the matter of interest in this review) and photocatalysis. According to the IUPAC (International Union of Pure and Applied Chemistry) photocatalysis is defined as "change in the rate of chemical reaction or its initiation under the action of ultraviolet, visible, or infrared radiation in the presence of a substance – the photocatalyst – that absorbs light and is involved in the chemical transformation of the reaction partners". The reaction fulfilling this requirement is then called photocatalytic.

At the beginning of the twentieth century, scientists felt that irradiation could be a method for catalysing a reaction. Giacomo Ciamician is the first scientist who devoted a scientific effort (during 1900 – 1920) to understand the chemical effect of light.[20] The terms *photokatalyse* and *photocatalytisch* appeared probably for the first time in the textbook *Photochemie*, published by Plotnikov.[21] However, the development of photocatalysis as a discipline specifically began in 1970s. [22, 23]

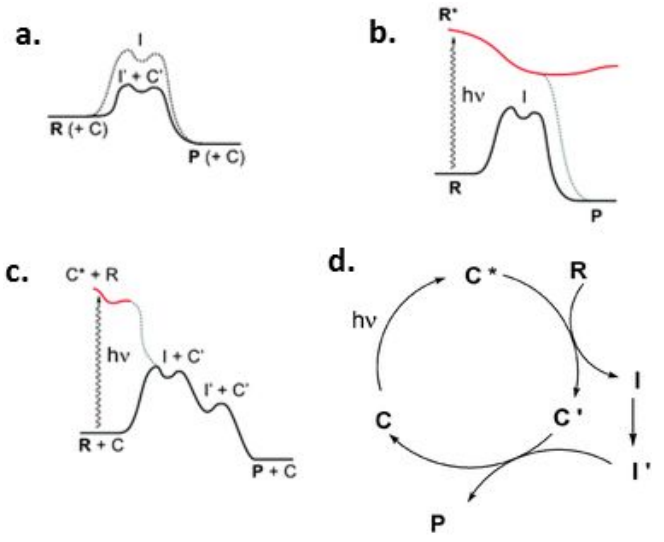

Fig. 1 a) a thermal reaction (R→P) catalyzed by C via intermediate I′, b) a photochemical reaction where the chemical reaction starts from the excited state surface of the reagent R*, c) a photocatalyzed reaction where the catalyst C is active only in the excited state, but the chemical transformation of R occurs entirely on the ground state surface, and d) C acts as a

photocatalyst in the R→P reaction. Adopted with permission from.[24] Royal Society of Chemistry (2009).

Catalytical transformation of a reagent (R) to product P via intermediates (I', C') has been depicted in Fig. 1a). In photocatalysis, the activation of R happens when the excited state (**C***) of a photocatalyst transfers an electron, while in thermal catalysis, it happens through the physical step of energy transfer (see, Fig. 1 b, c)). In photocatalysis, electronically activated R produces an intermediate **I** (a radical or radical ion), which in principle can be formed also through a thermal process. **C***, after transfer of the electrons, it becomes deactivated **C'**. The intermediate **I** gives the final product P (possibly through further intermediates **I')** and regenerates **C** in the final state. The overall reaction results in the transformation of **R** into **P** by absorbed light in the presence of non-consumed **C** (see Fig. 1d). The entire chemical transformation **R→P** occurs on the lowest potential energy surface at any configuration where the chemical path in part occurs on an excited state surface (from **R***, Fig. 1b). This is called photocatalysis since a new path on the ground state surface becomes accessible.[24, 25]

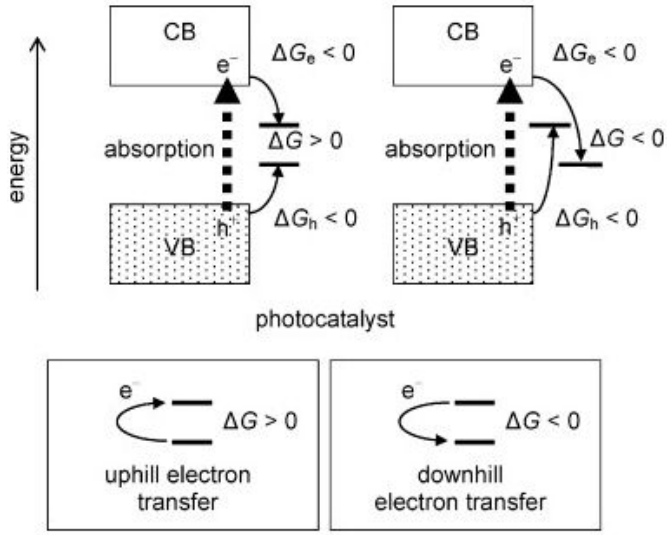

Fig. 2 Gibbs-energy change in photocatalytic reactions. Adopted with permission from.[26] Elsevier (2010).

The change in Gibbs energy (ΔG) is another significant criterion that differs between photocatalytic and ordinary thermal catalytic reactions. ΔG could be either negative and positive. A negative ΔG implies release of energy while a positive one means absorption/storing of energy. Ordinary catalyses are limited only to reactions of negative ΔG. This is because a thermal catalyst reduces the activation energy of the chemical reaction by changing the intermediate states and thereby accelerating the reaction which proceeds spontaneously with negative Gibbs energy change. However, both situations are possible in photocatalytic reactions.[26] The reason for a reaction of positive Δ*G* which does not proceed spontaneously is that an overall redox reaction can proceed, even if its Δ*G* is positive. It is just required that the reduction and oxidation steps are spatially or chemically separated; otherwise reaction between reduction and oxidation products proceeds to give no net products. Under these conditions, both Gibbs energy change for reactions of e^- with oxidant (ΔG_e) and h^+ with reductant (ΔG_h) are required to be negative, i.e. reactions by e^- and h^+ proceed spontaneously after photoexcitation (Fig. 2). Thermodynamic requirements for photocatalytic reaction is (i) more cathodic and anodic levels of the conduction band (CB) bottom and valence band (VB) top of photocatalyst material compared with the standard electrode potential of an oxidant and a reductant, respectively, to make Gibbs energy change of both reactions negative, and (ii) separation of reduction and oxidation by e^- and h^+, respectively, for both types of reaction with positive and negative Δ*G*.[26]

3. Selection criteria for a hydrogen evolution photocatalyst

The water-splitting process is an uphill reaction with a change in Gibbs energy of ΔG = 237 kJ/mol.[27] Therefore, the minimum energy (i.e. $E^0 = -\ \Delta G/nF$) required for an overall water-splitting is 1.23 eV, where E^0 is the electrode potential; *n* is the number of electrons per mole product and *F* is the Faraday constant in C mol^{-1}. [28] The proton reduction potential (H^+/H_2) is (0 - 0.59pH, V *vs.* NHE, normal hydrogen electrode), and the water oxidation potential (O_2/H_2O) is (1.23 - 0.59pH, V *vs.* NHE).[29] Therefore, pure water-splitting (pH = 7) requires -0.41 V for hydrogen evolution and 0.82 V for oxygen evolution, respectively. It indicates that the semiconductor photocatalyst should have a minimum bandgap of 1.23 eV to accommodate the water-splitting reactions considering standard conditions of zero over potential and zero reorganization energies for interfacial charge transfer reactions. However, in practice, an overpotential is unavoidable for hydrogen production. Therefore, a bandgap greater than 1.23 eV is always desirable. Along with the bandgap requirements, a material needs to have a CB minimum positions at a more negative potential than the reduction potential, and the VB maximum position at a more positive potential than the oxidation potential.

4. Fundamental physicochemical processes in Photocatalytic hydrogen production

Photocatalytic hydrogen production involves a series of photophysical and electrochemical processes (see Fig. 3). The photophysical process is comprised of photon absorption and charge carrier generation, and separation and transport of charge carrier to the reaction sites, while the electrochemical process includes redox reactions for water-splitting.

Under irradiation of light, a photocatalyst absorbs photons of defined wavelengths based on its intrinsic bandgap. The photon with energy equivalent or greater than the bandgap energy of the photocatalyst would have sufficient driving force to lift an electron from the valence band (VB) to the conduction band (CB), leaving behind empty holes in the VB. Absorption of photons is accompanied by generation of excited holes and electrons. To maintain the equilibrium, excited electrons in the CB might fall back radiatively/nonradiatively to the VB, and then

recombine with holes. Recombination annihilates the free electron-hole pairs. This is an unavoidable photophysical process regardless of the type of semiconductor used as a photocatalyst.[30, 31] Recombination is one of the critical factors responsible for low quantum efficiency of a photocatalyst.[32, 33]

The electrons and holes that survive recombination then need to be transported to the surface where HER and OER will be taken place. The transfer of photoexcited carriers to the surface active sites might occur either by diffusion or electric fields associated with the semiconductor/electrolyte and semiconductor/cocatalyst interfaces. [34]

The generation of excitons occurs on a time scale below 100 fs. The average lifetime of excitons typically limited to a few hundred picoseconds. Depending on the diffusion coefficient, the electron diffusion process will last, at most, a few picoseconds whilst the corresponding transition time for holes might be below 100–300 fs.[35, 36] Electron and hole transport are sometimes limited by trap states associated with the semiconductors. Electron/hole diffusion coefficients decrease proportionally with the number of (deep) traps present in the catalyst particle and are created by the network morphology (porosity, secondary particle size) at interfaces of the porous material.[37, 38] The time scale of trapping ranges from picoseconds to milliseconds or even a fraction of a second, and always competes with the charge recombination process. Hole trapping, relaxation and transfer to surface species processes all appear to be significantly faster and occur in the pico- and nanosecond region whilst electron trapping with shorter lifetimes than a few microseconds.[35, 39-41] The above mentioned time scales are depicted in Fig. 4.

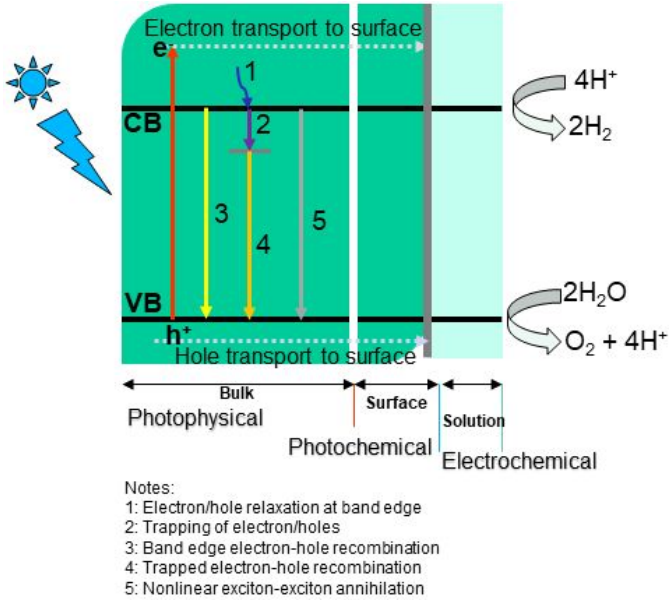

Fig. 3 Three key dynamics processes (photophysical, photochemical and electrochemical) involved in water-splitting. Following excitation across the bandgap: 1) electron/hole relaxation (tens to hundreds of fs); (2) trapping of electrons/holes into trap states due to defects or surface states within hundreds of fs to tens of ps; (3) radiative and nonradiative band edge electron-hole or exciton recombination within tens of ps; (4) radiative and nonradiative trapped electron-hole or relaxed exciton recombination within hundreds of ps to a few ns; and (5) nonlinear and nonradiative exciton-exciton annihilation within hundreds of fs to tens of ps. Adopted with permission from. [33] Copyright 2019, American Chemical Society.

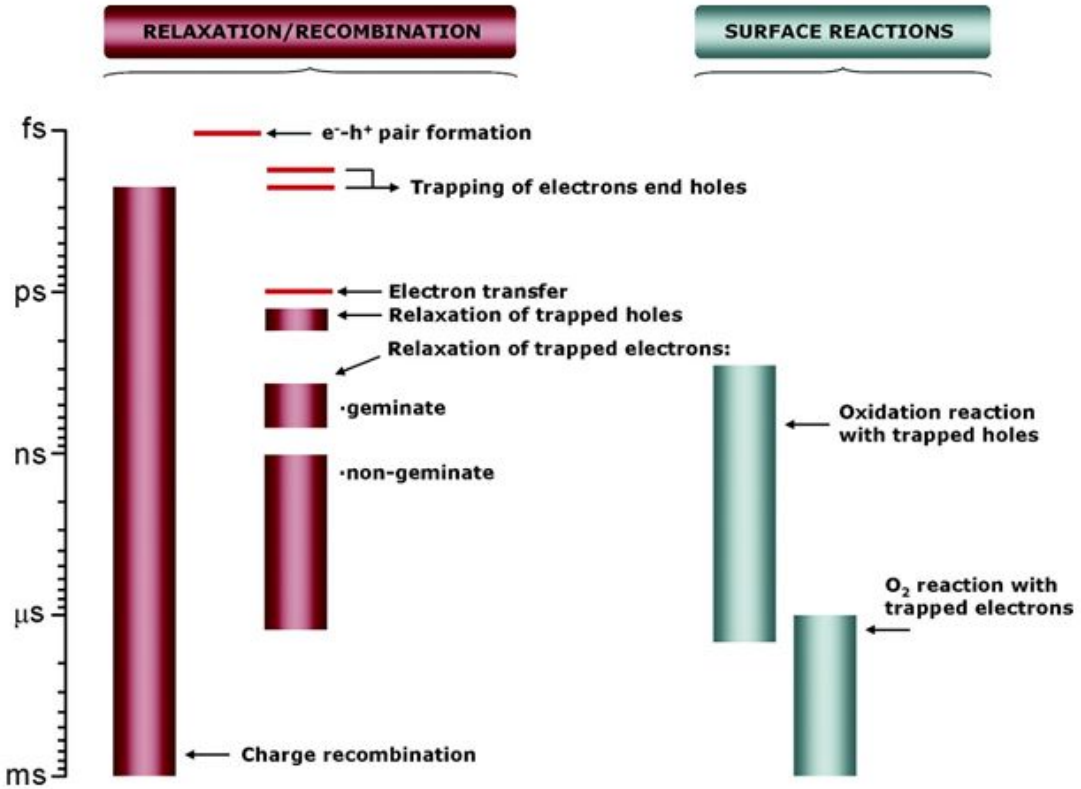

Fig. 4 Time scales of "elemental steps" occurring in a prototypical photocatalytic process. Adopted with permission from.[39] American Chemical Society (2012).

5. Photocatalytic hydrogen production systems

Hydrogen can be produced through a half-reaction of water-splitting (only the reduction reaction) or overall water-splitting (both reduction and oxidation reaction simultaneously).

The half reaction of water-splitting can be realized using an appropriate sacrificial electron donor/hole scavenger, for example, triethanolamine, alcohol, etc. When the photocatalytic half reaction is carried out in an aqueous solution which contains a reducing agent, photogenerated holes in the photocatalyst material irreversibly oxidize the reducing agent instead of water. It thus enriches electrons in a photocatalyst if only the hydrogen evolution reaction (HER) is taking place. However, hydrogen production in the presence of sacrificial agents must not be confused to be the water-splitting process. Because water-splitting means to split water into H_2 and O_2 in a stoichiometric amount in the absence of sacrificial agents.

There are one-step (single-photon) and two-step (two-photon) systems available for overall water-splitting under visible light irradiation[8] as shown in Fig. 5. The two photon photocatalyst systems are also known as Z-scheme processes.[42]

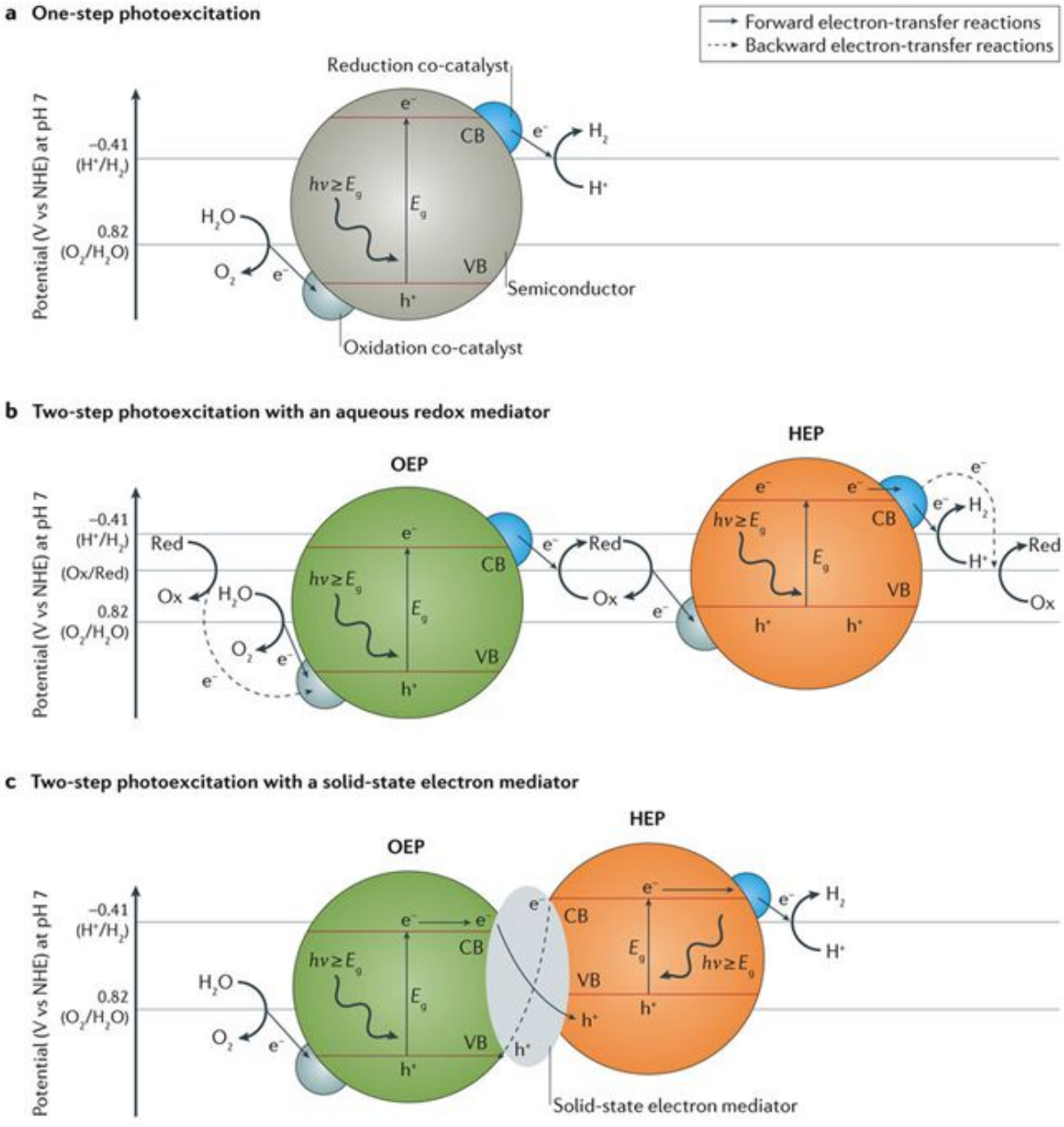

Fig. 5 Schematic illustration of different photocatalytic water-splitting systems. Adopted with permission from,[29] Nature Publishing Group (2017).

The system for one-step overall water-splitting employs only one semiconductor having appropriate band-edge positions compatible with the H^+/H_2 and O_2/H_2O potentials. In a two-step system, that is, a Z-scheme water splitting system, one hydrogen evolution photocatalyst (HEP) and one oxygen evolution photocatalyst (OEP) are employed to separately evolve H_2 and O_2. It is to be noted that it is not a hard and fast rule for HEP and OEP photocatalysts in a Z-scheme to be independently capable for overall water-splitting. Practically, semiconductors active in either HER or OER only may be

employed in this system. Therefore, the Z-scheme provides a larger driving force in alleviating the thermodynamic requirements for water splitting.

Contrary to a one step system, the photoexcited electrons and holes remain in the HEP and the OEP, respectively, in a Z-scheme system. Additionally, holes in the HEP and electrons in the OEP are recombined via an aqueous redox mediator (Fig. 5b) or a solid-state electron mediator (Fig. 5c) to complete the photocatalytic cycle in the Z-scheme system. Therefore, eight electrons are needed to complete the photocatalytic cycle in two-steps while four electrons could complete the photocatalytic cycle in a one-step system. Consequently, a one-step photoexcitation process produces two times the quantity of H_2 and O_2 compared with that of a two-step photoexcitation system at AQY and light absorbance values of unity. [29]

The Z-scheme system is prone to backward electron-transfer that makes this process kinetically more challenging than the one-step system. In addition to preventing backward electron transfer, control over the interparticle charge transfer between the HEP and OEP is also a limiting key factor for efficient overall water-splitting via the Z-scheme.

6. Trends in photocatalytic water-splitting research

In their seminal note published in *Nature* (1972), Fujishima and Honda demonstrated that water could be photolyzed electrochemically at an illuminated TiO_2 and dark Pt electrode combination to yield H_2 and O_2. [23] In the late 1970s, a strong push in that direction was led by Bard and his colleagues [43]. They described some of the principles and applications of semiconductor electrodes in photoelectrochemical (PEC) cell and the possible uses of heterogeneous photocatalysts in designing PEC cells. Since 1980, a great research effort has been undertaken regarding the pursuit of developing highly efficient, rugged and cost effective heterogeneous photocatalysts.[44]

Wide bandgap metal oxides consisting of d^0 (empty d orbitals) cations (i.e. Ti^{4+}, Zr^{4+}, Ce^{4+}, Nb^{5+} , Ta^{5+} and W^{6+}) or d^{10} (filled d orbitals) cations (i.e. Zn^{2+},Ga^{3+}, In^{3+}, Ge^{4+},Sn^{4+},Sb^{5+} , Mo^{6+}etc.) are considered as the effective photocatalyst for ultraviolet (UV) light in the solar spectrum.[5, 8] Among all, because of its appropriate energy levels to initiate the water splitting reaction, TiO_2 is the most reported active photocatalyst under UV light.[40] Nitrides consisting of d^{10} metal cations are also active water splitting photocatalysts under UV irradiation. For example, Ge_3N_4 and co-catalyst doped GaN are well known non-oxide powder photocatalysts. [45-47]

Since UV light accounts for only ~4% of the entire solar energy spectrum, [48] wide bandgap (Eg > 3 eV) photocatalysts can't be effectively used for efficient solar energy harvesting and conversion. The bandgap engineering via metal /non-metal ion doping and visible light sensitizers are being used to enhance photon absorption of wide bandgap photocatalyst.[49-55] However, the elements used for narrowing the bandgap suppress the redox potentials of photogenerated charge carriers and also serve as recombination centers for electrons and holes. [51, 53] The most efficient sensitizers used to date are noble metals (Au, Ag, Pt, Rh etc.). The metal nanoparticles are also widely used as cocatalysts, and Ag and Au have attracted increasing attention in plasmonic photocatalysts.[56, 57] However, they are expensive and thus won't lead to large scale application in the future. The use of organic dyes as sensitizers suffers from their instability and they readily decompose under longer time irradiation. Narrow band gap semiconductor sensitizers have inherently led to the photocorrosion of the photocatalyst and for this reason, the photocatalyst eventually becomes completely ineffective. [58] Hence, the development of a visible-light active photocatalyst that splits water efficiently is indispensable.

There are two types of oxide photocatalyst that could work under visible light irradiation, such as, (i) photocatalysts for H_2 or O_2 evolution from an aqueous solution in the presence of sacrificial agents and (ii) photocatalysts for overall water splitting. For example, WO_3 is a stable photocatalyst for O_2 evolution under visible light in the presence of a suitable electron acceptor. [59, 60] $InTaO_4$ and $YBiWO_6$ have been reported for overall water splitting as single photocatalyst under visible light. [61-63] Photocatalysts that work only for half reactions of water splitting (only H_2 or O_2 evolution) can be used to construct Z-scheme systems.

Oxide photocatalysts have already been established as efficient under UV light, as discussed above. Empty d orbitals of transition metals or s, p orbitals of typical metals construct the conduction band (CB) of metal oxide photocatalyst. [64] The CB lies above the water reduction potential of water (0 V vs. NHE at pH0). The potential of the valence band (VB) which consists of O 2p orbitals (ca. +3 V) is more positive than the water oxidation potential (1.23 V). [64] This makes the band gap too large to harvest visible light but suggests metal oxide photocatalysts have sufficient potential to oxidize water under visible light if appropriate band structuring is done. The approaches adapted so far for a wide band gap metal oxide to make it sensitive to visible light are (i) doping transition metals having a d^n ($0 < n < 10$) electronic configuration, (ii) valence band control using an anion's *p* orbitals or the orbitals of *p*-block metals ions and (iii) spectral sensitization. [5, 8]

When a wide band gap metal oxide is doped with a transition metal cation or anion, a donor or acceptor level is formed in the forbidden gap as a center for visible light absorption. But the doping has some adverse effects. It is to be noted that the dopant introduces a discrete energy level rather than an energy band in the host material which hinders the rapid migration of photogenerated carriers. Maintaining charge balance also becomes critical because dopants sometimes act as recombination centers. [65, 66] Therefore, the formation of the valence band by orbitals not associated with O 2p but with other element is very important for oxide photocatalysts to be able to work under visible light. [67-71] The application of a visible light sensitizer in wide band gap oxide semiconductor photocatalysts has been also studied to inject electrons into the conduction band of the oxide photocatalyst to evolve H_2. The organic dyes or narrow band gap semiconductors are usually exploited as sensitizers. The sensitizers must have a more negative excited

state potential than the conduction band of the metal oxide photocatalyst for efficient charge injection. [72, 73] Another inclusion is supported oxide nanosystems (e.g. Ag/ZnO nanocomposites,[74] Si/Co_3O_4 nanopyramid[75, 76], CuO/ZnO nanrod arrays[77] etc.) for photoactivated H_2 production.[78, 79]

Metal sulphides are also attractive visible light driven photocatalyst. Many metal sulphide photocatalysts have been reported.[80-88] The VB of sulfide photocatalysts is formed by the S 3p orbitals which are more negative than O2p orbitals. For example, CdS is a very well-known narrow band gap (2.4 eV) visible light photocatalyst. It possesses the appropriate band levels for water reduction and oxidation in the presence of sacrificial agents.[89] ZnS (3.6 eV) doped with various metal cations shows excellent photocatalytic H_2 evolution performance from aqueous solutions containing S^{2-} and/or SO_3^{2-} as electron donors under visible light. [90, 91] Solid solutions of CdS-ZnS, $AgInS_2$-ZnS, $CuInS_2$-ZnS, $CuInS_2$-$AgInS_2$-ZnS and $AgGa_{0.9}In_{0.1}S_2$ are also active for H_2 evolution under visible light.[81, 86-88, 90, 92]

Although sulfide photocatalysts have very suitable band levels for water splitting under visible light irradiation, they become unstable and deactivated due to photocorrosion or self-oxidation rather than evolving O_2. [93-95]

Non-oxide compounds such as (oxy)nitrides and oxysulfides having d^0 and d^{10} electronic configurations have been reported in [96-106] as a new type of visible light driven photocatalyst for overall water splitting. The band gap narrowing of these materials results from the valence band formation by N 2p and S 3p orbitals in addition to O 2p orbitals. The absorption band of these materials is in the range 500 – 750 nm which corresponds to 1.7 – 2.5 eV for a band gap energy.[5, 8] (Oxy)nitrides and oxysulfides differs from materials doped with nitrogen or sulphur. These non-oxide materials are regarded as a valence band-controlled photocatalyst as the constituent anion component forms a valence band rather than a discrete impurity level. However, they are not stable in strong acids, for example, in aqua regia and hot concentrated H_2SO_4. [51, 102] In most cases, (oxy)nitrides are partially decomposed by the photogenerated holes instead of undergoing water oxidation at the initial stages of photocatalytic reaction accompanied with low level N_2 evolution. However, the N_2 production gets completely suppressed as the reaction progress. Although (oxy)nitrides have stable water reduction and oxidation reactions, the necessary performance for overall water splitting has yet to be achieved due to low level H_2 evolution. Moreover, some of the (oxy)nitrides consisting of d^0 metal cations, such as, Ti^{4+}, Nb^{5+} and Ta^{5+} are not active for H_2 or O_2 evolution in the absence of sacrificial agents. [101, 102, 107, 108]

Wang et al., in their seminal works reported graphitic carbon nitride (g-C_3N_4) for the first time as a visible light active metal free photocatalyst for the purposes of water splitting in 2009. [109] The graphitic carbon nitride is a medium band gap (2.7 eV) semiconductor with good physiochemical stability and adjustable band structure. This organic semiconductor can be prepared via a one-step polymerization of cheap feed stocks like cyanamide, urea, thiourea, melamine and dicyandiamide.[11] The graphitic planes are constructed from tri-s-triazine units connected by planar amino groups.

The visible light response of g-C_3N_4 originates from the electron transitions from the valence band populated by N2p orbitals to the conduction band formed by C2p orbitals. Copolymerization of, for example, dicyandiamide with barbituric acid also extend the absorption band up to 750 nm.[110] The as prepared g-C_3N_4 exhibited photocatalytic H_2 evolution from water at wavelength > 420 nm, even without using a cocatalyst.

Besides compound photocatalysts, some elemental semiconductors (i.e., Si, P, S and Se) have also shown their potential as a new class of visible light active photocatalysts. [14] Among them crystalline Si (1.12 eV) has been studied extensively. But Si hasn't become a material of interest due to its instability in aqueous solution and unsuitable band edges for redox reactions. [111] Wang et al. [112] first demonstrated the photocatalytic behavior of red P. They revealed that crystalline monoclinic red P could produce H_2 from water. Amorphous P has a wide photon absorption range compared with crystalline P, but it has small surface area and large number of electron-hole trapping sites. However, the photocatalytic performance of P is somewhat low. Among more than 30 allotropes of elemental sulfur, recent investigations have shown α-sulfur (2.79 eV) as a promising visible light active photocatalyst. [113] But it has poor hydrophilicity which weakens its phocatalytic activity. Modifying the sulfur crystal structure could possibly solve this problem. Se has amorphous and crystalline forms. The ability of amorphous Se (1.99 eV) as a photocatalyst has also been demonstrated. [114] One of the drawbacks of amorphous Se is its instability with annealing temperature. As annealing temperature increases, amorphous Se begins to be converted to crystalline Se.

The elemental photocatalysts are still in the infancy stage and there are huge issues in developing them. If special strategies could develop, more exciting properties of elemental semiconductors might be explored. For example, forming heterojunctions of elemental photocatalysts or constructing heterostructures with their respective sulfides, phosphides and selenides may results in some unusual photocatalytic activities. Exploring special co-catalysts that might fit well with elemental photocatalysts may be another way to improve their performance.

The recent addition to metal-free photocatalysts are the organic materials having C-C/C-H bonds in their π-conjugated organic frame works.[115-118] The timeline of key developments in photocatalysts research is shown in Fig. 6.

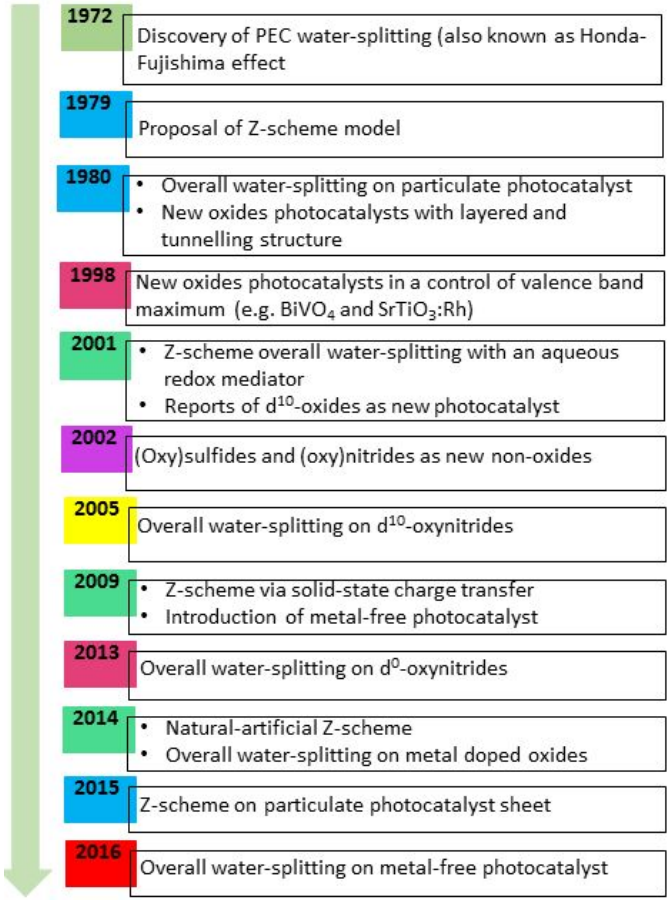

Fig. 6 Timeline of key developments in photocatalytic water-splitting.

7. Metal-free elemental photocatalysts for hydrogen production.

In the past, much research has been directed to the development of compounds semiconductors as photocatalysts. Elemental S, P, B, Se, C, and Si are narrow to medium bandgap semiconductors. Therefore, they have the potential to be applied to photocatalytic water-splitting. Among them, only carbon dots, P, and S have been used to date as a hydrogen evolution photocatalyst. Elemental semiconductors therefore represent a new class of photocatalysts for solar energy conversion.

7.1 Boron (B)

Boron has 17 polymorphs with each having B_{12} icosahedral clusters as a common basic building block. Among these polymorphs, only four main polymorphs (i.e., α-tetragonal, α-rhombohedral, β-tetragonal, and β-rhombohedral boron) form under ambient conditions, while β-rhombohedral boron is the most thermodynamically stable form. β-rhombohedral boron has a bandgap of 1.5–1.6 eV, sufficient for visible light active photocatalysis. Indeed, it is photocatalytically active in generating ·OH radicals under irradiation with visible light.[119] This result encourages the exploration of the effectiveness of elemental boron for photocatalytic water-splitting. However, there are no such reports to date, to the best of our knowledge.

7.2 Carbon (C)

Because of the lack of a sufficient bandgap, elemental carbon and its derivatives (e.g., graphene) are not suitable for use as a standalone photocatalyst but instead as a cocatalyst or as a photosensitizer to a photocatalyst.[120] Research has been made to widen the bandgap of carbon materials through morphological tuning and heteroatom doping. For example, carbon dots were shown to produce hydrogen at a rate of 423.7 μmol h^{-1} g^{-1} and 3615.3 μmol h^{-1} g^{-1} from pure water and from 20 vol. % aqueous methanol solution, respectively, under UV-light irradiation without a co-catalyst. [121] Recently, Reisner et al. reported N-doped carbon dots as a visible light active hydrogen evolution photocatalyst.[122] It has been shown that nitrogen doping could increase the hole scavenging by electron donors, extending the lifetime of electrons, resulting in high charge extraction creating efficient photocatalysis.

There is a long list of graphene based photocatalysts in which graphene was used as a dopant or as one of the heterostructure components. [123] However, expectedly, pristine graphene is not suitable for water-splitting. With doping heteroatoms (e.g. N, P etc.), gapless metallic graphene can be turned into a semiconductor.[124, 125] For example, Garcia et al.[124] reported P-doped graphene with a bandgap of 2.85 eV, and demonstrated visible light hydrogen evolution with a rate of 282 μmol g^{-1} h^{-1} in the presence of a triethanolamine sacrificial electron donor and Pt co-catalysts under visible light irradiation. Interestingly, P-doped graphene was shown to exhibit about one order of magnitude greater photocatalytic activities than that of graphene oxide (GO). N-doped graphene was also shown to be an active photocatalyst under UV- (355 nm) and visible-light (532 nm) irradiation.[125]

Graphene derivatives are now routinely combined with other semiconductor photocatalysts (mostly metal-based) for hydrogen evolution.[126]

7.3 Phosphorous (P)

Out of three allotropes (white, red, and black), red and black phosphorous were reported as hydrogen evolution photocatalysts.[127, 28] Elemental red-P has poor photocatalytic performance having an AQE of less than 1%. Recently, black phosphorous (BP) has gained significant interest. BP is a layered material where layers are held together by weak van der Waals interlayer interactions. [128, 129] It is therefore convenient to exfoliate BP nanosheets of few layers to a monolayer, known as phosphorene.[128, 130] Rahman et al. reviewed the fundamental properties of phosphorene and predicted its suitability as a water-splitting photocatalyst in 2016.[28]

In 2017, few layer BP was reported as a hydrogen evolution photocatalyst for the first time.[131] The BP nanosheets showed ~18 times greater photocatalytic performance than that of bulk BP. Yet the AQE (< 0.5%) of the hydrogen evolution was poor. Hu et al.[132] proposed a mechanism to improve the photocatalytic efficiency of phosphorene nanoribbons (PNRs). DFT calculations showed that pseudohalogen (CN and OCN) passivated PNRs would have the desired VBM and CBM band

edges for both water oxidation and hydrogen reduction reactions. A maximum of 20% energy conversion efficiency was predicted for photocatalytic water splitting.

Recently, Tian et al. reported few-layer BP nanosheets with a hydrogen production rate of ~0.36 µmol h^{-1} and ~11.1 µmol h^{-1} without and with Pt (20 wt. %), respectively, at 420 nm.[133] Clearly, a high rate of hydrogen evolution depends on the high loading of Pt. However, it is recommended to avoid the use of Pt for low-cost hydrogen production. Pt, in this representative case, appeared unavoidable to ensure the efficient charge transfer for catalytic reactions. It indicated that BP is somewhat inactive without Pt.

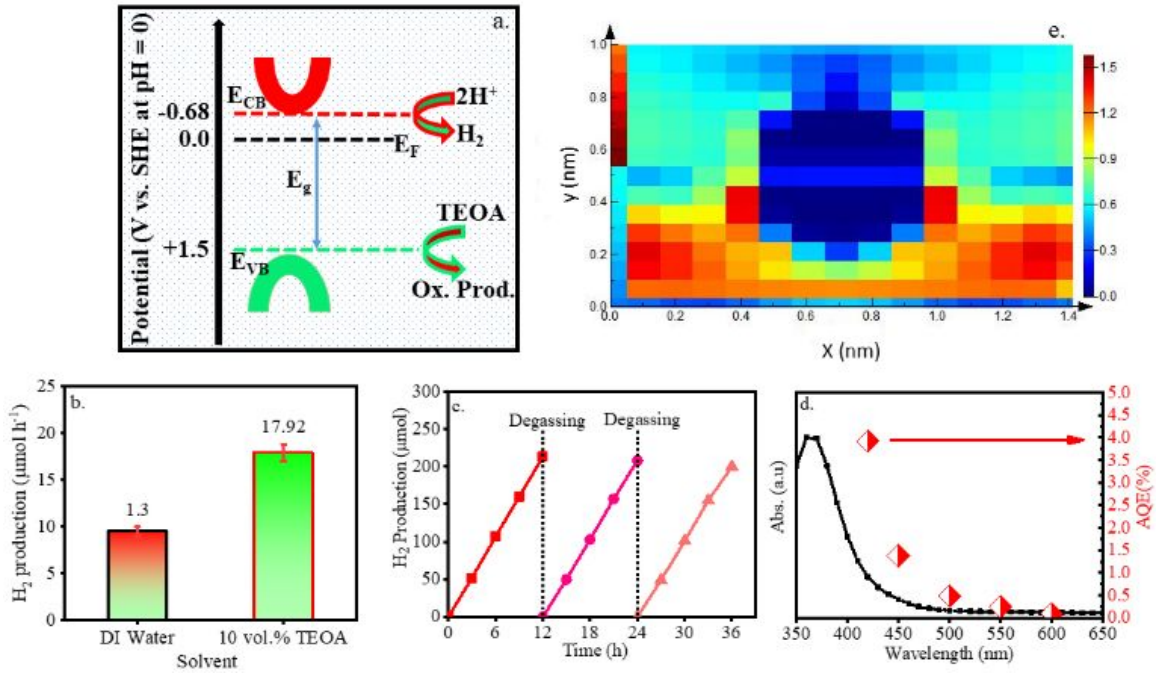

Fig. 7 a) Hypothetical schematic presentation of energy level of conduction band (E_{CB}) and valence band (E_{VB}) with respect to Fermi energy level (E_F), showing BP-nanosheets have sufficient electronic potential to drive HER, b) Rate of hydrogen production DI water and water-triethanolamine solution, respectively under visible light (420 nm) irradiation, c) Cyclic hydrogen production under visible light (420 nm) irradiation for probing photocatalytic stability, d) Wavelength dependent hydrogen production, and e) Understanding the probabilistic distribution of charge carriers through FDTD simulations. Adopted with permission from. [134] Royal Society of Chemistry (2018).

To overcome the problems with poor stability, poor AQE, and over dependence on noble metal cocatalysts, Rahman et al. reported few layer BP with a record high AQE of ~ 4 % at 420 nm, Fig. 7.[134] This unprecedented improvement in AQE was reported to stem from a low level of material oxidation that impedes the degradation of BP under ambient conditions, strong absorption of photons at the surface, and a conduction band edge position that favourably facilitates the proton reduction reaction. These BP-nanosheets also exhibited a superior performance to g-C_3N_4, carbon dots, and red-P under identical experimental conditions.

The elemental red-P and BP are now routinely been used to construct heterostructure photocatalysts for hydrogen evolution.[135]

7.4 Sulfur (S)

Sulfur (S) is the 16th most abundant element in the earth crust. [136] Sulfur has been known since ancient time, which was referred to in Genesis as brimstone (i.e., a stone that burns). The word 'Sulfur' was derived from *sulvere* (Sanskrit) and *sulphur* (Latin), respectively. Unlike many sulfur-containing compounds (e.g. mercaptans, thioethers, and disulfides that possess remarkably foul odours), elemental S is odourless, tasteless, and nontoxic. A commercial process for recovery of S from coal, ores, and minerals was developed by Herman Frasch in the 1890s.[137] Among more than 30 allotropes of elemental S, orthorhombic S_8 (α-S) is the most stable configuration at standard temperature and pressure (STP).[138]

The amber-colored α-S powder (Fig. 8 inset) is an intrinsic semiconductor with a bandgap that varies between 2.4 to 2.8 eV.[139, 140] Clearly, α-S is able to absorb visible light. The UV–vis absorption spectrum of α-S is shown in Fig. 8. Therefore, α-S is suitable for use as a photocatalyst. However, elemental S as a standalone photocatalyst has seldom been studied, while it was extensively used in the synthesis of sulfide photocatalysts or as a dopant in both metal and metal-free photocatalysts.

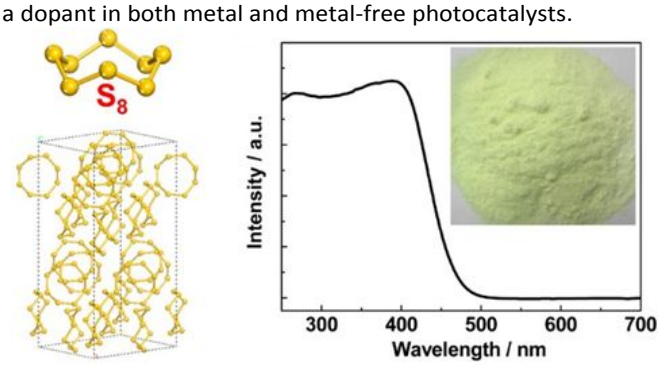

Fig. 8 (left) Schematic illustration of the unit cell of an α-S crystal constructed from S_8 molecules. (right) UV–vis absorption spectrum of α-S crystal powder. The inset is a photograph of the α-S crystal powder. Adopted with permission from. [140] American Chemical Society (2012).

7.5 Selenium (Se)

Selenium (1.99 eV) has also been applied to photocatalytic ·OH radical formation,[114] but yet to be applied for water-splitting applications, to the best of our knowledge.

7.6 Silicon (Si)

Si has an indirect bandgap of around 1.1 eV. This bandgap is lower than the minimum potential required for water splitting (i.e. 1.23 eV). Additionally, the CBM lies below the proton reduction potential- inferring that Si is not suitable for hydrogen evolution reaction. This disadvantage can be overcome by applying a bias. Therefore, Si is widely used as a photoelectrode in photoelectrochemical water-splitting, while its application as a particulate photocatalyst is rather limited.[27]

Moreover, Bare Si, when submerged into an aqueous solution, becomes affected by the pH of solutions, forms a passive oxide layer and corrodes subsequently. The instability of Si in aqueous solution is therefore a great challenge to overcome prior to its sustainable application in water-splitting. Taking quantum size effects into account, nanoscaling would be a recommended strategy to tune the band edges to be compatible to redox levels.[141] However, nanoscalling also adversely influences the instability of Si in an aqueous solution. For instance, it was demonstrated that H-terminated Si nanowires would have a higher oxidation rate with increasing pH of the solution.[111]

8. Metal-free binary photocatalysts for hydrogen production.

8.1 BC_3

Bulk BC_3 is metallic crystal with graphite-like structure, Fig. 9 a. It was first synthesized through the interaction of boron trichloride with benzene at 800 °C: $2BCl_3 + C_6H_6 \rightarrow 2BC_3 + 6HCl$.[142] Later on, BC_3 was epitaxially grown on the $NbB_2(001)$ surface through a carbon-substituted technique in a boron honeycomb matrix.[143, 144] BC_3 is a layered material of stacked sheets where the sheets are 3–4 Å apart.[143] Like graphene, the nanosheets may also be peeled from stacked layers of BC_3 through physical/chemical exfoliation, or single/multilayers sheets may be grown by using chemical vapor deposition or epitaxial growth methods on a suitable substrate.

Theoretical calculations suggested a bandgap of 1.83 eV for the BC_3 monolayer (Fig. 9 b) that is well-above the overall redox potential (1.23 eV) to be used as a water-splitting photocatalyst.[145] The calculated chemical potentials of conduction-band electrons and valence-band holes of the BC_3 monolayer are +0.15 and +1.98 V (vs E_{NHE}), respectively (Fig. 9 c). If the holes in the valence-band would have a chemical potential of +1.0 to +3.5 V (vs E_{NHE}), it would be considered as a good oxidant. Similarly, if the electrons in the conduction-band would have a chemical potential between +0.5 to −1.5 V (vs E_{NHE}), it would be considered as a good reductant. To be noted, the redox potential of a normal hydrogen electrode (NHE) is $E_{NHE} = -4.5$ V with respect to the absolute vacuum scale $E_{AVS} = 0$ V.

Clearly, the BC_3 monolayer is promising for the oxygen evolution reaction when compared to the reference potential for water-oxidation, i.e. H_2O/O_2 = 1.23 vs E_{NHE} at pH of 0. However, the calculated reduction potential (+0.15 vs E_{NHE} at pH = 0) of BC_3 monolayer falls below the reference potential for water reduction (H^+/H_2) = 0 vs E_{NHE} at pH = 0) - meaning that it might not be suitable for the hydrogen evolution reaction. Given the uncertainty and underestimation of theoretical bandgap and band position calculations using DFT, it suggests more research in the synthesis of nanosheets of BC_3 experimentally and determination of the experimental band positions.

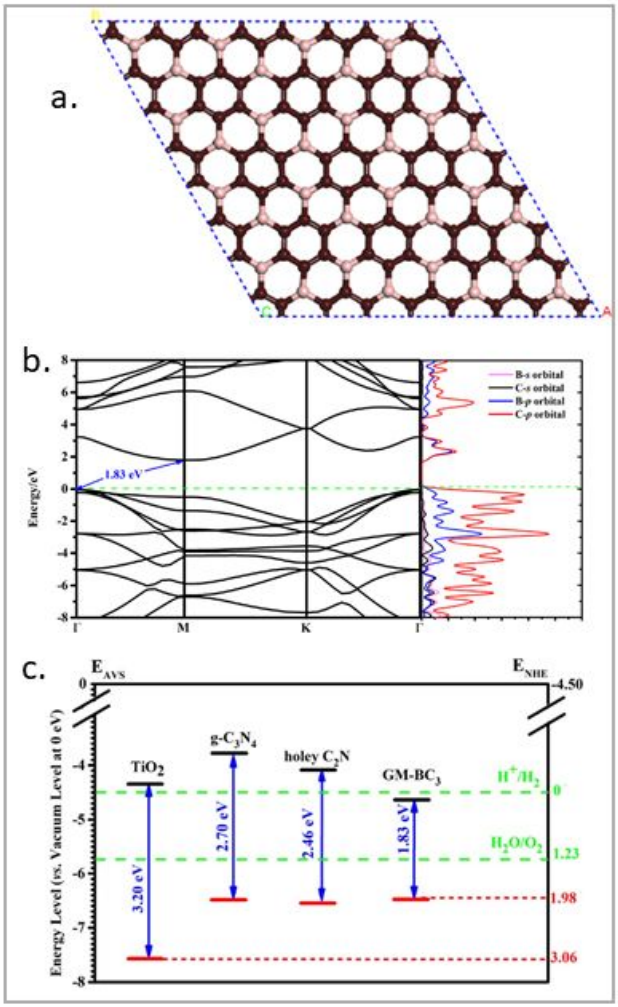

Fig. 9 a) BC_3 equilibrium structures, b) Band structures computed by HSE06 functionals. The green dashed line in the band structure represents the Fermi level at 0 eV, and c) Band edge positions of BC_3 monolayer, TiO_2, g-C_3N_4, and holey C_2N crystals. The redox potentials of H^+/H^2 = 0 vs E_{NHE}) and H_2O/O_2 = 1.23 vs E_{NHE}) at pH = 0 are also given as a reference. Adopted with permission from.[145] American Chemical Society (2018).

8.2 B_4C

Boron carbides consist of a α-rhombohedral structure (space group $R\bar{3}m$) that are composed of slightly distorted B_{12} or $B_{11}C$ icosahedra at each vertex, and are connected by linear three-atom chains on the main cell diagonal in the crystallographic *c*-direction.[146] Disordered combinations of the 12-atom icosahedra and three-atom chains (C-B-C, B-Vacancy-B, C-B-B) therefore offer the possibilities to construct elementary cells with different stoichiometric

compositions. Its homogeneity range extends from $B_{4.3}C$ at the carbon-rich limit to $B_{\sim 11}C$ at the boron-rich limit.[146, 147] Like other common crystalline solids, there is no unit cell representation of the whole structure of boron carbide. Rather, the structure is characterized by elementary cells.

Boron carbide is often incorrectly denoted as B_4C. As has already been proven by numerous studies, the compound B_4C does not exist.[148] The actual chemical composition consists of the compound $B_{4.3}C$ and precipitated graphitic free carbon. Regardless of synthesis and compositions, boron carbides contain a small amount of free graphitic carbon.

The electronic structure of boron carbide is evolved from a completely filled valence band and high density gap states that are partly filled by electrons generated by B substituted C atoms. The Fermi level is pinned at the valence states that result in p-type semiconducting behavior.[149, 150] Boron carbides display dark coloration and high absorption from 310–800 nm by UV/Vis diffused reflectance spectra. The intrinsic bandgap of boron carbides was reported to be ~2.0 eV.[151, 152] It implies that boron carbides might be employed as a photocatalyst for water splitting under visible light irradiation. Recent photoluminescence studies revealed the existence of a stronger excitonic level at 1.56 eV and a weaker one near 1.57 eV.[151]

$B_{4.3}C$ and $B_{13}C_2$ were shown to evolve hydrogen at a rate of 2.9 µmol h^{-1}/0.2 g and ca. 0.9 µmol h^{-1}/0.2 g, respectively, from a 25 % methanol aqueous solution at 420 nm. With 2 wt % Pt, the H_2 evolution rates of $B_{4.3}C$ and $B_{13}C_2$ were 6.2 µmol h^{-1}/0.2 g and1.6 µmol h^{-1}/0.2 g, respectively. $B_{4.3}C$ and $B_{13}C_2$ exhibited stable H_2 evolution rates for a long 100 h. Despite the fact that boron carbides contain a small amount of free graphitic carbon, the graphitic carbon was reported to be not active in photocatalytic water splitting.[152]

8.3 B_6O

Boron suboxide (B_6O), a member of α-rhombohedral boron-rich compounds, consists of eight B_{12} icosahedral units situated at the vertexes of a rhombohedral unit cell, whereas two oxygen atoms are located in the interstices along the (111) rhombohedral direction (see Fig. 10 a, b). Hubert et al. synthesized orange–red color icosahedra B_6O particles via a Mackay packing at high temperatures (1700–1800 °C) and pressures (4–5.5 GPa).[153] The icosahedra B_6O has a bandgap of 2.0 eV that is sufficient to be used as visible-light active photocatalyst.

In contrast to the high temperature (>1300 °C) and pressure (>1 GPa) synthesis of icosahedra B_6O particles, Luo et al. developed a synthesis method to obtain crystalline B_6O at ambient pressure and a low temperature of 90 °C, and demonstrated the activities of photocatalytic hydrogen evolution with B_6O. [154] They have studied two types of B_6O (e.g. R-B_6O and L-B_6O) and compared with elemental B for H_2 evolution from water under visible light irradiation. The H_2 evolution rates of R-B_6O, L-B_6O, and crystalline B are about 5.48, 1.34, and 2.48 µmol g^{-1} h^{-1}, respectively, at >400 nm in the absence of any metal cocatalysts. The absorption spectra and time dependent H_2 evolution of R-B_6O, L-B_6O, and crystalline B are shown in Fig. 10 c, d.

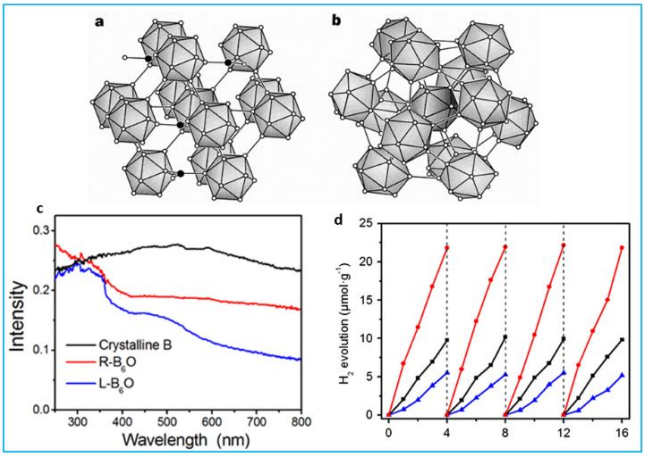

Fig. 10 a) A part of the B_6O structure showing c.c.p. packing (slightly distorted) of B_{12} icosahedra with O atoms (filled circles) in the close-packed layers, b) A fragment of the β-rhombohedral boron structure. The central B_{12} unit is surrounded by 12 other B_{12} icosahedra whose centres are at the vertices of an icosahedron. Adopted with permission from.[153] Copyright 1998, Nature Publishing Group. c) UV-Vis spectra and d) Time course for H_2 evolution by crystalline B (black), L-B_6O (blue), and R-B_6O (red) at > 400 nm. Adopted with permission from. [154] Wiley-VCH (2019).

8.4 Boron phosphide (BP)

Boron phosphide (BP) is a III–V compound made up of covalently bonded boron and phosphorus, and has a cubic zinc-blende structure. The crystal structure of BP was first investigated in 1957.[155] Among the notable properties, BP is chemically highly stable and is resistant to chemical corrosion even in contact with concentrated mineral acids or aqueous alkali solution. BP is also thermally very stable as is evident from its resistance to oxidation and decomposition in air up to 800–1000 °C.[156]

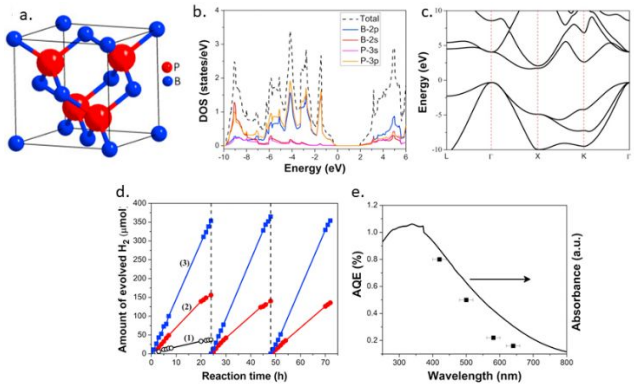

Fig. 11 Electronic properties and photocatalytic activities of BP. a) unit cell structure, b) Density of states (DOS), c) bandgap calculations, d) time course of hydrogen evolution and e) wavelength dependent hydrogen evolution at 420 nm. Adopted with permission from.[157] Elsevier (2016).

BP has an indirect band gap of 2.0 eV. [156] BP can be either *p* or *n*-type. Excess B will produce *p*-type, while excess P will produce *n*-type BP.[158] The *n*-type BP usually shows higher charge mobility and lower resistivity than *p*-type. Endowed with excellent chemical, thermal, mechanical and electronic properties, BP is a material of choice for electronic devices to work in extreme conditions at high temperature and intense radiation. [158] Despite its widespread use in electronic devices, BP has rarely been used in photocatalytic applications. It might

due to the difficulties in materials development. Synthesis of BP requires a high-pressure flux that is difficult to be realized in many laboratories. [159]

Lee et al. reported a *p*-type BP photoelectrode for photoelectrochemical splitting of water under visible light. [159] Ye et al. reported *n*-type BP as a photocatalyst for H_2 evolution under visible light, even without loading a precious metal cocatalyst. The H_2 evolution activity of bare BP was 2.0 μmol h^{-1} without a Pt cocatalyst, and 6.9 μmol h^{-1} with a Pt cocatalyst, see Fig. 11.[157]

8.5 *h*-BN

Pristine h-BN has a bandgap > 5 eV that is not suitable for being used as a photocatalyst. Therefore, its bandgap and band positions need to be adjusted to be compatible with redox potentials. Recently, S doped h-BN nanosheets (3.907 eV) were reported to be active in visible light photocatalytic hydrogen production in the presence of sacrificial electron donors and a Pt cocatalyst.[160] However, at least two questions remained unanswered. Firstly, scaling down from bulk to nanosheets incurs a blue-shift in optical absorption- meaning that the nanosheets would have a larger bandgap than the bulk. Secondly, how could visible light absorption happen when the reported bandgap of 3.907 eV is not suitable for absorption of photons from visible light? Indeed, it should not be able to absorb photons beyond ~320 nm. In our opinion, visible light absorption might stem from S that has bandgap < 3.0eV,[139] and S is itself an elemental photocatalyst.[140] It therefore demands more controlled measurements to conclude the actual interplay of S doping (or other heteroatoms) in the photocatalytic behavior of h-BN.

8.6 Carbon nitride (C_xN_y)

The history of the synthesis of the early genre of carbon nitride dates back to Liebig's melon in 1834.[161] Several research groups have contributed in the development and understanding of the fundamental properties of carbon nitride over the years.[11, 162-165] However, the first breakthrough in using carbon nitride as a water-splitting photocatalyst happened in 2009 with the collaborative research efforts of the Domen and Antonietti groups when they reported graphitic carbon nitride (g-C_3N_4) as a photocatalyst.[109] In the midst of metal-based photocatalysts, g-C_3N_4 began a new era of metal-free photocatalysts. As might be expected, it drew unprecedented interest among researchers as evident by the hundreds of peer-reviewed publications in the subsequent years.[9, 10] Facile synthesis from earth abundant and inexpensive raw materials, suitable bandgaps (~ 2.7 eV), exceptional stability, and non-toxicity cumulatively sparked the interest in g-C_3N_4.

However, pristine g-C_3N_4 exhibits very poor photocatalytic performance regarding hydrogen evolution with an AQE < 1% under visible light irradiation.[109] Research has been directed to improve the photocatalytic performance of this exotic metal-free photocatalyst. For example, incomplete polycondensation of the precursor and structural destruction g-C_3N_4 nanosheets were serious problems. Rahman et al. developed a combined three-step method including co-polymerization, surface activation and exfoliation that resulted in structurally very robust and catalytically highly efficient g-C_3N_4 nanosheets as evidenced by a 38 fold enhancement in hydrogen production as compared to pristine g-C_3N_4.[166] In addition to semicrystalline g-C_3N_4, they also engineered a sponge-like hierarchical structure of amorphous g-C_3N_4 (ACN) to overcome the mismatch between light-absorption and charge-collection that limited the AQE to < 0.5 % under visible light irradiation.[167] The modified ACN exhibited 40 % enhanced light-trapping and a ~23 times longer electron lifetime that led to a new benchmark for hydrogen production with an apparent quantum efficiency (AQE) of 6.1 % at 420 nm.[168] Traditional fabrication methods for g-C_3N_4 nanosheets result in a blue shift in optical absorption, which is considered a major cause of poor efficiency. Recently, a fabrication method was demonstrated to counteract this blue-shift that resulted in a AQE of 16% at 420 nm.[169]

g-C_3N_4 is considered as a wide bandgap semiconductor for photocatalytic applications. Its absorption edge is confined to the ultraviolet and blue fraction of the solar spectrum (λ < 450 nm) which limits its photocatalytic performance. Benefits of metal and non-metal doping with various heteroatoms (e.g. Ag, Cu, Rh, Pt, Na, P, F, B S etc.) are frequently exploited to tune the bandgap of g-C_3N_4 for improved visible light absorption.[170] However, doped g-C_3N_4 suffers from the innate drawback of carrier recombination. Alternatively, surface modification using soft and hard templating, copolymerization of two or more precursors, nanostructuring of bulk material, coupling with other semiconductors/metal complexes to form heterojunctions, etc., are routinely employed to improve the photocatalytic performance of g-C_3N_4.[171-180] These conventional techniques are already been comprehensively reviewed elsewhere.[9-11, 170]

Beyond those above mentioned techniques, molecular tuning of the structure, compositions, and electrochemical surface states of carbon nitride were achieved by combining advanced computational quantum chemistry and nanotechnology. Research has progressed significantly regarding the in-depth mechanistic understanding of photochemical, electrochemical, and electro-optical processes in carbon nitride. Supramolecular assembly, metal-to-ligand charge transfer, surface chemical modification, construction of surface bonding states, self-sensitization, homogeneous self-modification of vacancies, stabilizing single metal atoms, monomer functionalization, etc., are some of the notable techniques for molecular tuning of the intrinsic catalytic activities of carbon nitride. We have recently reported the latest progress in molecular tuning of carbon nitride.[12] In this contribution, our focus is therefore to cover the new developments in carbon nitride based photocatalysts.

8.6.1 New derivatives of carbon nitride beyond C_3N_4

Recently, tuning the band structure of g-C3N4 through self-modification of chemical structure has emerged to synthesize the carbon nitride framework with entirely new physicochemical properties for efficient photocatalytic applications. This can be done by either reducing the nitrogen content or adding extra nitrogen-rich moieties in the g-C_3N_4 scaffold. For the case of nitrogen reduction, the nitrogen

content is reduced to an extent such that C/N > 1. Thus, the end product is a carbon rich carbon nitride which is sometimes called carbon-subnitride. Theoretically, there could be many variations in carbon-subnitride. However, C_3N and C_2N (1.96 eV) are the only experimentally demonstrated representatives of carbon-subnitride to date.[181-183] Contrarily, upon addition of extra nitrogen such that C/N < 1, the product is a nitrogen rich carbon nitride (C_3N_{4+x}) which is sometime also called carbon supernitride. For example, Vinu et al. demonstrated the synthesis of N-rich carbon nitrides, C_3N_5 (2.2 eV, HER at 267 μmol h^{-1} at 420 nm) and C_3N_6 (2.25–2.5 eV, HER at 31.5 μmol h^{-1} at 420 nm).[184, 185] However, stand-alone C_3N and C_2N are yet to be applied for photocatalytic hydrogen production. Interestingly, Co and Ru supported C_2N exhibited electrocatalytic hydrogen evolution.[186, 187]

The carbon sub/super nitrides constitute new and different bonding structures compared with g-C_3N_4. For example, skeleton of C_3N_5 is formed from two *s*-heptazine units that are bridged together with an azo linkage. In contrast, g-C_3N_4 has three heptazine units that are linked together with tertiary nitrogen. C_3N_5 is attributed with extended conjugation of an aromatic π network of heptazine units compared with g-C_3N_4 that lead to an upward shift of the valence band maximum. Extended π-conjugation and distribution of the lone pair electrons in the N atom to the heptazine motif can reduce the bandgap significantly.

Following the report of Vinu et al., recently, , Shankar et al. reported the synthesis of a C_3N_5 with a C/N ratio of 0.6 and an electronic bandgap of 1.76 eV by thermal deammoniation of the melem hydrazine precursor.[188] Clearly, Shankar's C_3N_5 has an extended absorption range compared with Vinu's C_3N_5. However, this extended absorption range comes with a penalty in the VB band position that makes it unsuitable for water-splitting. For example, its CB edge is positioned at −0.72 V, while the VB edge is at +1.04 V vs NHE at pH 0. Considering the proton reduction potential (0.0 V at pH 0), the CB edge is suitable for proton reduction in the presence of a sacrificial electron donor, although It is yet to be applied to photocatalytic hydrogen production. However, it is not suitable as a stand-alone catalyst for the overall splitting of water, because water oxidation (H_2O/O_2) requires a VB position at least at +1.23 V vs NHE at pH 0. Nevertheless, owing to the excellent visible light absorption, C_3N_5 was applied as a photosensitizer to increase the photocatalytic performance of TiO_2. [188] Compared to C_3N_4, C_3N_5 was found to have a higher charge transfer resistance and a high rate of charge carrier recombination that are detrimental to photocatalytic performance. Clearly, intense research is needed to adjust its band positions and overcome its charge transport related problems to be suitable as a water-splitting photocatalysts.

Rahman et al. reported a topological carbon nitride (TCN) as a new type of carbon nitride with built-in polycrystalline and amorphous phases.[189] In the synthesis of TCN, a new concept of 'repairing the crystallinity of the amorphous phase' was developed. This comes with the realization of localized photon absorption for the first time for any carbon nitride photocatalyst. This attribute is highly desirable to limit wasted photon absorption at the regions where charge carriers are most likely to undergo recombination. This research provided new understanding of entropy assisted charge carrier separation. These attributes enable cocatalyst-free hydrogen production in TCN, while other carbon nitride based photocatalysts are dependent on a precious metal (i.e. Pt) cocatalyst.

8.6.2 Dealing with bottleneck of charge transport for Pt-free hydrogen production

A long-standing problem with CN is its dependence on metal cocatalysts, such as platinum for photocatalytic hydrogen evolution. Sluggish charge transfer kinetics and a high activation energy for proton reduction makes pristine CN dependent on a high loading of precious Pt-cocatalyst for hydrogen evolution. Recently, it was shown that the limiting factors of Pt-dependent hydrogen production could be overcome by amorphization with a mechanistic understanding of the origin of cocatalyst-free hydrogen evolution.[190]

Dissociation of electron-hole pairs into free electrons and holes in CN also suffers from an inherent high recombination rate.[29] Conventionally, the suppression of recombination is preferentially dealt with a heterojunction but inherently depends on the precious metal cocatalyst. [191] To overcome the dependency on precious metals, it has been reported that coupling two energetically optimized carbon nitrides, but with different phases in the form of a hybrid could significantly inhibit charge carrier recombination and facilitate the charge transfer processes.[192, 193] It was found that the potential gradient in this homojunction delocalizes electrons and holes, and increases the spatial charge separation. Therefore, this led to a high AQE of 5% for photocatalytic H_2 production from water under visible light irradiation in the absence of a precious metal (e.g., Pt) cocatalyst.[32]

Clearly, efficient photogeneration of charge is the key for enhanced hydrogen production via water-splitting. Photogeneration implies the sequential steps of exciton generation followed by dissociation of the excitons, and finally, diffusion of excitons to the surface/interface for redox reactions.[33] Excitons are Coulombically strongly bound in CN [194] which makes dissociation of excitons into free electrons and holes difficult.[195] In the process of exciton generation to dissociation into free charge carriers, the recombination/trapping of charge carriers is the undesired but unavoidable problem. Therefore, a predictive understanding of the relationship between charge transport related phenomena and photocatalytic performance is crucial for rational design of the photocatalyst materials. Much relevant research has been to make morphological fine-tuning from the bulk-to-nanoscale and to construct heterojunctions to deal with the charge transport problems in CN. However, there are only a few reports regarding the mechanistic understanding of charge transport phenomena in CN at the atomic level.[9, 191]

Based on transient spectroscopy measurements, a cascade of charge transfer kinetics was found in CN[196] that showed preferentially 1D diffusive hopping transport along the interplanar direction, Fig. 12. [197] The dissociated excitons

migrate independently between nearest neighbor monomers in a manner of diffusive hopping transport, and exciton relaxation follows a path of nonradiative decay. Recombination depends on the dimensionality (1D, 2D, 3D) of the spatial region. For higher dimension, a strong decrease in excitation density and weaker recombination prevailed.[197]

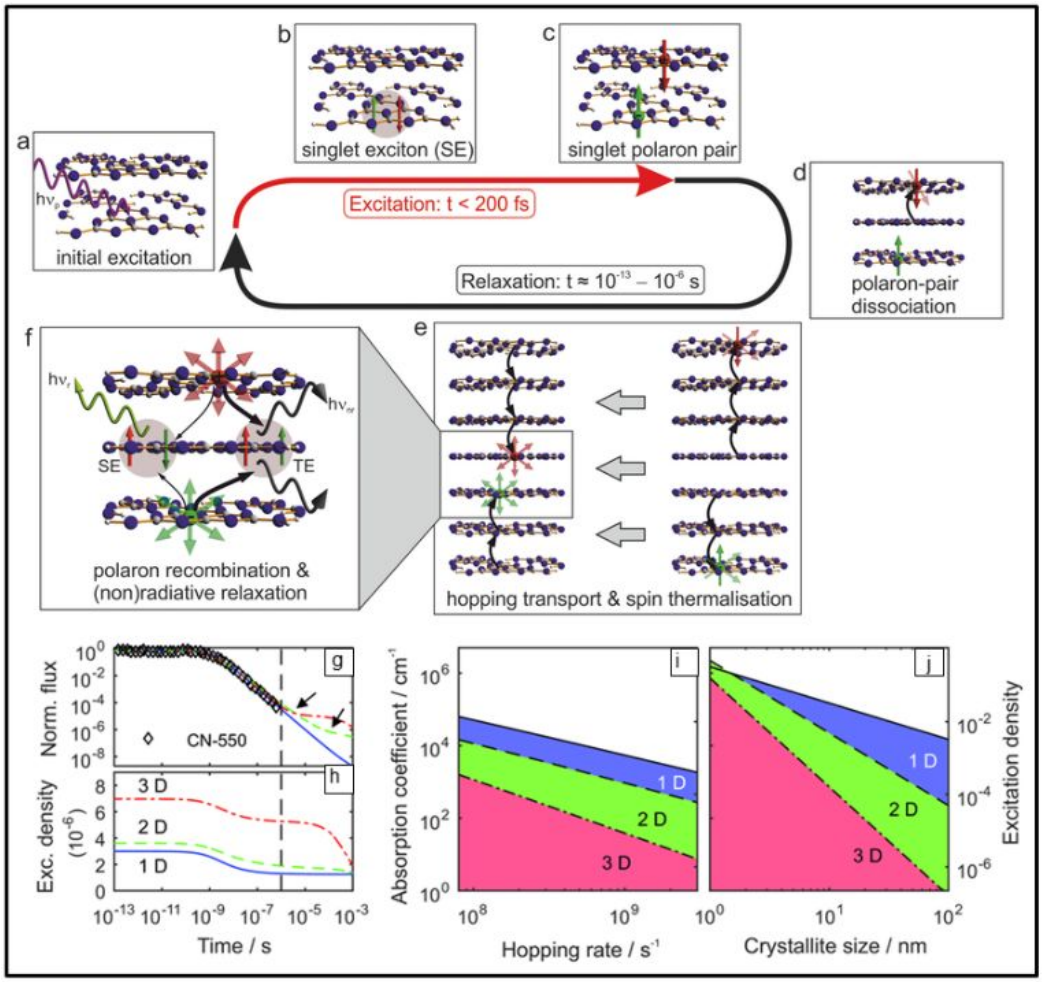

Fig. 12 Light induce charge transport in CN. a, b) Photoexcitation and generation of singlet excitons (SE), c) rapid dissociation (< 200 fs) of SE into singlet polaron pairs, d) further dissociation into free polarons, e) diffusive Brownian motion of free polarons, f) recombination of free polarons, and recovery of singlet (SE) or triplet (TE) excitons. Effect of dimensionality on g) the time-dependent luminescent flux and h) associated excitation density. Allowed ranges of excitation densities and absorption coefficients for 1D, 2D, and 3D scenarios in i) the diffusion-limited case and j) domain-size-limited case. Reproduced with permission from ref. 16. [197] Wiley-VCH (2015).

Based on the charge trapping model for CN proposed by Durrant el at. [198] (Fig. 13), a photogenerated electron may undergo one of the two events in the course of transition to the conduction band. It may either transit directly to the conduction band to create an emissive state (EM) or become trapped forever in deep or shallow trap states. Even if the electron succeeds in going to the conduction band from the ground state, an excited electron may fall back to the ground state (GS) and recombine with holes, or be trapped in the trap states. [199] Electron trapping is inversely related to recombination. Regardless of the recombination or the trapping of electrons, it will reduce the concentration of free charge carriers, and therefore, decrease the nominal charge transfer rate. [198] Consequently, there would be fewer electrons and holes to be transferred to catalytic active sites for redox reactions.

Singlet excitons in carbon nitride were found to be confined to the tri-s-triazine unit, and are influenced by a strong Coulombic attraction along with electron-lattice and electron-electron interactions that causes a large binding energy, greater than the thermal energy.[194, 200] The dissociation of the exciton requires overcoming this binding energy within its lifetime. [195] Following dissociation, the excitons may also recombine and might never reach the catalytic sites.[32, 195] Both the photocatalytic activity and exciton dissociation are therefore statistical in nature- varying with the wavelength of the photoexcitation.[201]

It has been shown that if triplet-to-singlet conversion process could be attained, it would significantly enhance the HER mechanism.[202] For example, triplet-to-singlet conversion would promote the availability of more electrons to be transferred to the active sites for HER by delaying carrier recombination lifetime from nanoseconds to microseconds. A half-metallic semiconductor may avail the triplet-to-singlet conversion due to spontaneous spin polarization that makes the electronic structure around the Fermi level split into spin-up and spin-down.[203]

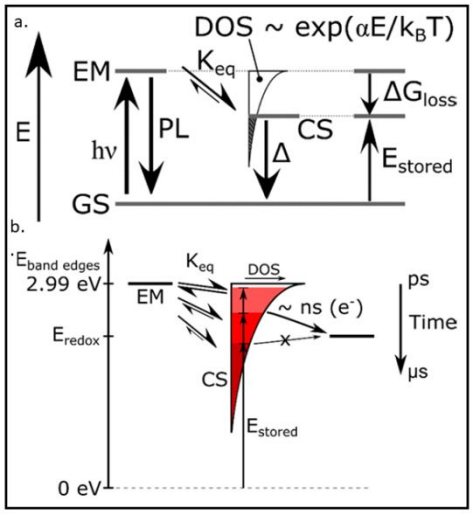

Fig. 13 Schematic representation of a) charge trapping model, and b) influence of trapping on charge transfer reactions. Reproduced with permission from ref. 24. [198] American Chemical Society (2017).

DFT calculations reveal that when OH^- comes in close vicinity of CN, photogenerated electrons in carbon nitride transfer to the empty molecular orbitals of OH^-. Consequently, it become difficult for OH^- to be oxidized to the hydroxyl radical unless sacrificial reagents are used to sweep the electrons. The sacrificial electron scavenger depletes the electrons and promotes the holes migration to OH^-, and therefore, enhances the photo-oxidation reaction rate. [204] As a result, the sacrificial hole/electron scavengers are now being routinely employed to suppress HER or OER. A reverse hole/electron transfer, RH(E)T process from adsorbate-to-substrate governs the efficacy of hole/electron scavengers.[205] An ideal hole/electron scavenger should capture the holes from the substrate as quickly as possible and retain the captured holes/electrons as long as possible. The timescale for RH(E)T is the measure of highly efficient hole/electron scavengers.

8.6.3 Achieving AQE > 50% with visible light

Thermally-induced polycondensation of nitrogen-containing precursors is the most commonly used method to synthesize pristine g-C3N4. This traditional technique typically results in a g-C3N4 with lower crystallinity, poor charge transport, and therefore, moderate photocatalytic activity. Therefore, the synthesis of a fully condensed and crystalline g-CN is desirable with the vision that the improved crystallinity would reduce the defect related recombination centers for electron–hole pairs in the photocatalyst which will, in turn, enhance the photocatalytic activity.

To address this problem, a molten salt method was developed to synthesize crystalline g-CN. For example, crystalline g-C3N4 was synthesized from a preheated melamine precursor using KCl/LiCl salts, which showed impressive rates of hydrogen production from phosphate solution with an AQE of 50.7 % at 405 nm.[175] This high AQE was attributed with enhanced crystallinity of the extended conjugated system that reduces the density of surface defects, decreases unpaired electron density, and suppresses electron–hole pair recombination.

Antonietti and co-workers have significantly advanced the molten-salt assisted synthesis of crystalline carbon nitrides with AQE > 50% under visible light irradiation. For example, they synthesized a crystalline carbon nitride from co-condensation of urea and oxamide using KCl/LiCl that exhibited a narrow bandgap of 2.56 eV and a maximum π–π layer stacking distance of heptazine units of 0.292 nm (while it is ~0.326 nm for pristine g-C3N4). The narrow bandgap provided extended spectral overlapping for harvesting low energy photons, while compact interlayer stacking improved the lateral charge transport and interlayer exciton dissociation. As a result, it showed hydrogen evolution with an AQE of 57 % at 420 nm.[172] Recently, they have also investigated the combination of different salts in the synthesis of crystalline carbon nitride and their photocatalytic performance, see Fig 14. It was found that ionothermal synthesis of carbon nitride in NaCl/KCL salts resulted in an AQE of 60% at 420 nm.[206] This is the highest AQE reported to date for any type of carbon nitride based photocatalyst.

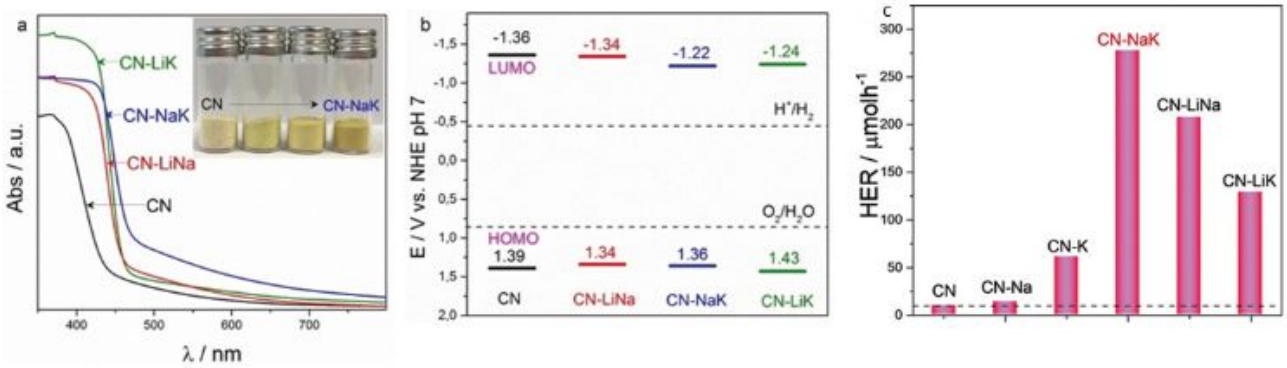

Fig. 14 a) UV/Vis absorption (inset: digital photograph). b) HOMO and LUMO positions determined by Mott–Schottky plots and UPS analysis. c) Photocatalytic H_2 evolution rates at 420 nm. Adopted with permission from. [206] Wiley-VCH (2018).

8.6.4 Binary heterojunction photocatalysts

A binary heterojunction is comprised of two different materials. It is a purpose built and custom made structure to accommodate one or more of the followings actions: increasing the window of photon absorption from the UV to the IR, to deal with the kinetic competition between charge recombination and separation, and set band edges to be compatible to redox potentials. We discuss some notable binary heterojunctions of metal-free photocatalysts below.

Most of the metal-free heterojunction photocatalysts have been made having g-C_3N_4 as a base with another metal or semiconductor that is incorporated with it to form a heterostructure. For instance, g-C_3N_4 is composed of carbon materials, e.g., multiwalled carbon nanotubes, carbon black, or carbon nanodots etc., in which carbon materials act as a conductive material to transfer the photogenerated electrons to catalysts for H_2O_2 decomposition.[207, 208] Endowed with high conductivity, intrinsic carrier mobility, and specific surface area, graphene is also a commonly used material to promote charge transport because of the area of graphene. A graphene/g-C_3N_4 heterostructure photocatalyst for hydrogen evolution was reported[209] for hydrogen evolution with a rate of be 451 µmol h^{-1} g^{-1} in the presence of methanol as an electron donor and Pt as a cocatalyst. In this heterostructure, the graphene was used to provide electronic conductive channels for efficient separation of the photogenerated charge carriers. For an optimal graphene content (~1.0 wt %), graphene/g-C_3N_4 heterostructure photocatalysts could produce at rate that was ~3 times greater than that of pristine g-C_3N_4. Recently, a sandwich of graphene-carbon nitride-graphene (titled GR-CN-GR) was reported for simultaneous photocatalytic hydrogen generation and capsule storage, Fig. 15. [210] Among the carbon materials, carbon dots are used to prepare 2D/0D heterostructure photocatalyst. The carbon dots here function as a photosensitizer to expand visible light absorption regions and suppress the recombination of photo-induced carriers. A carbon dot/g-C_3N_4 photocatalyst exhibited hydrogen evolution at a rate of 88.1 µmol h^{-1} under visible light irradiation from 5 vol. % methanol aqueous solution with 2 wt. % Pt. [211]

While the above mentioned heterostructure photocatalysts were dependent on precious metal Pt- cocatalysts for hydrogen evolution, Han et al.[212] reported an interconnected framework of mesoporous g-C_3N_4 nanofibers merged with in situ incorporated N-rich carbon (g-C_3N_4@C) that exhibited hydrogen evolution at a rate of 16885 µmol h^{-1} g^{-1} without any cocatalysts that achieved an AQE 14.3 % at 420 nm. In this heterostructure of C_3N_4@C, excitons generated in g-C_3N_4 were transferred to carbon or nitrogen atoms on N-carbon where the proton reduction reaction was taking place to generate H_2. This 3D porous skeleton of C_3N_4@C resulted in high surface area, efficient charge separation and transfer, and enhanced light-absorption. The highest AQE of 77.4 % at 420 nm was reported for a metal-free heterojunction photocatalyst of P3HT/g-C_3N_4.

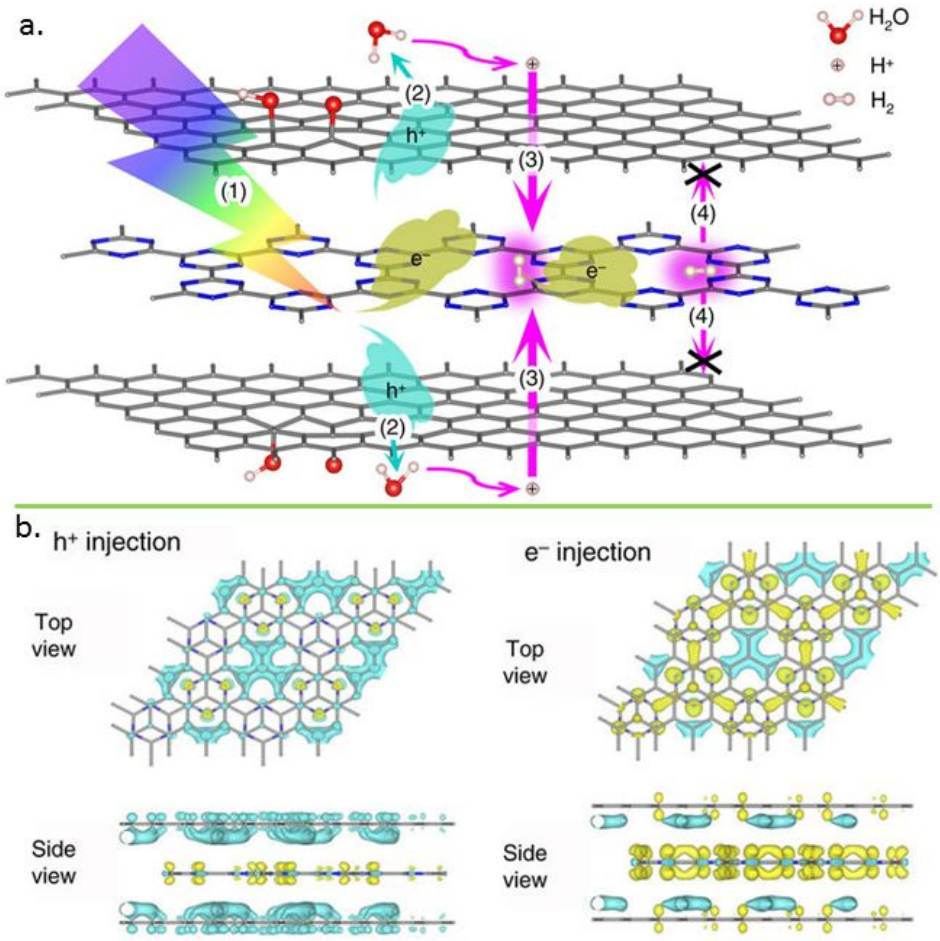

Fig. 15 a) The photocatalytic (water-splitting) hydrogen evolution and capsule storage scheme: (1) photo-generated electrons (e^-) and holes (h^+) separating; (2) water splitting to produce protons (H^+) through holes (h^+) attacking; (3) protons (H^+) penetrating through GR and producing H_2 molecules; (4) H_2 molecules are prohibited from moving out of the sandwich. b) Charge distribution computed as Bader charge differences between GR–CN–GR sandwich. Yellow and blue bubbles represent respectively electron and hole charges with isosurface value of 0.0005, e $Å^{-3}$. Adopted with permission from. [210] Nature Publishing Group (2017).

Such a high AQE was a result of wide visible light absorption, efficient charge transfer at the interface, and a suitable oxidation half-reaction caused by the sacrificial reagent. [213] Other notable metal-free heterojunctions include fullerenes/carbon nitride and polytriazine/heptazine carbon nitride for photocatalytic hydrogen evolution. [214-216] Beyond carbon based materials, phosphorous was also coupled with carbon nitride with broadband solar absorption from the UV to near-infrared region of the solar spectrum. For example, a red-P/g-C_3N_4 and BP/carbon nitride were demonstrated, respectively for hydrogen evolution in the presence of sacrificial electron donors and a Pt cocatalyst. [217, 218]

In addition to broadband photon absorption, the phosphorus built heterojunction also provided prevention of charge trapping into deep and photocatalytically inactive trap states of g-C_3N_4 in which neither participate in the charge transfer reaction nor reduce electron acceptors on the surface or in solution during the photocatalytic process.[198, 219] Because of these highly beneficial attributes, the red P/g-C_3N_4 heterojunction exhibited a remarkable hydrogen production of 2565 μmol h^{-1} g^{-1}. [220]

By exploiting the *in situ* bond modulation through a defect-induced self-functionalization process,[221] a molecular polymer heterojunction of GCN with polyfluorene family polymers was reported with an AQE of 27%.[222] This molecular heterojunction accommodates intermolecular π – π interactions, and an optimized band structure for efficient exciton dissociation and extended visible light absorption.

All of the above discussed heterojunctions are active in only hydrogen production via a half reaction of water-splitting while overall water-splitting remains great challenge. In opposition to challenging the four electron pathway for oxygen evolution, recently, a two electron pathway to release O_2 from water was reported in a heterojunction of carbon dots/C_3N_4, where water is oxidized via a two-electron reaction to H_2O_2 and H_2, followed by H_2O_2 decomposition to O_2 and H_2O (i.e. $2H_2O \rightarrow H_2O_2 + H_2$; $2H_2O_2 \rightarrow 2H_2O + O_2$). [223] This heterojunction demonstrated overall water-splitting with a solar-to-hydrogen conversion efficiency of ~2%. This is indeed a milestone achievement for a metal-free photocatalyst reported to date. Inspired by this work, a heterostructure of C_{ring}-C_3N_4 was reported for hydrogen evolution via overall water-splitting. [224] In this heterostructure, a strong in-built electric field that was produced by a sp^2-hybridized π-conjugated system with different work functions. This internal electric field provides an intrinsic driving force for delocalization of the photocarrier around the photoexcited sites, and promotes electron–hole pair separation and transport. Additionally, high electron density around the Fermi level introduced by the carbon ring increases the photocarrier diffusion length and lifetime significantly (10 times) relative to those of pristine g-C_3N_4. As a result, the C_{ring}–C_3N_4 heterostructure produced hydrogen at a rate of 371 μmol g^{-1} h^{-1} with an AQE of 5 % at 420 nm.

9. Metal-free ternary photocatalysts for hydrogen evolution

9.1 Borocarbonitride (BCN)

BCN is different from B-, N-codoped graphene[225] both from compositional and structural aspects. The electronic properties of BCN can be tuned between graphene (gapless) and BN (insulator) by varying the B:C:N ratio or by configurational changes in the structure of BCN. **[226]**

Want et al. reported BCN tubes (~2.72 eV) as a hydrogen evolution photocatalyst. BCN tubes exhibited hydrogen evolution with an AQE of 0.32% at 405 nm.**[227]** They recently reported a boron-rich ceramic aerogel-like 3D porous BCN photocatalyst that was synthesized by a eutectic molten salt method. The BCN aerogel showed absorption in the range of 420 to 650 nm that corresponds to an optical gap of 2.92 eV to 2.72 eV. The optimum BCN aerogel evolved hydrogen at a rate of 7.3 μmol h^{-1} with an AQE of 0.82 % at 420 nm.**[228]**

9.2 h-BN/graphene hybrid

The BN family includes amorphous BN (a-BN), hexagonal BN (h-BN), cubic BN (c-BN), and the relatively rare wurtzite BN (w-BN).[229] Among them h-BN only has a layered structure. Hexagonal boron nitride (h-BN), also referred to as white graphene or boronitrene, is a layered honeycomb allotrope of boron nitride.[230] In contrast to ideal graphene (a gapless material), h-BN features a wide band gap (> 5 eV). Because the bandgaps of these layered materials do not fall within the thermodynamic limit of water-splitting redox potentials; neither graphene nor h-BN, Individually, can be used as a photocatalyst. Therefore, bandgap engineering is the foremost issue to deal with. In this regard, merging h-BN and graphene in the same lattice to form the so-called h-BN/graphene hybrids therefore is of great research interest.[230-234]

Quantum chemical computations reveal that size modifications of h-BN segments confined in a given graphene host may induce dramatic electrical property variations.[235, 236] Interestingly, theoretical studies revealed that h-BN fragments embedded in graphene hosts may induce precisely the reverse effect on band gap related properties, that may vary from 0.7 eV to 4.0 eV.[236] Additionally, when finite sections of h-BN are confined in the graphene flakes, exceptional nonlinear optical properties might emerge.

Layered BN has a structural analogue of graphite with strong in-plane bonds and weak coupling between layers. Honeycomb lattice h-BN can be thought as of graphene by substituting carbon (C) atoms in graphite with alternating boron (B) and nitrogen (N) atoms. Therefore, C, B, and N atoms can coexist as atomic sheets in a layered structure. Because, h-BN and graphene share similar lattice parameters and crystal structure, therefore, hybridization of h-BN and graphene together with the mixture of C, B and N atoms will result in a ternary B–C–N system with interesting characteristics. Boron carbonitride (BxCyNz) nanostructures may be of particular interest.[231] Recently, carbon doped BN (denoted as BCN-30, E_g = 2.9 eV) was reported as a hydrogen evolution photocatalyst with an AQE value of 0.54% at 405nm in presence of Pt (3 wt.%) as cocatalyst and TEoA (10 vol%) as a sacrificial electron donor.[237] Theoretical studies showed that semi-hydrogenated graphitic BN sheet[238] may also be a water-splitting photocatalyst. However, its

synthesis and practical demonstration in water-splitting applications has yet to be proven.

BN is not much studied as a water-splitting photocatalyst. Lack of facile synthesis methods to prepare hybrid or ternary structures of the B–C–N system, and yet found effective tuning of their bandgaps for suitable photocatalysis are the remaining challenges for widespread applications. A meaningful combination of C, B and N atoms could offer different (B–C–N) layered configurations of binary and ternary compounds with different stoichiometry, such as BCN, BC_2N, BC_4N, BC_3 etc. Recent progress in synthesis of different $B_xC_yN_z$ nanostructures such as nanotubes and microspheres could be taken as guidance to develop photocatalyst grade BCN structures.[239] Nanotubes were synthesized by Pyrolysis of the BH_3–trimethylamine adduct[240] or by chemical vapour deposition,[241] while microspheres were produced by the reaction of low-surface area carbon spheres with urea and boric acid.[242] However, these nanostructures were not demonstrated for any photocatalytic applications. Future research needs to be directed to explore this avenue.

9.3 Metal-free ternary heterojunction photocatalysts

Efficient charge transport is key for enhanced hydrogen production. In a heterojunction, due to offset of the conduction and valence bands, the band-offset facilitates delocalization of charge carriers and retards back-recombination of electron-hole pairs. [243-245] A semiconductor heterojunction is therefore highly sought after in heterogeneous photocatalysis. [246, 247] With the plethora of inorganic semiconductors, metal-free binary heterostructure are emerging. However, metal-free ternary heterostructure (combining three materials) are rare, because of the limited number of metal-free semiconductors, hybridization constraints and intricate synthesis procedures.

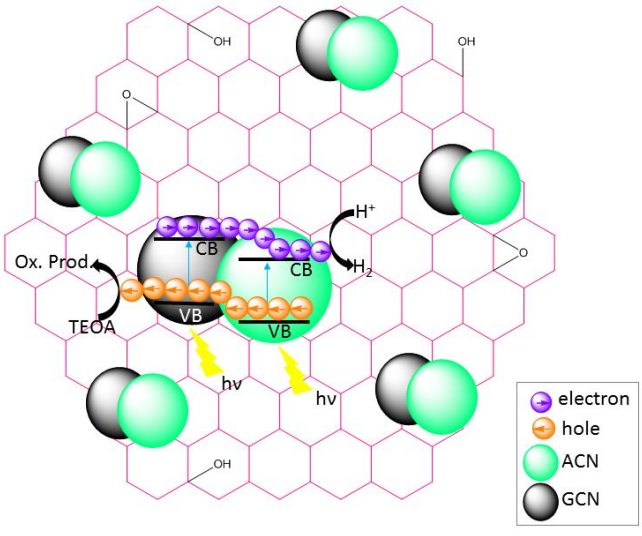

Fig. 16 Schematic illustration of charge transfer process for photocatalytic hydrogen in GCN/ACN/rGO. The band offsets between GCN and ACN helps in delocalizing the electrons in conduction band of ACN while holes in valence band of GCN. rGO enhances the transfer of surface electrons to water for proton reduction. Reproduced with permission.[248] Royal Society of Chemistry (2017).

Rahman et al reported, for the first time, a ternary metal-free heterojunction photocatalyst for hydrogen production by combining GCN, ACN and rGO (reduced graphene oxide) with an AQE of 6.3% at 420 nm, see Fig. 16. [248] This ternary heterojunction was built by in-plane stitching of 2D domains of GCN, ACN and rGO with similar aromatic structures that induced an intrinsic driving force for delocalization of photocarriers in photoexcited states. [249] The difference in work functions induced a strong electric field for efficient charge separation. [250]

10. Organic photocatalysts

Because of the flexibility in molecular engineering and precise tuning of optoelectronic properties, organic π-conjugated polymers have emerged as a promising alternative to the widely accepted inorganic semiconductor photocatalysts.[251, 252] Noticeably, while inorganic photocatalysts have limited photon absorption beyond 550 nm, a new era of 600 nm-class photocatalyst begins with organic materials for solar fuel production. In 1985, for the first time, linear poly(*p*-phenylene)s were reported as an organic photocatalyst for H_2 evolution with an apparent quantum efficiency (AQE) of 0.006 % under UV-light irradiation (λ>366 nm).[253] However, the interest in polymeric photocatalysts for photocatalytic H_2 evolution waned over the time due to instabilities and extremely poor AQE values. Recently, a renewed interest in this area has been noticed. Conjugated microporous polymers (CMPs), conjugated organic frameworks (COF), conjugated triazine frameworks (TzF), conjugated phosphinine frameworks (CPF), and silicate conjugate frameworks (SiCOF) are the most notable polymeric photocatalysts.[11, 181, 182, 186, 189, 254-271] In the following subsections, we will discuss the progress with regard to hydrogen production from polymeric photocatalysts.

10.1 COF

Covalent organic frameworks (COF) are structures that are made by stitching organic molecules together through strong covalent bonds using the principles of reticular synthesis.[272] Notably, COFs are the first example demonstrating covalent bonds beyond molecules to organic solids that are entirely composed of light elements, and therefore begins the era of 'the chemistry of the framework'.[273] COFs are geometric constructs from molecules, while molecules are geometric constructs from atoms. Making covalent bonds between the molecules to form COFs, linkers (building units) and linkages (bond formed between those units upon reticulation) are essential.

Synthesis of COFs start with linkers and ends with reticulation of the linkers by stitching them with appropriate linkages to form an extended framework.[274] Fig. 17 illustrates the approaches of the reticular synthesis of COFs of various dimension and structure. Over the years, organic chemists have mastered the art of controlling covalent bond formation from 0D to 3D by utilizing the principles of dynamic covalent chemistry (DCC). [275-279] Fig. 18 represents the chronological progress in the synthesis of COFs with various dimensions.

Because direct crystallization of COFs has yet to be proven feasible, reversible condensation reaction mechanisms such as the Schiff base reaction, spiro-borane condensation, Knoevenagel condensation and imide condensation, etc., are being routinely used to construct crystalline COFs.[278-281] The reversibility in bond formation endures the possibilities of self-healing and error correction (i.e., if any bond formation happens in an undesired direction, the system will repair it through back reaction and bond reformation) during the crystallization.[278] In DCC, a specific chemical agents are used to maintain the reversibility to render ordered COF structures with high crystallinity. COFs are mainly targeted for gas storage, however, recently it has also been considered for heterogeneous catalysis applications.

The interest in COF-based photocatalysts is increasing because of favourable physicochemical properties pertinent to photocatalytic water-splitting reactions. Light harvesting, charge transport phenomena and catalytic reactions sites can be precisely tuned by selecting appropriate molecular building blocks and their reticulation within COFs. Some of the most notable characteristics of COFs includes high structural porosity, high surface areas, crystallinity, low density, and stability regardless of the pH of oxidative and reductive environments.

These attributes facilitate the rapid diffusion of charges to the surface for increased interaction with secondary catalytic enhancers (i.e., sensitizers, electrolytes, sacrificial agents, cocatalysts etc.), enhance the lifetimes of the excited states and charge carrier mobility, suppress recombination of charge carriers, and offer high gravimetric performance.[275] Therefore the modular, porous, and crystalline COFs are gradually becoming one of the most prominent metal-free photocatalysts for hydrogen evolution. Since the first demonstration of a hydrazone-based COF (TFPT–COF) as a hydrogen evolution photocatalyst in 2014,[282] continuous growth in this field of research is slowly but steadily emerging (see Table 1 and Fig. 19).[283-287]

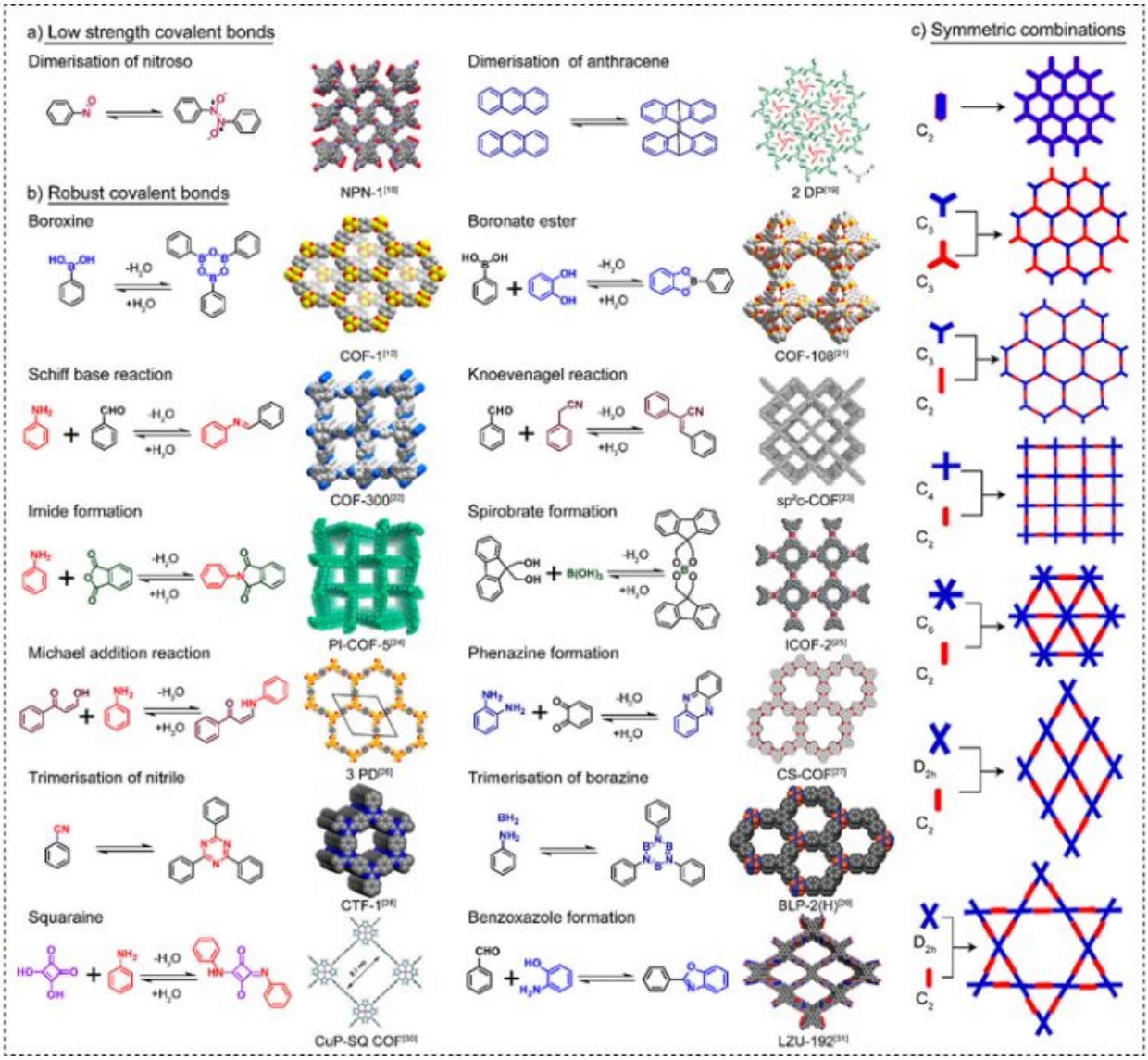

Fig. 17 Approaches for reticular synthesis of COFs. (a, b) reversible organic reactions used for COF construction, and (c) symmetric combinations used for 2D COF construction. Adopted with permission from[278]. American Chemical Society (2019).

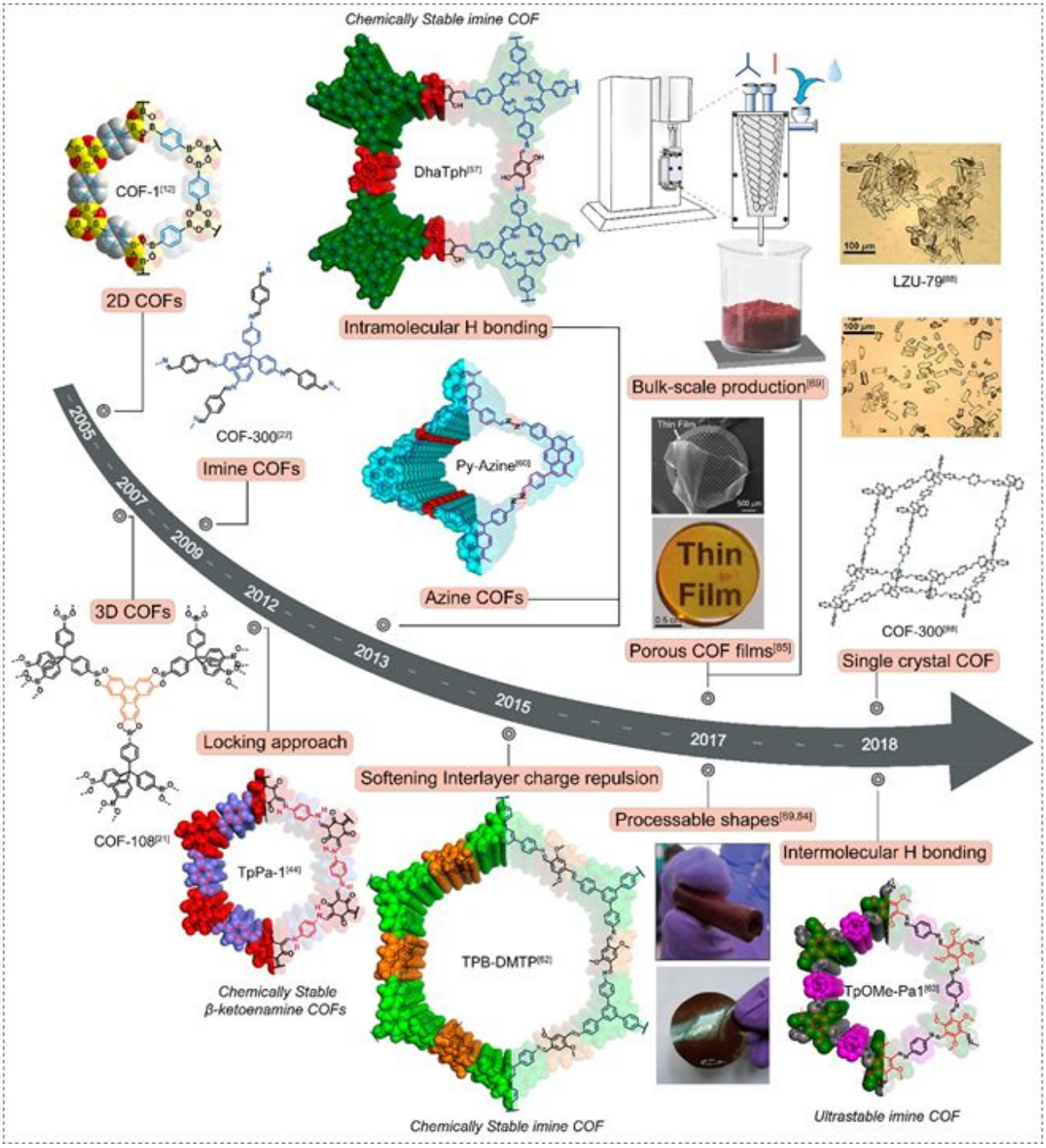

Fig. 18 Chronological advancement in COF synthesis. Adopted with permission from[278]. American Chemical Society (2019).

In 2015, aryl triphenyl azine COFs (N*x*-COFs) were synthesized and demonstrated for H_2 evolution.[283] A stepwise increase in the nitrogen content of the central aromatic ring was shown to lead to a progressive increase in photocatalytic hydrogen evolution. Later on, research was extended to study the structure–property–activity relationships in such materials.[286] The enhanced hydrogen evolution activity in N*x*-COFs with increased nitrogen content in the central aryl ring were traced back to intrinsic electronic factors that can possibly influence the hydrogen evolution rate, such as the band gap, the absolute HOMO and LUMO levels with respect to the hydrogen evolution potential, and charge carrier delocalization in the excited state. Apart from electronic factors, the radical anion stabilization energy, crystallinity, and surface area were

also found correlated with the HE activity, which are higher in the N2/N3-COFs and lower in the N0/N1-COFs. However, in depth understanding of the interplay and relative weight of the structure–property–activity relations remains elusive. While the peripheral rather than the central aryl ring in N*x*-COFs were substituted with nitrogen atoms, the resulting PTP-COF also showed photocatalytic hydrogen evolution in the presence of triethanolamine as the sacrificial electron donor and a Pt co-catalyst. [286] The HE rate of PTP-COF was reported to be 83.83 μmol h^{-1} g^{-1} which is comparable to that of N1-COF (90 μmol h^{-1} g^{-1}), while an order of magnitude lower than that of N3-COF (1703 μmol h^{-1} g^{-1}). [283, 286]

In another study, synthesis and photocatalytic applications of novel β-ketoenamine COFs, such as TP-DTP, TP-EDDA and TP-BDDA having acetylene (−C≡C−) and diacetylene moieties (−C≡C−C≡C−) was reported.[259] TP-BDDA showed a continuous hydrogen evolution at a rate of 324 ± 10 μmol h^{-1} g^{-1}, whereas the hydrogen evolution rate for TP-DTP and TP-EDDA was 20 ± 5 μmol h^{-1} g^{-1} and 30 ± 5 μmol h^{-1} g^{-1}, respectively. Higher hydrogen evolution rates for the case of TP-BDDA implies that the conjugated diacetylene moiety has an important role for enhanced activity. It was found that diacetylene moiety was responsible for the reduced bandgap, high charge career mobility, and facile migration of photogenerated excitons to the surface of the photocatalyst which was confirmed by photocurrent response measurements and electrochemical impedance spectroscopy analyses. A maximum AQE of 1.8% was obtained in TP-BDDA under the irradiation of 520 nm light. Wang et al. reported a crystalline COF based on a benzo-bis(benzothiophene sulfone) moiety (FS-COF) that showed an excellent hydrogen evolution rate up to 16.3 mmol g^{-1} h^{-1} under long-term visible irradiation in the presence of a sacrificial electron donor and 8 wt.% Pt cocatalyst for at least 50 hours. [268] The obtained AQE was 3.2% at 420 nm. The high quantum efficiency of FS-COF was attributed to its crystallinity, strong visible light absorption, and hydrophilic 3.2 nm mesopores.

Table 1: List of COF based photocatalysts for hydrogen evolution

COF	Eg (eV)	Sacrificial agent	Co-catalyst	AQE	Ref.
TFT-COF	2.8	TEoA	Pt	3.9% at 420 nm	282
N_3-COF	2.7	TEoA	Pt	0.44% at 450 nm	283
PTP-COF	2.1	TEoA	Pt	0.87% at AM1.5	286
N_2-COF	-	TEoA	Co-1	0.16% at 400 nm	285
β-ketoenamine COF	2.31-2.42	TEoA	Pt	1.8% at 520 nm	259
TpDTz-COF	2.07	TEoA	nickel-thiolate	0.2% at 450 nm	287
FS-COF	1.85	Ascorbic acid	Pt	3.2% at 420 nm	268
Sp^2-c-COF	1.9	TEoA	Pt	-	288

Recently, a fully π conjugated COF (sp^2 c-COF) has been synthesized for photocatalytic applications.[288] The sp^2 c-COF constitutes an all sp^2 carbon-based tetragonal skeleton in which the conjugated 2D sheets stack to form an ordered layered structure that enables exciton migration over the framework which splits into charges at the donor–acceptor interface as demonstrated by photocurrent measurements. The π columns therefore offer a pathway for charge delocalization to prevent backward electron transfer. The sp^2 c-COF has a bandgap of 1.9 eV with HOMO and LUMO levels suitable for water reduction, and is exceptionally stable in organic solvents, concentrated HCl solution, and aqueous NaOH solution (14 M). Moreover, the sp^2 c-COF has a pore size of 2 nm that facilitate the trapping of Pt nanoparticles for a favourable interface between pore wall and reaction center. The sp^2 c-COF is attributed with the mechanisms for light harvesting, exciton migration and splitting, electron transfer, and charge transport. Endowed with these beneficial properties, the sp^2 c-COF exhibited a hydrogen evolution rate of 2120 μmol h^{-1} g^{-1}at λ ⩾ 420 nm. Most notably, it is the only COF reported to date which showed some activity for oxygen evolution.

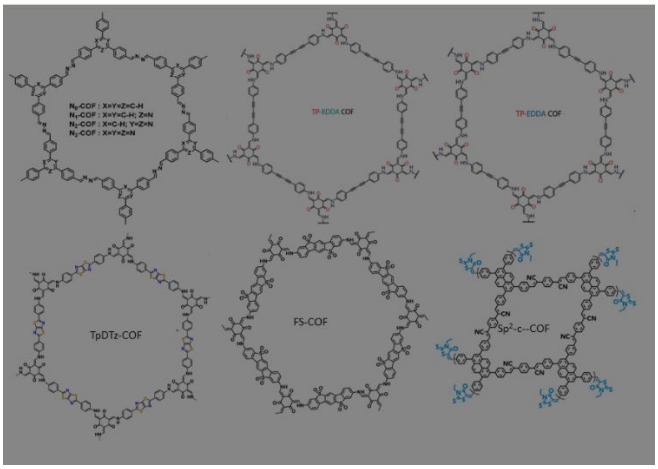

Fig. 19 Selected COFs based photocatalysts for hydrogen production. This figure has been adapted from ref 259, 283, 287 and 288 with permission from American Chemical Society, copyright 2018, and Elsevier, copyright 2019.

Research has also been directed toward developing earth-abundant, non-precious-metal-based co-catalysts in place of platinum to be incorporated with COFs to reduce the overpotential of H_2 generation. However, coupling molecular co-catalysts into the COF while ensuring efficient light harvesting and charge-percolation processes is a great challenge. For the first time, cobaloxime co-catalysts (Co-1) have been incorporated with an azine-linked COF (N2-COF) for hydrogen evolution with an AQE of 0.027% under AM 1.5 illumination and, an AQE of 0.16% under 400 nm irradiation. [285] The concern was the limited photostability whilst the catalyst often converts to an inactive form within a few hours (<6 h) of H_2 evolution, possibly due to ligand decomposition or hydrogenation. Recently, a new type of cocatalyst based on a nickel-thiolate hexameric cluster was incorporated with thiazolo[5,4-*d*]thiazole-linked COF (TpDTz - COF) as the

photoabsorber *in situ* in water that enables long-term (70 h) H_2 production in TpDTz - COF at a maximum rate of 941 µmol h^{-1} g^{-1} with a maximum AQE of 0.2% at 400 nm. [287] These AQE values are not impressive; however, they show the possibilities from thinking of cocatalysts beyond the commonly used Pt.

In those above reports on COF based photocatalysts, researchers have shown a tendency to compare their results with pristine g-C3N4 to claim that the reported COFs are better photocatalyst than g-C3N4. Actually, this is not the case (see ref. 7 for the latest developments in g-C_3N_4-based photocatalysts). [7] We urge prospective authors to compare their photocatalysts in terms of quantum yield or solar-to-hydrogen (STH) conversion efficiency rather than hydrogen production rate. Additionally, the hydrogen production rate should not be normalized by the mass of the spent photocatalysts because the rate does not vary with the mass.[12, 15] For the case of carbon nitride based photocatalysts, the AQE reaches as high as 60% under visible light irradiation,[206] while the COF-based photocatalysts are still struggling to overcome their inaugural AQE of 3.9%. Moreover, COFs have not yet proved active to produce H_2 without an added electrocatalyst at the COF backbone. Clearly, carbon nitride based photocatalysts outweigh COFs in every aspect of synthesis, performance and stability. Therefore, the carbon nitride is more promising as a scalable photocatalyst for large-scale implementation of photocatalytic hydrogen production in the long-run.

Despite many beneficial attributes, the quantum efficiency of hydrogen yield in COFs is < 4%. It infers that the plausibly beneficial physicochemical properties need to be well-orchestrated to maximize the H_2 evolution efficiency. Further improvements in the photocatalytic efficiency might be achieved by an appropriate selection of building blocks and linkers for a custom made COF with controlled delocalization of the π-electron system both in the axial and in-plane direction. With this careful design, electron-rich terminal groups may facilitate the charge separation and possibly increase the excited-state lifetimes to maximize the charge separation and transport. Another avenue worth exploring is engineering the interfacial chemistry of COFs/sacrificial agents. Because COFs have not yet been observed to produce H_2 without an added electrocatalyst, similarly, it also demands attention in optimization of the COF/electrocatalyst interface. Research needs to be carried out for the optimization of the kinetic overpotential associated with the charge-transfer and bond formation processes for H_2 evolution in COFs. One recommended approach to accomplish this involves finding the dedicated catalytic reaction sites at the COF backbone. Currently, Pt is commonly use to trap electrons from the COFs, and to provides effective proton reduction sites for H_2 formation. However, finding appropriate coordination sites for Pt on the COF backbone remains unexplored. Pt is the most celebrated cocatalyst because it is endowed with a large work function and a low Fermi level ideal for acting as an electron sink. However, platinum needs to be replaced with earth-abundant nonprecious cocatalysts. We also know little about how the pH and reaction environment affect the hydrogen evolution in COFs. Because the microstructure of the polymer, degree of its solvation, and polarity of solvent influence the charge transfer and thermodynamic driving forces for hydrogen evolution activity. [289] Moreover, dielectric permittivity of solvent environment controls the population of polarons for proton reduction.[290]

10.2 Covalent Triazine Frameworks (CTFs)

CTFs are new class of metal-free photocatalysts that are endowed with the excellent stability of triazine based carbon nitrides and the functionalities of extended π-conjugated COFs. However, unlike carbon nitrides, CTFs are inherently micro-mesoporous. Although a considerable amount of research has been invested in developing different routes from high temperature to room temperature for synthesis of CTFs,[165, 291-295] the progress on CTF based photocatalysts was rather insignificant till 2016 evident by only few reports for hydrogen evolution.[296-298] There are excellent reviews that cover the development of CTF-based photocatalysts up until 2016.[251, 252] We therefore limit our discussion to selected CTFs reported thereafter. [206, 257, 258, 299-302]

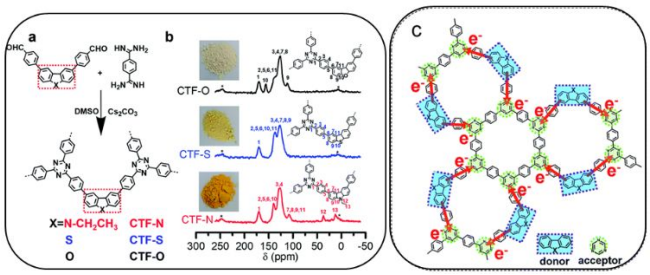

Fig. 20 a) Synthetic scheme of CTFs, b) CP-MAS solid-state ^{13}C-NMR and the digital photographs of corresponding CTFs, and c) the path of excited electron transfer in donor–acceptor CTFs. Adopted with permission from.[300] Royal Society of Chemistry (2018).

Lotsch and co-workers made the early breakthroughs in CTF based photocatalysts,[296] and reported an AQE of as high as ~9.9% under UV-Vis light (>250 nm) irradiation.[298] However, the AQE was < 3.5 % under visible light irradiation. To maximize the hydrogen quantum yield, CTF has been incorporated with donor–acceptor pairs and doping with heteroatoms.[257, 303] A series of heteroatom (N, S, O) doped CTFs (namely, CTF-N, CTF-S and CTF-O) was synthesized using fluorene analogue building blocks, Fig. 20 a,b.[300] The band gaps of CTF-N, CTF-S and CTF-O were calculated to be 2.17 eV, 2.47 eV and 2.67 eV, respectively. In these CTFs, the triazine rings can function as electron acceptors while the fluorene-like building blocks can act as electron donors. The benzene ring provides the bridge to transfer electrons from the donor to acceptor in a push–pull interaction. Under visible light irradiation, the excited electrons migrate from fluorene-like units (donor, blue part) to triazine rings (acceptor, green part), See Fig. 20 c. Because of the narrow bandgap (extended spectral overlapping for light absorption) and better charge transfer, CTF-N exhibited an AQE value of 4.11% at 420 nm. While synthesis of CTFs is a time consuming (> 20h) process, Thomas et al. developed a technique to not only synthesize CTFs with a shorter reaction time (~10 min), but also showed that these are highly active in hydrogen evolution as evident by an AQE of 9.2% at 450 nm.[258] Cooper et al.

reported the synthesis of an amorphous CTF (named as CTF-HUST) via polycondensation under mild conditions (≤120 °C, no strong acids) as opposed to the commonly used ionothermal route at high temperature and under harsh acidic conditions. CTF-HUSTs showed hydrogen evolution at a maximum rate of 2647 μmol h^{-1} g^{-1} under visible light.[299]

In addition to amorphous CTF-HUSTs, Tan el at. reported highly crystalline CTF-HUSTs by in-situ oxidation of alcohols to aldehyde monomers.[304] Crystalline CTF-HUSTs evolved hydrogen as a rate of up to 5100 μmol $h^{-1}g^{-1}$ at 420 nm. Crystalline CTFs are comparably highly efficient than amorphous CTFs because of better electronic transport and light absorption. Research has been directed to investigate the impact of morphological features rather than structural changes. It was found that a hollow-spherical morphology of CTF could render a hydrogen evolution rate of 6040 μmol h^{-1} g^{-1} with an AQE of 4.2% at 420 nm, (see Fig. 21).[305] These hollow-structures facilitate the mass transfer of guest molecules and guide the migration of photogenerated charges to enhance the collection and separation of charges on the interface.

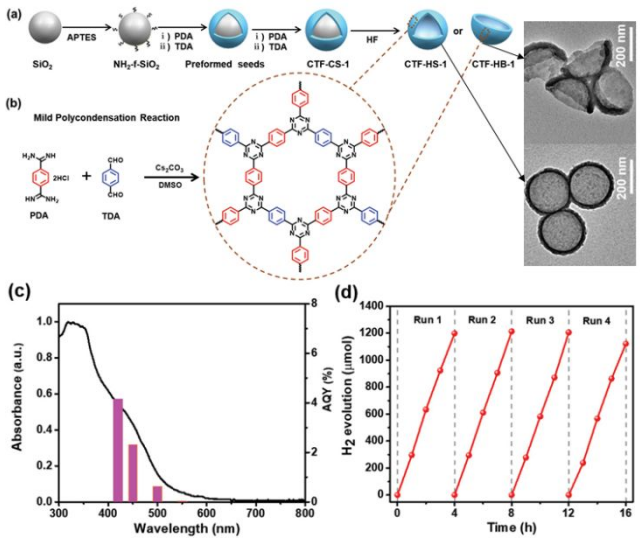

Fig. 21 a) The synthetic routes of of hollow CTF (CTF-HS) and bowl-like CTF (CTF-HB). b) Reaction path. c) Wavelength-dependent AQY for photocatalytic hydrogen evolution. d) Recycling hydrogen evolution tests with 3 wt% Pt deposited at 420 nm. Adopted with permission from. [305] Wiley-VCH (2019).

In a plethora of CTF based hydrogen evolution photocatalysts, to date, only one CTF has demonstrated oxygen evolution; it was synthesized in a very mild microwave-assisted polymerization approach.[306] This CTF demonstrated oxygen evolution with an AQE of nearly 4%, and hydrogen evolution with an AQE of 6% at 420 nm in the presence of sacrificial agents. This polymer holds potential for overall water splitting or to be integrated into a Z-scheme water splitting system. The performance is attributed to its well-defined and ordered structure, low carbonization, and superior band positions.

10.3 Conjugated Microporous Polymer (CMP)

IUPAC classified three types of porous materials according to pore size, namely, macroporous materials having pore sizes greater than 50 nm, mesoporous materials having pore sizes between 2 and 50 nm, and microporous materials having pore sizes less than 2 nm.[307] The skeletons of microporous polymers are built up from organic matter connected by covalent bonds.[308] Unlike crystalline COFs, CMPs bring their own set of issues because of the diverse synthetic concepts that range from metal catalyzed couplings to metal-free condensation reactions.[309, 310] The microporosity (pores of diameters below 2 nm) and high surface areas (> 6000 m^2 g^{-1})[311] are the trademark properties of CMPs.[312] The microporosity and high surface areas result from the polymerization of tectones (monomer building blocks) into the contorted molecular structures, and subsequent crosslinking of these contorted molecules. The contorted structures prohibit the space-efficient packing of polymers- therefore, creating a large free volume seen as microporosity, and the crosslinking of structures impede packing of the polymer backbone- resulting in high surface areas. [309, 312]

The first CMPs were reported in 2007;[313] however, CMP was not reported as a hydrogen evolution photocatalyst until 2015. [263, 314] In sharp contrast to crystalline COFs, CMPs are amorphous and show no long-range molecular order. However, this lack of order does not come as an obstacle to tune the micropore size distribution and surface area by varying the length of the rigid organic linkers as demonstrated for ordered crystalline materials.

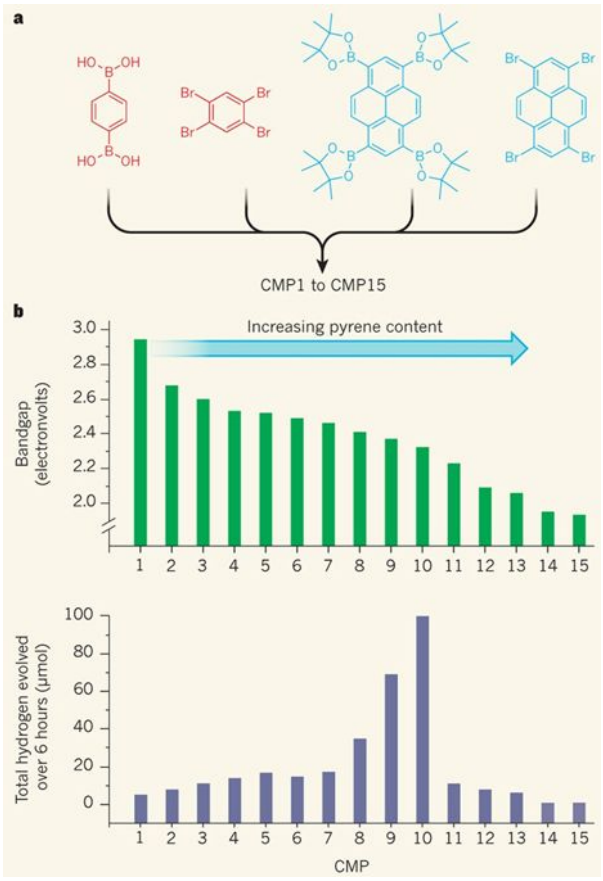

Fig. 22 a) synthesis of 15 conjugated microporous polymers (CMP1 to CMP15) from a mixture of phenylene-containing (red) and pyrene-containing (blue) building blocks. b) The optical bandgap and related rate of hydrogen

evolution. Copyright 2015, Adopted with permission from.[315] Nature publishing Group (2018).

It suggests that order is not a prerequisite for fine control over the microporous properties of organic networks. Most importantly, because CMPs are composed solely of carbon–carbon and carbon–hydrogen bonds, they are thermally more robust and chemically more stable than many COFs and MOFs.[313, 316]Additionally, CMPs, a subclass of hypercrosslinked polymers, may combine the well-known properties of conjugated linear polymers as well as incorporate a wide range of chemical functional groups to tune the physicochemical properties for desired applications. Moreover, linking of carbon atoms in a conjugated manner lends CMPs to the use of metal catalysis under relatively mild conditions. [312] In particular, their synthesis lends itself to fine control over photophysical properties, such as the optical gap that is beneficial for photocatalytic water-splitting. Sprick *et al*. demonstrated CMPs, for the first time, as photocatalysts,[263] and opened a new window of opportunities for systematic engineering and manipulation of the properties that are deemed essential to improve the photocatalytic efficiency of CMPs.

Sprick *et al*. used palladium-catalysed reactions route to prepare a series of 15 different CMPs from phenylene and pyrene building blocks (Fig. 22 a). These polymers exhibited a red-shift in optical absorption as evident by decreasing bandgap from 2.95 eV to 1.94 eV with increasing the pyrene content. In addition to enabling low-energy optical excitations, the structural effects such as the formation of cyclic substructures (rings) and the strain within CMPs becomes more dominant as the pyrene component increases. The bandgaps are suitable for hydrogen evolution via water-splitting reactions under visible light irradiation. Indeed, all of the polymers promoted stable hydrogen evolution, and hydrogen evolution reaches a peak for CMPs with a bandgap of 2.33 eV (Fig. 22 b). The lower photocatalytic activities of CMPs with smaller bandgaps were postulated to have enhanced recombination of separated charge carriers and increased kinetic barriers to electron transfer.

Sprick's CMPs inspired other research groups to synthesize a series of microporous conjugated polymers through palladium-mediated polycondensation of chromophore monomers with biphenyl and bipyridyl comonomers. Chromophores enhance the light harvesting while comonomers provide better wettability, local ordering structure, and an improved charge separation process.[317] The optical gap was shown to be tuned between 1.81 eV to 2.89 eV by varying the mole fraction of comonomers. The highest hydrogen production rate was ~33 µmol/h at full-arc irradiation, while it was only ~6.7 µmol/h with visible light (400 nm). The highest AQE was 0.34% at 350 nm. These results are an indication of the first demonstration of developing CMPs through copolymerization of a strong electron donor and weak electron acceptor in the same polymer chain. The rate of hydrogen production was further enhanced to 164 µmol/h with an AQE of 1.8% at 350 nm by loading 2 wt % of Pt cocatalyst in addition to the residual palladium that was present in the CMP network.

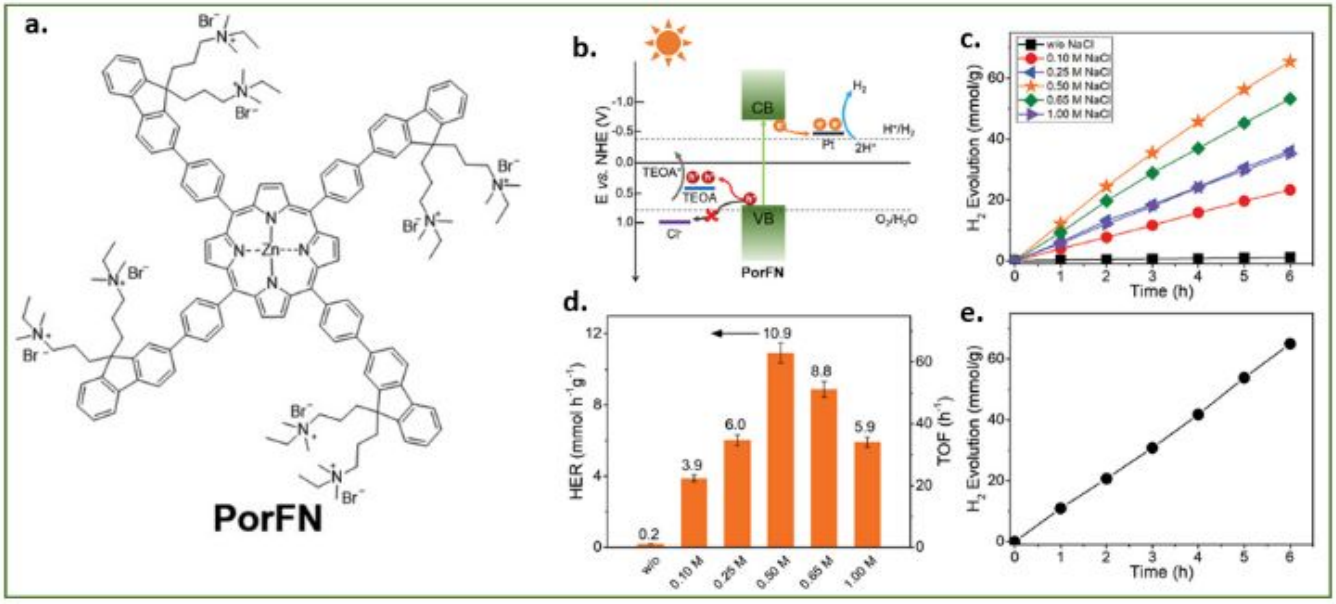

Fig. 23 a) chemical structure of PorFN. b) Energy level alignment of PorFN, chlorine ions, and TEOA at pH = 7. c) Photocatalytic experiment results in presence of TEOA and Pt under simulated solar light (AM 1.5G, 100 mW cm^{-2}). d) Hydrogen evolution rate (HER) and corresponding turnover frequency (TOF). d) Photocatalytic experiment in simulated seawater. Adopted with permission from[318]. Wiley-VCH (2019).

Other studies showed that copolymerizing the electron-withdrawing benzothiadiazole units at different positions on phenyl rings, various CMPs with defined energy-band structures and charge-transfer and charge-separation abilities could be obtained, and the effect of the molecular structure on their catalytic activity was investigated. These CMPs exhibited photocatalytic H_2 evolution efficiencies up to 116 µmol h^{-1} with an AQE of 4.01 % at 420 nm in the presence of TEoA as the sacrificial agent.[319] Zhu et al. reported a series of CMPs from benzothiadiazole which had

electron-donating CH_3O– and electron-withdrawing F-substitutions which enable proton-coupled electron-transfer mechanisms. These CMPs showed H_2 production with an AQE of 5.7% at 420 nm.[320] Jiang and co-workers reported perylene-containing conjugated microporous polymers (PrCMPs) with a hydrogen evolution rate of 12.1 μmol h^{-1} under UV–vis light irradiation.[321]

One common feature of the above discussed CMPs is their insolubility in water. Recently, water soluble dibenzo[*b*,*d*]thiophene sulfone polymers (S-CMPs) showed the highest hydrogen evolution rates of 6076 μmol h^{-1} g^{-1} (λ > 295 nm) and 3106 μmol h^{-1} g^{-1} (λ > 420 nm) with an AQE of 13.2% at 420 nm. It indicates that enhanced wettability of the material particles and its pores play a significant role in improving hydrogen evolution. [267] An added candidate in this category is a newly developed CMP called PorFN, which was synthesized from a zinc–porphyrin core (Fig. 23 a).[318] Noted that porphyrins are the most famous derivatives of natural chlorophyll molecules with large π-conjugated macrocycles, and have a high absorbance coefficient and high degree of electron delocalization. Structurally, PorFN consists of four fluorene units connected at the *meso*-position via phenyl bridge groups. The π-conjugated PorFN is endowed with enhanced light absorption, electron-donating ability, and efficient charge generation and transport. Notably, PorFN showed a red emission peak at 625 nm, but completely quenched blue emission, implying it could efficiently transfer excitation energy from the fluorene arms to the porphyrin core. As per cyclic voltammetry (CV) measurements, the unoccupied molecular orbital (LUMO) energy level of PorFN is -0.74 V vs the normal hydrogen electrode (NHE), which is suitable for HER (Fig. 23 b). PorFN exhibited a hydrogen evolution rate of 10.8 mmol h^{-1} g^{-1} (≈TOF = 63 h^{-1}) in simulated seawater (0.5 m NaCl, very close to the concentration of natural seawater) which was more than 50 times greater than that in pure water under 1 sun of sunlight irradiation (AM 1.5G, 100 mW cm^{-2}). The light-driven hydrogen evolution activity of PorFN is shown in Fig. 23 c-e. Interestingly, a donor (1,3,6,8-Tetrabromopyrene)-acceptor (3,8-Dibromophenanthroline) copolymerized CMP has been demonstrated for hydrogen evolution from deionized water, municipal water, commercial mineral water, and simulated seawater (NaCl 3 wt %).[322] In the best case, it showed a hydrogen evolution rate of 42 μmol h^{-1} (equal to 4200 μmol g^{-1} h^{-1}) with an AQE of 1.5 % under visible light irradiation (λ ≥ 400 nm).

High-efficiency CMP photocatalysts can also be made from dibenzothiophene-*S*, *S*-dioxide-based building blocks due to their planar molecular structure and strong electron-withdrawing ability.[264, 323, 324] These photocatalyst features include a broad visible light adsorption ability, proper band gap, and efficient photogenerated electron and hole transport and separation capabilities. For example, Cooper et al. reported a family of photocatalysts produced from phenyl and dibenzothiophene-*S*, *S*-dioxide that showed a hydrogen evolution rate of 3.68 mmol h^{-1} g^{-1} with an AQE of 2.3 % at 420 nm. [22] Liu et al. demonstrated CMPs from fluorene and dibenzothiophene-*S*, *S*-dioxide that showed a hydrogen evolution rate of 5.04 mmol h^{-1} g^{-1} with an AQE of 2.13 % at 420 nm.[323] Jiang et al reported CMPs made from dibenzothiophene-*S*, *S*-dioxide and a phenyl cross-linker with an impressive a hydrogen evolution rate of 9200 μmol h^{-1} g^{-1} with an AQE of 3.3% at 400 nm.[324] Jiang et al showed that a short-length phenyl cross-linker is the key for an improved hydrogen evolution rate. Peng et al reported porphyrin-based CMPs that exhibited a photocatalytic H_2 generation rate of 43 μmol h^{-1} with an AQE of 7.36% at λ = 400 nm (monochromatic light).[325]

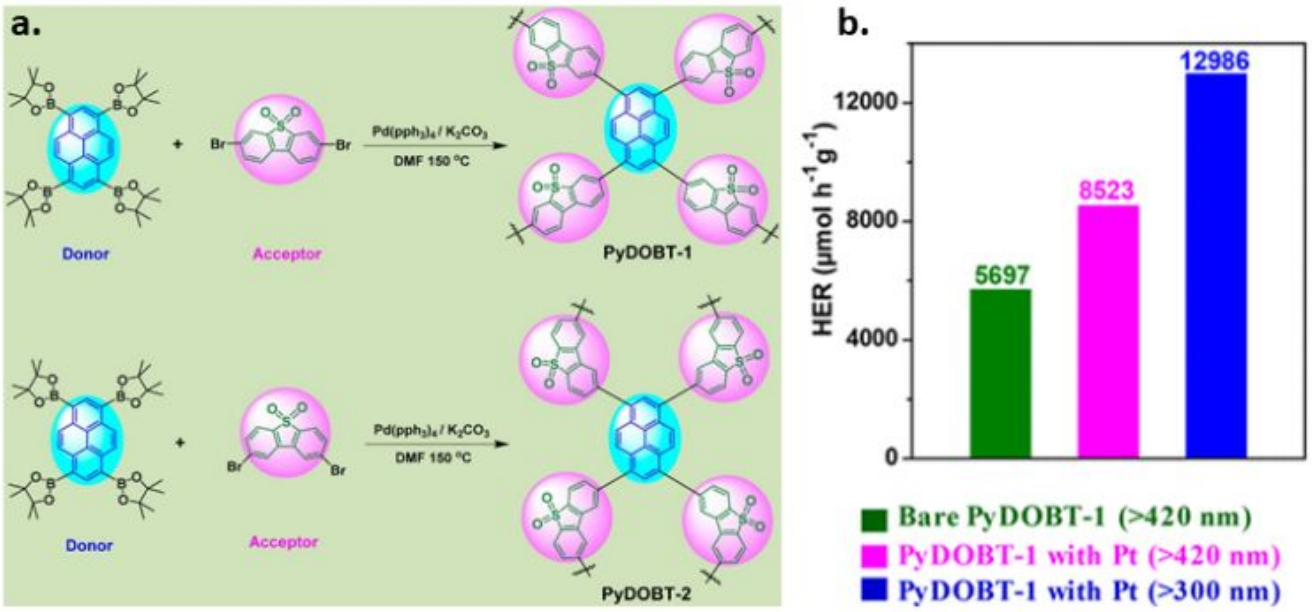

Fig. 24 a) synthesis routes for PyDOBT-1 and PyDOBT-2, and b) photocatalytic activities. Adopted with permission from[326]. American Chemical Society (2018).

More recently, it has been demonstrated that CMPs built with a donor–acceptor module by using pyrene as donor and dibenzothiophene-*S*,*S*-dioxide as an acceptor could exhibit an attractive rate of hydrogen evolution of 12986 μmol h^{-1} g^{-1} under the full-arc spectrum (>300 nm).[326] Changing the substitution position of the dibenzothiophene-*S*,*S*-dioxide building block with pyrene linkers, two CMPs were synthesized, namely, thePyDOBT-1 photocatalyst with a 3,7-linking pattern that showed visible light activity with a HER rate of 8523 μmol h^{-1} g^{-1} compared to the 2,8-linked PyDOBT-2 (2650 μmol h^{-1} g^{-1}), Fig. 24. It was claimed that high hydrogen production with the 3, 7-linking pattern was because it could extend the conjugation degree and enhance the coplanarity of the polymer backbone, promoting photogenerated electron and hole migration along the polymer chain. Clearly, the linking pattern of the polymer skeleton plays a significant role in determining the photocatalytic performance of CMP photocatalysts. To date, the highest AQE for CMPs was reported to be 13.2% at 420 nm by Cooper et al.[267]

It should be noticed that Pd-catalyzed cross-coupling reactions are the most celebrated technique for synthesizing carbon–carbon-linked porous polymers. However, it was argued that metal-catalyzed cross-coupling reactions are usually an expensive and unsustainable technique, and the resulted polymers are low in stability. Beyond the commonly used Pd-catalyzed cross-coupling reactions, therefore, development of a metal-free-catalyzed carbon–carbon crosscoupling method is deemed necessary. Zhang et al.,[327] recently, reported new types of olefin-bridged CMPs through the condensation of tricyanomesitylene with different linear or branched polyphenylenes using a metal-free-catalyzed carbon–carbon coupling method. An organic base-catalyzed Knoevenagel reaction was adopted to avoid possible transition-metal contamination. The synthesis scheme, optoelectronic properties and photocatalytic activities are shown in Fig. 25 a-d, respectively. All of these CMPs showed hydrogen evolution activity under visible-light irradiation (λ > 420 nm) with the following order: OB-POP-1 < OB-POP-2 < OB-POP-4 < OB-POP-3 with an AQE up to 2.0% at 420 nm.

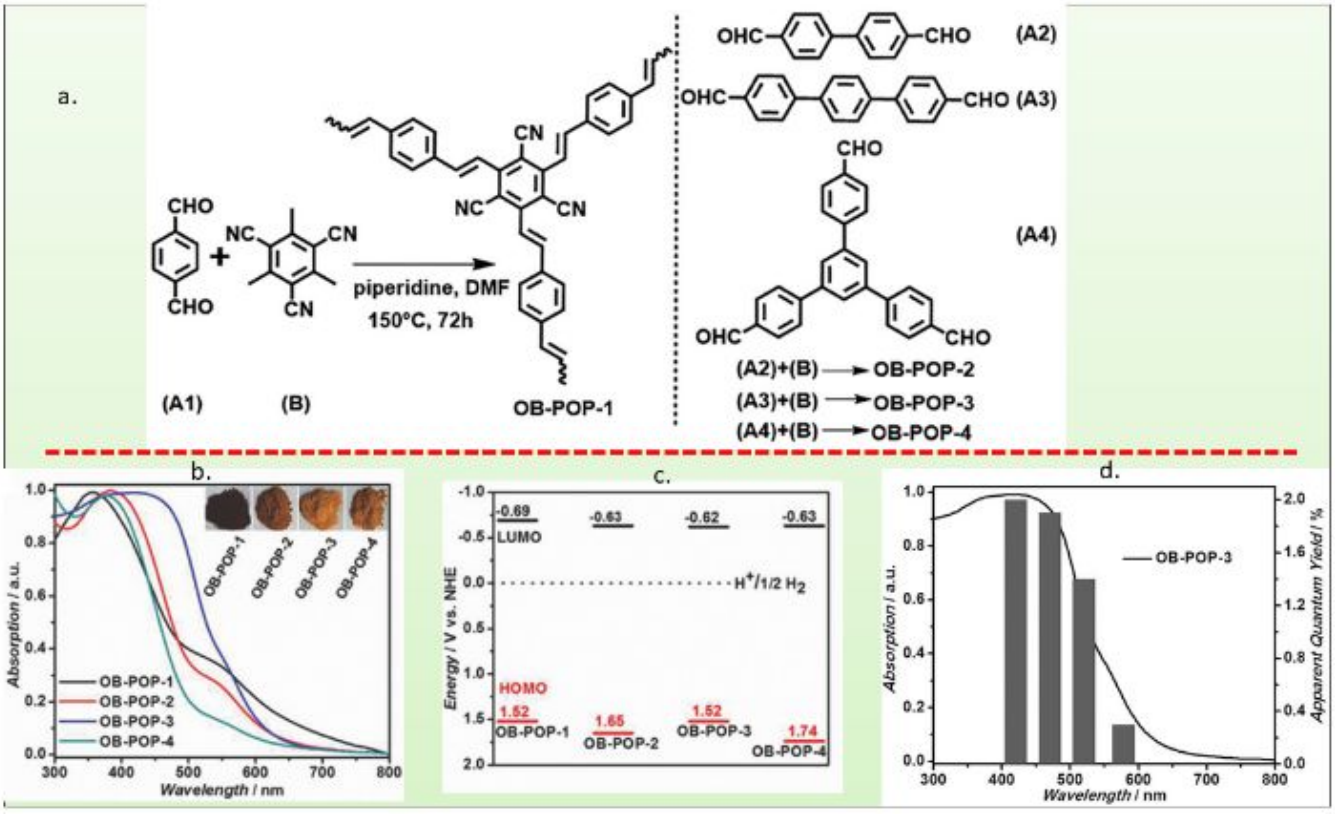

Fig. 25 a) Synthetic process of olefin-bridged porous organic polymers (OB-POPs), b) UV–vis diffuse reflectance spectra (DRS) and photographs (inset) of prepared OB-POP-1–4, c) OMO and LUMO band position of the polymers, and d) wavelength-specific AQE on H_2 evolution using Pt-modified OB-POP-3. Adopted with permission from. [327] Wiley-VCH (2017).

CMPs are highly promising photocatalysts. To Achieve further improvement in the photocatalytic efficiency requires more research regarding these materials. In particular, we do not yet understand the complex interplay between optical gap, charge mobility, excited state lifetime, and other properties such as particle size, porosity, and surface hydrophilicity. This is compounded by the fact that there are relatively few mechanistic studies for these materials, and it is often unclear whether these polymers act as light absorbers, as catalysts, or as both. Most CMPs are rather hydrophobic and even float on water. How protons reach and are reduced on the CMP surface is not yet understood. The surface polarity of CMPs also needs to be considered.

10.4 Covalent phosphinine framework (CPF)

Hypothetically, incorporating non-metal heteroatoms (i.e. S, N, Si, P, etc.) into countless number of organic building blocks offers the possibility to fabricate numerous type of covalent organic frameworks with tailored optoelectronic properties. For example, covalent triazine-based frameworks (CTFs) and silicate organic frameworks (SiCOFs) are notable examples that incorporate S, N and Si.[256, 262] Recently, P has been incorporated to develop a new kind of organic framework and termed a Covalent Phosphinine Framework (CPF).[261] A phosphinine (C_5P)[328] ring as the principle building block with the Pd-catalyzed Suzuki–Miyaura coupling reaction route has been used to design a π-conjugated CPF (See Fig. 26 a).[261] C_5P contains either λ^3-phosphinine (a trivalent phosphorus atom with a coordination number of 2) and λ^5-phosphinine (a pentavalent phosphorus atom with a coordination number of 4). λ^3-phosphinine showed electrophilic attack or nucleophilic attack preferentially at the P atom.[329] In contrast, λ^5-phosphinine is more stable because of the absence of phosphorus lone pairs. However, λ^5-phosphinine is susceptible to strong acids or bases that may attack the P atom during polymerization.[330] Selection of appropriate phosphinine-based monomers and polymerization routes are of the utmost importance for yielding P-containing π-conjugated frameworks.

Electronically, λ^5-Phosphinine is flexible enough to lose an electron and be oxidized to a radical cation at a lower oxidation potential than the λ^3-phosphinine.[331] CPF exhibited an absorption edge at around 620 nm, which is equivalent to a direct optical band gap of 2.19 eV and an indirect optical band gap of 1.64 eV (See Fig. 26 b, c). CPF was employed as a photocatalyst for hydrogen evolution under visible light (wavelength 380–780 nm) with triethanolamine as the sacrificial agent and 3 wt % Pt co-catalyst. It showed a hydrogen evolution rate of 29.3 μmol h^{-1} g^{-1} under UV and visible light (300–2500 nm). [261]

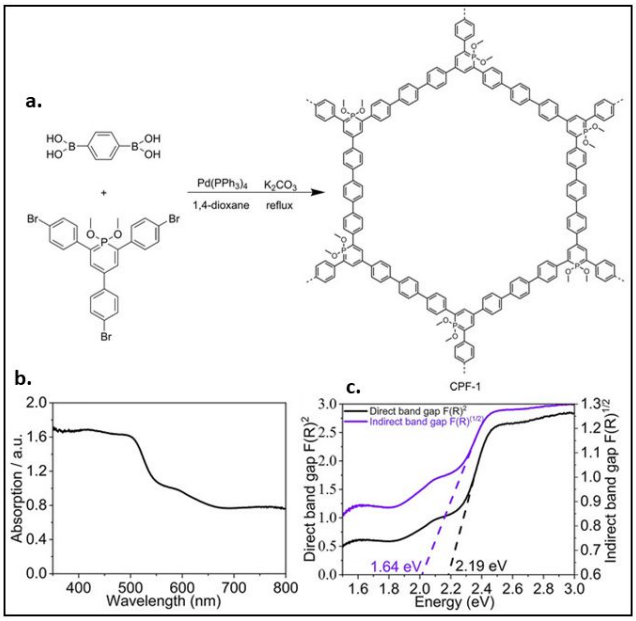

Fig. 26 a) Suzuki–Miyaura coupling polymerization route to CPF, b) Solid-state UV/Vis diffuse reflectance spectrum of CPF, and c) Kubelka-Munk plot for band gap determination. Adopted with permission from. [261] Wiley-VCH (2019).

10.5 Linear conjugated polymers (LCPs)

Linear conjugated organic polymers are relatively less studied for light-driven water splitting. In contrast to CMPs, we here consider linear polymers that show no microporosity.

Cooper et al. reported a series of LCP is based on phenylene oligomers (SM1–SM5) and poly(*p*-phenylene)s (P1K, P1S) and their planarized fluorene-type analogs ((FSM1–FSM3, P2–P7).[264] Unlike amorphous CP-CMPs, all of these LCPs were found semi-crystalline. These LCPs showed an increasing hydrogen evolution rate with the decreasing optical gap. The FSM-type analogs exhibited a red-shift in optical absorption, and therefore a higher rate of hydrogen evolution than that of phenylene oligomers (SM1–SM5) and poly(*p*-phenylene)s (P1K, P1S). The ionization potentials for the fluorene oligomers are always more negative than those of the equivalent phenylene. Moreover, extended conjugation of phenylene oligomers (SM1–SM5) and poly(*p*-phenylene)s (P1K, P1S) with flourene offers several advantages. For example, it lowers the phenylene-phenylene torsion angle and increases rigidity, shows a higher degree of conjugation, decreases the Coulomb binding energy for dissociating electron-hole pairs and hence increases exciton dissociation yields, and increases charge carrier mobility.[332, 333] The low photocatalytic activity of these LCPs were attempted to be overcome by deploying co-polymerisation strategies. Because, copolymerization leads to an optimum trade-off between various properties under a specific set of catalytic conditions.[334]

Copolymerization was effective previously for CTFs and CMPs etc. Most notably, isostructural CTFs with 1,4-phenylene-linkers of different lengths resulted in higher hydrogen evolution activity than pristine CTFs.[301] The hydrogen evolution activity of CMPs based on 1,2,4,5-connected benzene and 1,3,6,8-pyrene cores was enhance by linking *with* 1,4-connected phenylene linkers upon changing the phenylene fraction.[263] Based on these previous successes, the effect of co-polymerisation on the hydrogen evolution activity for structurally well-defined linear ordered co-polymers of 2,5-phenylene and 2,5-thiophene building blocks (Fig. 27) was studied recently.[335] Although phenylene homo-polymers as photocatalysts have been used since the mid-1980s,[253] polythiophene was a recent addition to the photocatalyst family.[336] Interestingly, all of the co-polymers were more active than the two homopolymers, and a maximum hydrogen evolution was observed for a co-polymer with 33 mol% thiophene content. DFT calculations revealed that the potentials of the free charge carriers and excitons in the different co-polymers increased while the driving force for the reduction of protons to hydrogen and the oxidation of sacrificial electron donors (or water) decreased significantly with increased thiophene content. [301]

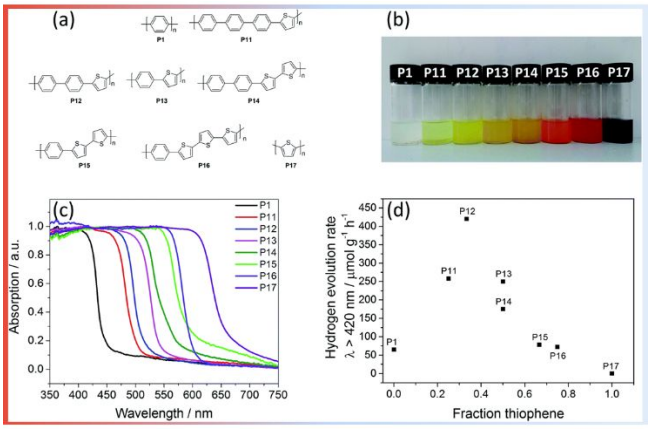

Fig. 27 (a) Structures of the polymer photocatalysts; (b) photographs of **P1**, **P11–P17** in THF suspension; (c) UV-vis reflectance spectra of **P1**, and **P11–P17** in the solid-state; (d) photocatalytic hydrogen evolution of **P1**, and **P11–P17**. Adopted with permission from. [301] Royal Society of Chemistry (2018).

Incorporating nitrogen heteroatoms in those LCPs also resulted in a better control over the driving forces for redox reactions. Consequently, LCPs exhibited a significantly increased photocatalytic performance with an AQE of 6.7% at 420 nm.[337] In contrast to electron-poor heteroatoms (i.e. nitrogen), incorporation of electron-rich heteroatom monomers shows a decrease in the photocatalytic performance. Electron-rich monomer led to a red-shift in the optical gap, however, the associated reduction in driving force for sacrificial electron donor oxidation counteracts the potential gains in photocatalytic activity. Recently, a new series of LCPs exhibited hydrogen evolution with external quantum efficiencies between 0.4 and 11.6%.[289] This study also investigated the influence of solvent. It was suggested that the localization of water around the polymer chain is crucial, and concluded that the polar solvent led to the production of long-lived electrons in these amphiphilic polymers for improved hydrogen evolution.

π-conjugated polymer nanostructures (CPNs) have emerged as a new class of photocatalysts.[116-118] Polypyrrole nanostructures (PPy NSs) modified with mono- and bimetallic nanoparticles of Pt, Ni, NiO exhibited photocatalytic hydrogen evolution.[118] Photocatalytic activity of PPy NSs was shown sensitive to the metal loading. For example, 0.2%Pt-PPy-NSs resulted in superior activity. Modification with nickel-based nanoparticles (5%Ni-PPy-NSs) forms heterojunction for enhanced the photocatalytic performance. However, Ni leaching led to a degraded the photocatalytic activity with time. Poly(3,4-ethylenedioxythiophene) (PEDOT) is a promising CPN. It has a bandgap of 1.69 eV and was demonstrated for photocatalytic water treatment without the assistance of sacrificial reagents or noble metal co-catalysts.[117] These results are very impressive to explore its potential for photocatalytic hydrogen production from water.

10.6 Conjugated Polymer Dots (CPDs)

Polymer dots (Pdots) are derivatives of polymeric micelles with size in the range of 1–100 nm. Pdots have attracted significant attention because of its facile synthetic methods, tunable optical gaps, tunable particle size and surface hydrophilicity, relatively long excited state lifetimes etc. In particular, Pdots, owing to their large π-conjugated structures with overlapping p-orbital clouds, facilitate the free movement of electrons within the polymer backbone through tunnelling, hopping, or other related mechanisms. [338, 339] These attributes are desirable for a photocatalyst. Nanoprecipitation, mini-emulsion and self-assembly are the frequently used methods to prepare Pdots. The nanoprecipitation method uses miscible organic solvents, whereas mini-emulsion method employs immiscible organic solvents. Notably, the physical size of Pdots depends on the methods used to prepare them.[339]

Compared with traditional organic small molecules, semiconductor quantum dots and inorganic nanomaterials, Pdots exhibit a higher extinction coefficient, better photostability and chemical stability.[340] Additionally, Pdots often have different reactive functional groups on their surface that can provide a platform to construct multifunctional and hybrid nanomaterials when conjugated with different chemical and biological molecules.[341] Importantly, compared with inorganic nanoparticles of heavy metals and semiconductors, the Pdots are biocompatible because of hydrophobic π-conjugate backbone and amphiphilic polymer matrixes, and therefore Pdots are not toxic like heavy metals.[341, 342] Pdots are being widely used in imaging, as chemical sensors and in phototherapy. [343, 344] They are now also being used as a photocatalyst to produce hydrogen. [345-348]

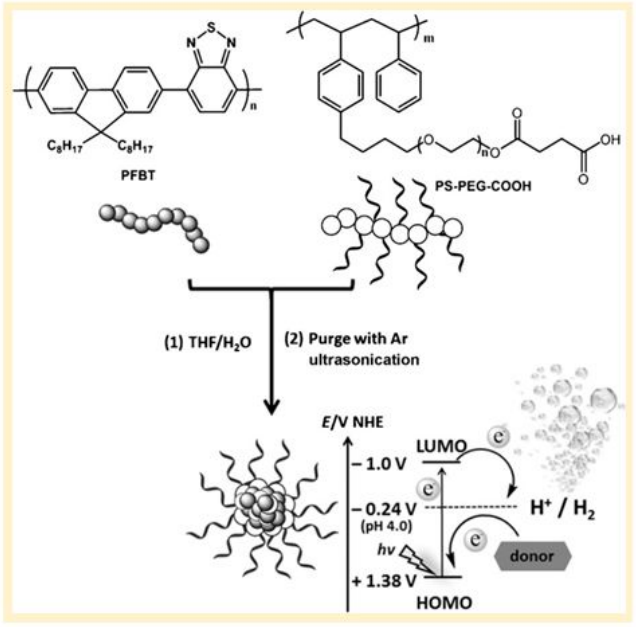

Fig. 28 Synthesis route for PFBT Pdots, and hypothetical diagram for hydrogen evolution reaction. Adopted with permission from. [347] Wiley-VCH (2016).

Inspired by the beneficial properties, Tian et al. reported water-soluble Pdots based on the conjugated polymer PFBT (Fig. 28) for photocatalytic hydrogen generation that showed a hydrogen generation rate of 8.3±0.2 mmol h^{-1} g^{-1} at λ>420 nm with an AQE of 0.5 % at 445 nm.[347] One interesting aspect about PFBT Pdots is their resistance to evolved oxygen. Oxygen is an inevitable byproduct in water splitting that may act as an

inhibitor to proton reduction reactions.[349] Therefore, an oxygen-resistant catalyst is the key for sustainable hydrogen production.

Following the reports of PFBT Pdots, a few other Pdots have been recently reported for photocatalytic hydrogen evolution.[345, 346, 348] Although, there is not much progress noticed in terms of quantum yield of hydrogen, Pdots are an important inclusion in the family of metal-free photocatalyst with much promise. One common feature of all of these reported Pdots are their effective extended absorption edge beyond 500 nm. This is highly desirable for harvesting low energy photons. Some Pdots are even active in harvesting photons up to 700 nm, [110] and can produce hydrogen in the absence of any organic solvent or co-catalyst.[345, 348] Below is the state of the art progress related to Pdots as a hydrogen evolution photocatalyst (Table 2).

Table 2. Activity of recently reported polymer dots (Pdots) for sacrificial hydrogen evolution under visible light irradiation.

Pdots	HER (mmol $g^{-1}h^{-1}$) at >420 nm	AQE (%)	Ref.
Hyperbranched	0.84	0.9 at 500 nm	345
Cycloplatinized	12.7	0.4 at 515 nm	346
PFBT	8.3	0.5 at 445 nm	347
PFODTBT	50.0	0.6 at 550 nm	348

10.7 Organic heterojunction photocatalysts

Efficient charge separation and suppression of charge carriers are the rate determining fundamental steps for high efficiency hydrogen production. In fact, hydrogen evolution is proportional to the number of free electrons available in reaction sites.[33, 168] Among many other strategies to enhance the hydrogen evolution in a photocatalyst, efficient charge separation and transport is the most recommended one regardless of the material (i.e. crystallinity, optical, electronic properties etc.) and chemical aspects (i.e. inorganic, organic, diffusion, mass transport etc.) of the photocatalyst. [169, 190]

A photocatalyst can sometimes suffer from a high recombination rate and poor charge separation. This problem can be overcome to a large extent by connecting two or more appropriate materials in the form of a heterojunction. Because of the band-offsets between two heterogeneous materials, it provides space for delocalization of photogenerated electrons and holes, thus avoiding recombination. Therefore, heterojunctions are the most frequently used technique to boost photocatalytic performance.[33] However, only a few polymeric heterojunctions beyond carbon nitride have been reported thus far.[350]. Here, we discuss polymer heterojunctions beyond carbon nitride.

Bojdys et al. reported the twinned growth of a 2D/3D van der Waals (vdW) heterostructure on a copper substrate by combining a sp^2 hybridized and crystalline 2D covalent triazine-based framework (TzF) with a sp^2–sp hybridized and amorphous 3D triazine-based graphdiyene (TzG), Fig. 29 a. This 2D/3D vdW heterostructure features promising structural motifs, such as open, porous structure and an intriguing donor–acceptor (D–A) motif having electron rich buta-1, 3-diyene (D) and electron poor triazines (A). These are interesting properties for photocatalytic water splitting, and open opportunities to fabricate conjugated heterostructure by incorporating different graphdiyne, a new two-dimensional (2D) carbon with unique sp–sp^2 carbon atoms, uniform pores, and highly pi-conjugated structure.[351-354] This mixed dimensional heterostructure evolved hydrogen at a rate of 34 µmol h^{-1} g^{-1} without a noble metal cocatalyst.[256] Despite a low hydrogen evolution rate, Bojdys et al. demonstrated a wet chemical approach in preparation of this 2D/3D vdW heterostructure in contrast to commonly used techniques, such as chemical (CVD) and physical vapor deposition (PVD) processes for preparation of 2D materials and their heterostructures.

However, CVD and PVD have synthetic limits that includes uncontrolled nucleation events that limit the homogeneity and size of the crystalline domains of the obtained materials. More importantly, vapor deposition techniques are incompatible with a majority of organic synthetic molecules. It is also difficult to predict bonding patterns for speculated materials, which may require complex postsynthetic treatment to obtain the desired materials. [355]

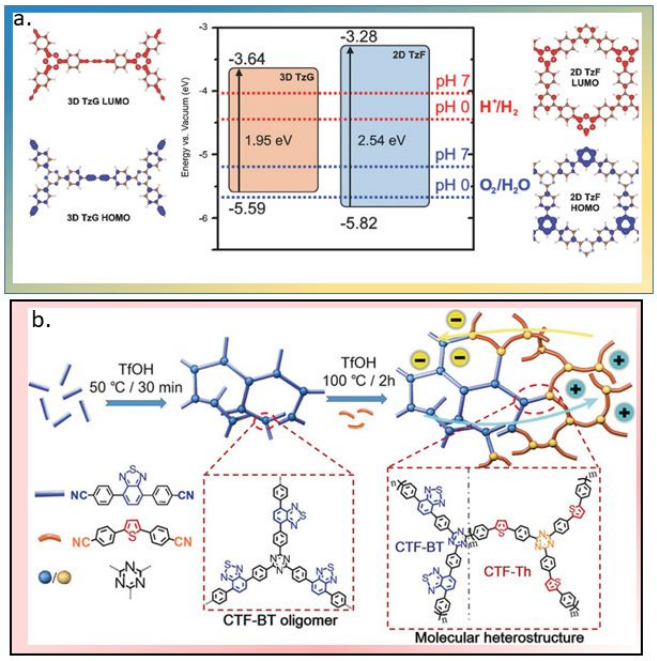

Fig. 29 a) Plot of orbital coefficients for the frontier orbitals of 3D TzG (left) and 2D TzF (right) as derived from DFT calculations. The relative locations of HOMO and LUMO for the TzF/TzG heterojunction (type I) are shown in the center with the redox potential of water indicated at pH 0 and 7. Adopted with permission from.[256] Wiley-VCH (2017). b) Sequential polymerization strategy toward covalently connected CTF-BT/Th. Adopted with permission from. [302] Wiley-VCH (2019).

Very recently, Li et al. reported a molecular heterostructure created via incorporation of benzothiadiazole (BT) and thiophene (Th) functionalities into a CTF as electron-withdrawing and electron-donating units, respectively, by the sequential polymerization of their nitrile precursors, Fig. 29 b.[302] Because of efficient charge-carrier-separation, it exhibited a hydrogen production

rate of 6600 µmol h^{-1} g^{-1} with an AQE of 7.3 % at 420 nm. This represents remarkable hydrogen evolution among the triazine-based polymer photocatalysts.

There are a large number of polymer photocatalysts that exist. Among the large pool of materials, researchers need to develop synthesis routes for creating more heterojunction photocatalysts.

10.8 Overall water-splitting with organic photocatalysts

Releasing hydrogen from water involves two simultaneous reactions, namely oxidation and reduction reactions. Research has pretty much progressed in realizing one of these two reactions while supressing the other in the presence of appropriate sacrificial agents. However, there are very few successes in accommodating both of these reactions in fulfilling the ultimate target of overall water-splitting into its constituents, hydrogen and oxygen.[356] Unfortunately, progress in overall water-splitting is rather insignificant, particularly, on polymeric based photocatalysts. The most challenging part of realizing direct water-splitting is the four-electron pathway involved in water-oxidation.

Xu et al. demonstrated overall water-splitting on CMPs nanosheets prepared by oxidative coupling of 1,3,5-tris-(4-ethynylphenyl)-benzene (TEPB) and 1,3,5-triethynylbenzene (TEB). These photocatalysts exhibited photocatalytic splitting of pure water (pH ≈ 7) into stoichiometric amounts of H_2 and O_2 with an AQE of 10.3% for TEPB and 7.6% for TEB at 420 nm, Fig. 30. The solar-to-hydrogen (STH) conversion efficiency of PTEPB and PTEB were 0.60% and 0.31%, respectively using the full solar spectrum. They also demonstrated a Z-scheme systems for overall water splitting using van der Waals heterostructures formed between nanosheets of aza-fused CMP and C_2N with a STH value of 0.23 % which was further increased to 0.40 % using reduced graphene oxide as the solid electron mediator.[357] The success behind this lies in the efficient charge separation and transport of photogenerated excitons by virtue of band alignment via heterostructuring.

Among the metal-free photocatalysts, the best STH value (~2 %) in overall water-splitting under visible light was reported for metal-free CDots/C_3N_4.[223] In contrast to the four-electron pathway, however, the overall water-splitting on CDots/C_3N_4 proceeded via a stepwise two-electron/two-electron process, in which H_2O oxidized into H_2O_2 was the first step followed by dissociation of H_2O_2 into H_2 and O_2 in the second step.

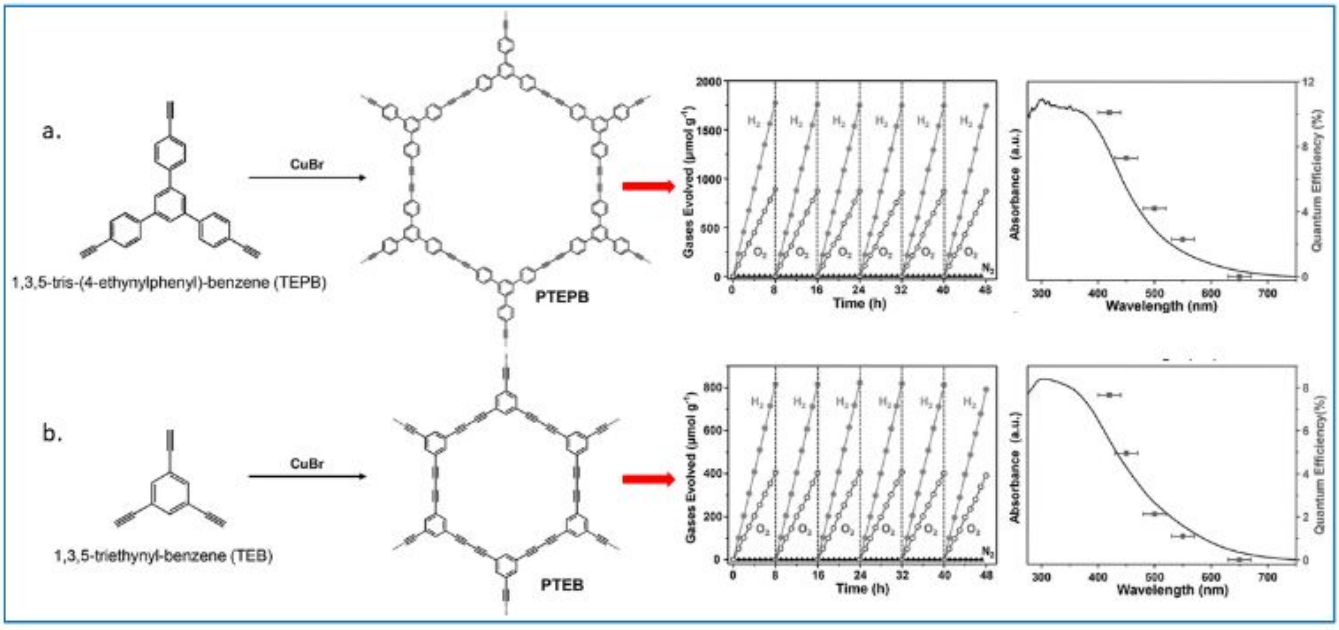

Fig. 30 Synthesis and overall water-splitting on a) PTEPB and b) PTEB. Adopted with permission from.[358] Wiley-VCH (2017).

10.9 Role of Pd in proton reduction reactions in polymeric photocatalysts

Linear and cross-linked conjugated polymer photocatalysts exhibited H_2 evolution under visible light irradiation without any added co-catalyst at a rate comparable to that of graphitic carbon nitride with added Pt cocatalyst.[263] These polymer photocatalysts are therefore attractive for cost-effective hydrogen production. However, a relatively unexplored feature of these linear and cross-linked conjugated polymers is the presence of residual Pd originating from their synthesis via Pd catalyzed polycondensation reactions, which could work as a built-in cocatalyst. [263, 266, 317, 359]

Recent studies reported that the Pd catalysts used in these reactions could turn into particles via aggregation and subsequent Ostwald ripening. Metallic Pd^0 cannot be removed completely from the polymer matrix using classical purification techniques.[360-362] It is well-known that similar to Pt^0, Pd^0 is a highly active proton reduction electrocatalyst.[363, 364] Expectedly, the dispersed residual Pd within these polymer structures plays a significant role in H_2 evolution. However, there are conflicting views in the literature in this regard. There are studies where it has been shown that there is no correlation between Pd concentration and the hydrogen evolution reaction rate for a range of CMPs, [21] and in a series of LCPs containing the

2,1,3-benzothiadiazole (BT) unit.[348] In those exemplary cases, it was concluded that it was not residual Pd but H-bonding from water to the N atoms on this unit that facilitated the proton reduction reaction. In contrast, a dependency of HER rate on Pd content was observed in COFs. [24] However, it was argued that varying the Pd catalyst loadings might alter the network's microstructure of the polymer due to a different degree of polymerization. An unambiguous conclusion was not possible to make whether these structural changes or the residual Pd had affected the HER rate. An added problem is that the reduction of Pd mass concentration below 400 ppm (0.04 wt.%) in the cross-linked structure of the polymer is difficult. Therefore, it remains a mystery whether these conjugated polymers could drive the HER without Pd or if Pd is the driving force behind accelerated HER rates.[365]

In a more recent study on Pd catalyzed poly(9,9-dioctylfluorene-alt-benzothiadiazole) (F8BT) systems, it was concluded that Pd was essential for any observable H_2 evolution.[366] Based on transient absorption spectroscopy (TAS) experiments, it showed that electron transfer to protons in the aqueous phase was impeded as the Pd content was reduced. Eventually, it was reported that very low Pd concentrations (<40 ppm) were sufficient to enhance the hydrogen evolution reaction which increases linearly with increasing Pd concentration from <1 ppm to approximately 100 ppm, after which the rate begins to saturate.

Despite these studies, more intense investigations need to be carried out to clearly answer the question regarding whether conjugated polymer systems are intrinsically able to drive photocatalytic H_2 production or whether they require a co-catalyst, i.e., Pd to drive the proton reduction reaction.

10.10 Screening and developing high-throughput and high efficiency polymer photocatalysts

Arguably, hydrogen production through photoreduction of water on polymer photocatalysts can be traced back to 1990.[253, 367, 368] Since then quite a few polymeric photocatalysts have been developed for solar hydrogen production. We are yet to find a conjugate polymer photocatalyst with comparable performance to that of inorganic counter parts. However, the reported photocatalysts are only a tiny fraction out of the possible chemical space for polymer photocatalysts. Given the available large pool of monomers, reaction pathways, and reaction conditions, the number of possible photocatalysts seems literally infinite.

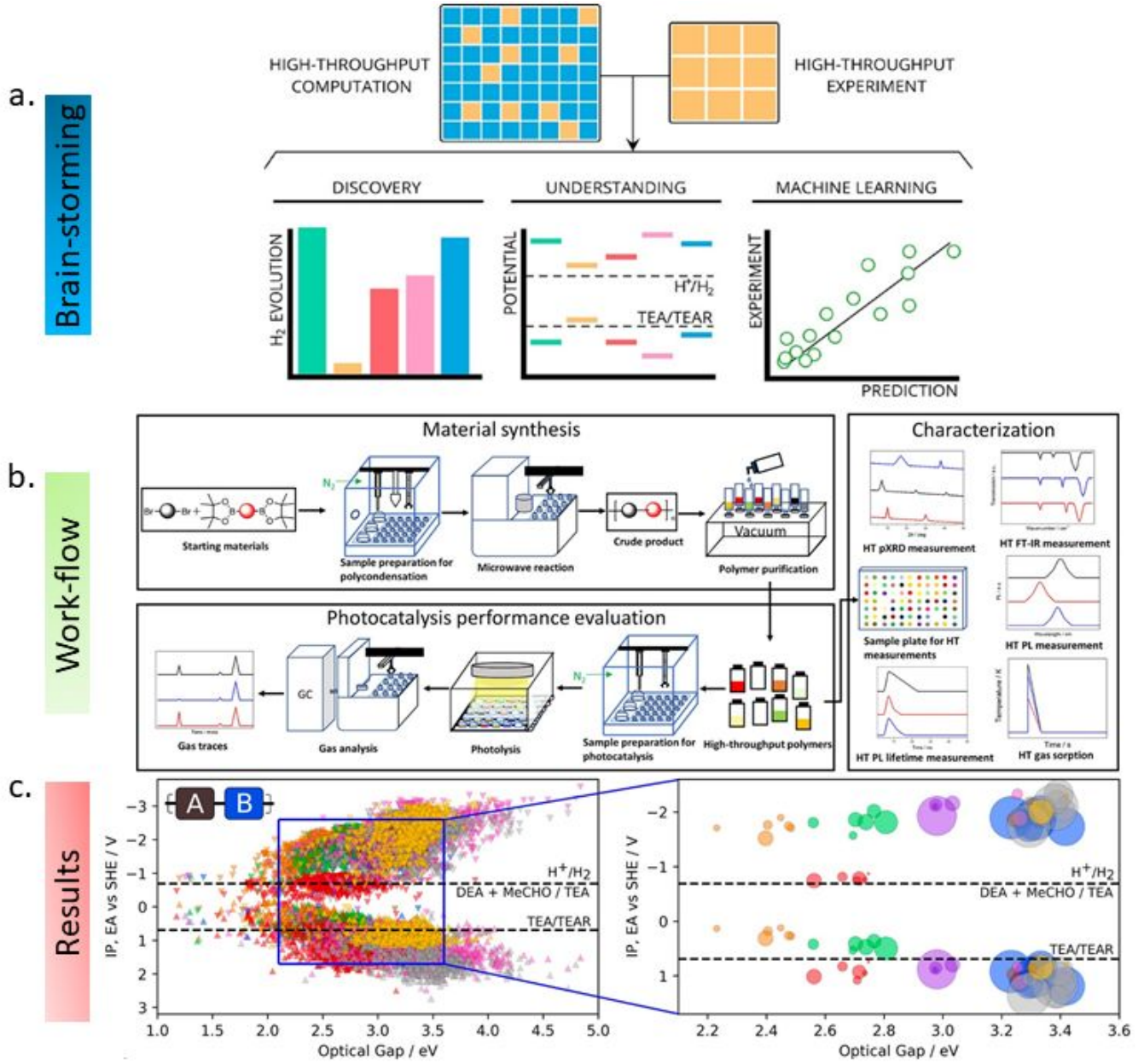

Fig. 31 a) Conceptual frameworks. b) Workflow for high-throughput synthesis and property screening of the conjugated polymer library. C) Prediction and comparison of optoelectronic properties for hydrogen evolution. Adopted with permission from. [269] American Chemical Society (2019).

It makes us optimistic that by a careful combination of these variables, we may find highly efficient organic photocatalysts. High-throughput screening of many diverse co-polymers, reduce the near impossible task of sorting out the suitable polymers from an appropriate combination and permutation of variables, however, artificial intelligence could be involved in a similar way to assist in sorting out the expected data from existing data banks. Recently, an integrated computational and experimental high-throughput approach for the screening of linear polymers as hydrogen evolution photocatalysts has been reported.[269] This integrated system was based on significant methodological development in computation, robotics, and automation, see Fig. 31.

This approach was exploited to rapidly sample chemical space and to identify high-activity photocatalysts for hydrogen evolution. Incredibly, a library of 706 candidate dibromo monomers and 9 diboronic acid/acid esters (6354 candidate co-polymers in total) was screened computationally, which explored structure–property relationships for families of closely related structures. Out of 6354 candidate co-polymers, more than 170 co-polymers were prepared and tested experimentally under photocatalytic conditions. A machine-learning model was used to predict and compare the HER, and correlate the HER with individual electronic properties of the polymer and how well it disperses in the reaction mixture.

Significantly, this data-driven approach will facilitate the development of the best-performing polymer photocatalysts in the future.

11. Limiting factors to the enhance quantum efficiency of hydrogen evolution

Three key dynamic processes, i.e., photophysical, photochemical and electrochemical processes need to be optimized for enhanced water-splitting.

A mechanistic understanding of how optical excitation contributes to the photogeneration of charge carriers is necessary for harvesting photons, and limiting the photogeneration at recombination active sites. There is clearly a lack of substantial systematic research endeavors for understanding this for the case of metal-free photocatalysts. In this regard, research therefore needs to focus on the analysis of the internal quantum efficiency as a function of photon energy to determine (i) the Coulombic binding and separation of the electron–hole pairs, (ii) the value of the band gap energy, and (iii) what fraction of photo-excitations can fully be separated for a given photon energy. Transient absorption spectroscopy and Finite Difference Time Domain (FDTD) Simulations would be useful tools to investigate these phenomena.[189]

11.1 Improving charge transport

Light induced photodecomposition of water into H_2 and O_2 molecules relies on the separation of excited state electron-hole pairs and the subsequent transfer of charge carrier to the relevant redox couples. The typical excited state lifetimes are in the range of 1–100 ps).[369] Unless separated within this time frame, the excited state electron-hole pairs undergo recombination with the release of captured light energy as heat or emission of a photon. It is therefore required that electron should be scavenged before the absorption of subsequent photons to sustain a multi-electron photo-redox reaction. Otherwise, the extraction of charges becomes more difficult, and imposes a limit to photocatalytic efficiency.

Most of the metal-free photocatalysts are low mobility materials, in which the kinetics of non-geminate recombination is strongly linked to the motion of charges. Additionally, these materials possess a significant disorder that could lead to unavoidable thermalization of photogenerated carriers in the heterogeneously broadened density of state distribution. Despite its general importance, knowledge about the kinetics of non-geminate recombination is not yet understood comprehensively. Researchers may employ time delayed collection field (TDCF) experiments to study the recombination of photogenerated charge on these materials.

Whether the recombination is dominant over the extraction or vice versa depends on a complex interplay among the effects of film thickness, charge transport, recombination strength and light intensity. A complete and systematic understanding of the interplay of all these factors will translate into significant improvements in the power-conversion efficiency. However, such understanding is still lacking. Detailed knowledge of the competition between charge extraction and recombination should be sought through combined time-resolved photoluminescence (TRPL), transient absorption (TAS), surface photo-voltage spectroscopy, and optical pump terahertz-probe spectroscopy experiments.

It is also recommended that research be extended to understand multi-photon/electron processes that involved binding singlet fission (SF) [370] and triplet–triplet annihilation (TTA-UC) [371] molecules. These SF and TTA-UC processes can act as a charge separation interface. With SF and TTA-UC, a theoretical solar conversion efficiency can be increased from 33% to 48%.[372, 373]

11.2 Understanding of sub-particle reaction mechanisms

Traditional approaches overlook inherent differences between the individual particles that make up a bulk material. It is to be noted that solid catalytic materials, even seemingly perfect crystals, contain atomic-scale imperfections at surfaces at which the reactions occur.[374] Therefore, understanding of sub-particle reaction mechanisms is necessary for probing the nanoscale electrochemical efficiency and redox reactivity of photocatalysts. We therefore need a method of 'filming' single catalytic events in real time on a solid crystal, allowing catalytic activity to be mapped over its whole surface.[375] This can be accomplished by using high-resolution fluorescence microscopy to observe a catalytic crystal at work in liquid-phase reactions. [374] This approach will enable monitoring of single catalytic events in real time by observing a 'reporter' molecule that becomes fluorescent only after catalytic action, and this may thus beautifully map the spatial distribution of active sites over a single catalytic crystal.

By doing so, it will also be able to analyse the number of electrons that could be withdrawn from the photocatalyst as different parts of it will be selectively illuminated. From these measurements, it will be able to deduce the efficiency with which an absorbed photon at a certain location gives rise to redox reactions or to an unwanted electron–hole recombination.

11.3 Rational engineering of catalyst-cocatalyst duo for improved operation

Minimizing the amount of photocatalyst and co-catalyst is essential not only to reduce costs, but also because co-catalysts compete for photons by scattering or absorbing them.[376] It should be achieved by identifying the oxidation and reduction hotspots to selectively deposit the oxygen/hydrogen evolution cocatalysts at hotspots or at regions with intrinsically low activity. These regions are currently not well-understood by researchers. The mapping of the locations of single oxidation and reduction reactions at the catalyst surface with nanometre-scale precision by using fluorogenic reactants may provide useful information.[377]

11.4 Improving electrocatalytic performance of a photocatalyst

The final step in water-splitting involves electrocatalytic reduction of proton and oxidation of water. Therefore, a photocatalyst should be endowed with electrocatalyst-like properties too. Enhanced HER and OER thus require the improvement of the electrocatalytic properties of a metal-free photocatalyst in terms of activity, selectivity, and durability to be comparable and compatible with that of high efficiency metal counterparts. The rational design of catalysts should be followed by in-depth understanding of the electrocatalytic reaction mechanisms involved at the molecular level through

fundamental and theoretical studies of model catalysts using in-situ, ex-situ and operando techniques.

The electrocatalytic performance of a photocatalyst toward specific reactions is described through measuring current density (j_0), overpotential (η), Tafel slope and so on. For example, the magnitude of j_0 is indicative of the intrinsic charge transfer rate between an OER electrocatalyst and the reactant intermediates. The Tafel slope evaluates the relationship between j and η, as such a smaller Tafel slope means a faster reaction rate constant (i.e., a faster increase in j with a smaller change in η).

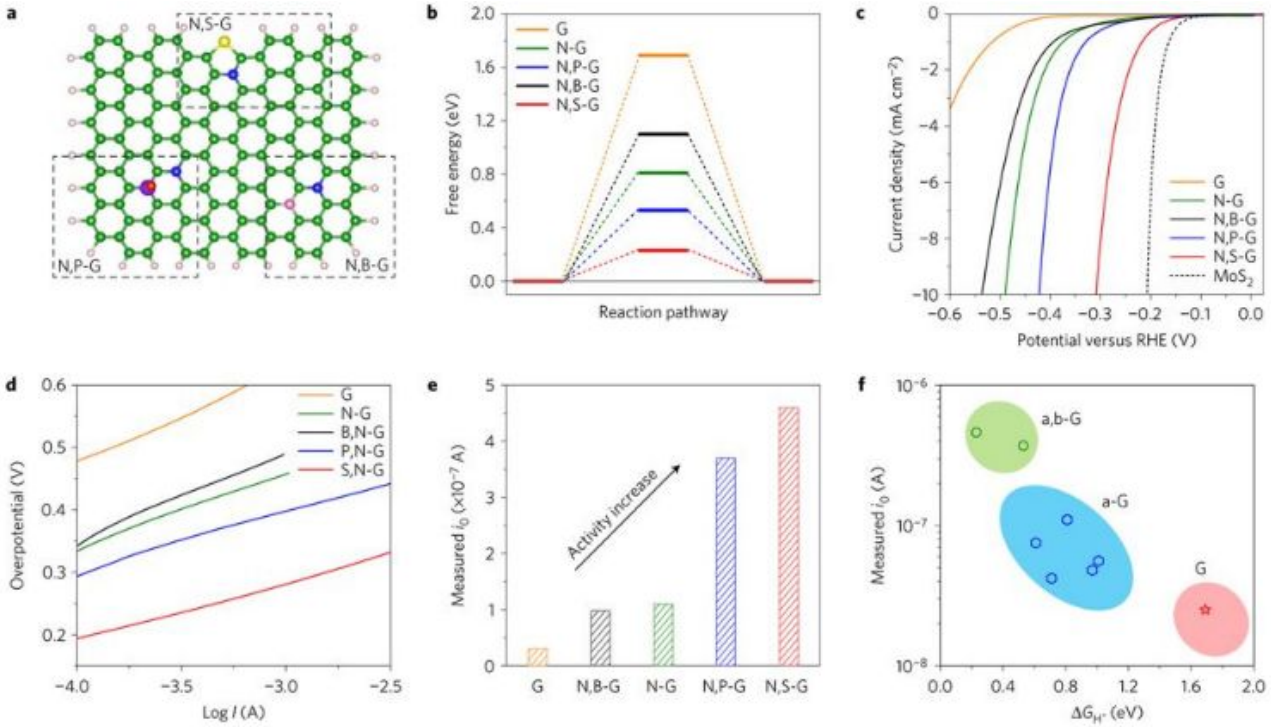

Fig. 32 a) Atomic configurations of three dual-doped graphene. **b**) The three-state free energy diagram for the pure, single- and dual-doped graphene models. c) polarization curves. **d**) Tafel slopes. **e**) exchange current. **f**) volcano plots. Adopted with permission from. [378] Nature Publishing group (2016).

In particular, of the change in η required to produce a j of 10 mA cm^{-2} is a commonly used parameter for comparing the performance of various electrocatalysts. [363] The geometry of the catalyst, its chemical composition and its electronic structure govern a specific reaction process.[379] Toward this end, DFT would be an essential tool for defining the adsorption energies, reaction thermodynamics and activation barriers, as well as accurate identification of the active sites on the surfaces of solid catalysts. [363] Unravelling the origin of reactivity should comprehensively be related to the experimentally measured specific reaction rate descriptors, for example, exchange current (i_0) and turnover frequency, and the resultant activity trend (that is, volcano plot). Combined theoretical and experimental studies are therefore necessary to establish a qualitative argument with defined quantitative data to tune the materials to achieve the best catalytic activities.[363, 379]

One of the most commonly used techniques is doping heteroatoms to tune the electro-chemical properties of the catalyst with tailored electronic properties and surface chemistry. Doping induces charge redistribution around the dopants and enhances the charge transfer process via a synergistic coupling effect. For example, it has been shown that heteroatom doped (e.g., N and S) graphene nanostructures can efficiently adjust the electron-donor properties and electrocatalytic activity of neighbouring C atoms that lead to a downshift in the valence bands of active C atoms. Heteroatom doping enhances favourable H* adsorption–desorption ability from graphene. As a result, dual-dopant doped graphene exhibits enhanced HER activity with a low onset potential and high exchange current, Fig 32.[378]

Forming heterostructure/hybrid-structure between two heterogeneous materials is another widely practiced strategy to deal with charge transfer for achieving better electrocatalytic performance. For example, a hybrid structure of g-C_3N_4 and CNT was shown to exhibit improved electrochemical OER activities compared with the IrO_2 benchmark electrocatalyst.[380] Electrostatic interactions and π–π stacking of exfoliated g-C_3N_4 nanosheets and carbon structures were shown to cause positive charge density on the nearby sp^2-hybridized C atoms that favoured the adsorption of OH^-, facilitated the electron transport between the reaction intermediates and catalyst surface, and consequently improved the electrochemical OER.

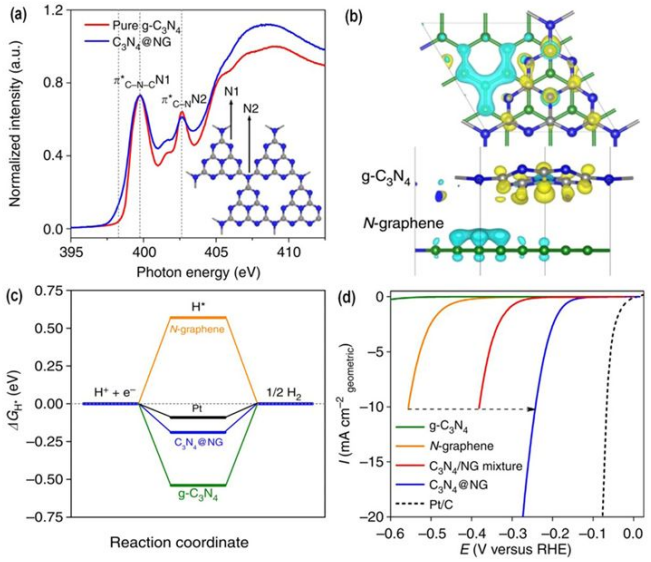

Fig. 33 a) N K-edge NEXAFS spectrum of g-C_3N_4 and C_3N_4@NG. b) Interfacial electron transfer in C_3N_4@NG. c) Simulated free-energy diagram at equilibrium potential. d) Comparison of HER activities. Adopted with permission from ref. [381] Nature Publishing Group (2014).

The overall reaction kinetics of the HER are largely determined by the Gibbs free energy of hydrogen adsorption, ΔG_{H^*}. Hydrogen adsorption is too weak if $\Delta G_{H^*} > 0$, while it is too strong if $\Delta G_{H^*} < 0$.[382] Both of these extreme cases may result in a poor apparent HER activity. Therefore, to make a trade-off between these values, a volcano shaped plot was developed by correlating the experimentally measured j_0 and the computed ΔG_{H^*}.[363] Such a relationship is beneficial in demonstrating the trend of HER activities. Recently, taking into account the excessive affinity of g- C_3N_4 nanosheets to adsorption of H* and very weak H* adsorption of N-doped graphene, a hybrid structure between g-C_3N_4 and N-doped graphene was demonstrated for better hydrogen evolution that is comparable to a commercial Pt/C catalyst. [381] The synergetic action between g-C_3N_4 and N-doped graphene induced moderate adsorption–desorption behavior of hydrogen on the surface of the hybrid that resulted in overall improved hydrogen evolution kinetics, Fig. 33.

12. Scaling up photocatalytic system for large-scale implementation

The hydrogen based economy will only become a reality if it can be produced at scale. Globally, countries will only transition their economies to hydrogen if the volumes of hydrogen needed to do so are achievable, available and, in the long term, at price parity with other forms of fuel. Therefore, getting to scale will be a major endeavour.

The United States Department of Energy set a goal of achieving a cost of 2.00–4.00 USD kg^{-1} H_2 by 2020 at daily AM 1.5G irradiation for 7.6 h (corresponding to 240 W m^{-2}). The associated constraints are a photocatalytic reaction system with an STH of 10%, a lifetime of 10 years, an annual depreciation rate of 4%, and an allowable cost of 102 USD m^{-2}. [383-385]

We therefore have to focus on improving the intrinsic factors of a photocatalyst (i.e., extending the spectral range of visible light absorption, enhancing photogenerated charge separation and transport, and facilitating the hydrogen and oxygen production reactions, stability etc.) to meet the external requirements (AQE, STH, modular level implementation etc.)

12.1 Performing reliable photocatalytic test and accurate reporting of hydrogen evolution and AQE

For reproducibility and benchmarking, reliable reporting of hydrogen production rate and apparent quantum yield is highly important. We recommend using AQE and/or STH values at specific wavelengths rather than gas evolution rates to compare the photocatalysts. Because gas evolution varies depending on the experimental conditions used. The gas evolution rates should be used to find the H_2/O_2 molar ratios to determine whether the process is an overall water-splitting or sacrificial reaction.

In the authors' opinion, reporting the hydrogen evolution rate per gram of catalyst used (i.e. $molh^{-1}g^{-1}$) is misleading to justify the photonic efficiency of a given photocatalyst. Because, up to a certain limit, the hydrogen evolution rate might be proportional to a linear increase of the amount of photocatalyst. However, light absorption becomes saturated after an optimal amount of photocatalyst, Fig. 34.[386] Therefore, it is recommended to report the optimal rate of hydrogen evolution (i.e. $molh^{-1}$) independent of the amount of photocatalyst used.[12, 386-388] The hydrogen evolution rate needs to be checked by varying the amount of photocatalyst to find out the optimal amount of photocatalyst.

A report of hydrogen production rate and apparent quantum yield should be accompanied with the type of reactor used (internal or external irradiation photocatalytic reactors), intensity of light source, wavelength of light, mass of the photocatalyst, and absence/presence of sacrificial agents and cocatalyst(s). A photocatalyst suspended in an internal irradiation type reactor usually gives greater gas evolution rates than an external type because of the close proximity to the light source. However, light-intensity distribution and irradiation area are irregular in an internal type reactor. Therefore, precise determination of the wavelength dependent hydrogen evolution and AQE is difficult. The external irradiation type reactor is better suited in this case. Care must be taken to ensure that the reactor is perfectly sealed or the reaction is performed under vacuum or under a flow of inert gas to avoid the intrusion of ambient air to avoid incorrect estimation of the evolved gases. It is typically done by degassing the reaction solution completely through inert gas flow. At the same time, the gas chromatograph must be carefully calibrated using standard gases to quantify the amount of evolved gas. If N_2 is detected in the gas chromatograph, it is an indication that the reaction solution was intruded by ambient air or inadequate removal of dissolved air. N_2 detection in the case of (oxy)nitride photocatalysts represent the self-oxidation of the photocatalyst. For either cases, N_2 evolution is not welcome in water-splitting reactions.

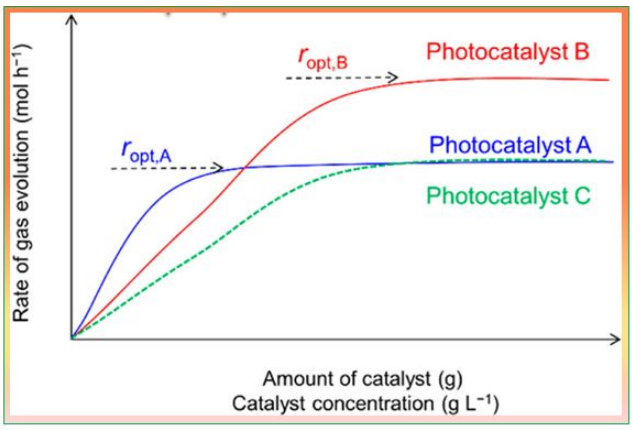

Fig. 34 Influence of amount of photocatalyst on the rate of gas evolution. Adopted with permission from. [386] American Chemical Society (2017).

To confirm that hydrogen/oxygen are evolved solely through photocatalytic reactions, it is recommended to test if the (i) catalytic reactions proceed in the dark, (ii) if evolved amounts of gases increase linearly with the irradiation time, and (iii) turnover number is greater than the quantity of hydrogen present within the catalyst. In overall water splitting, H_2 and O_2 should be evolved with a stoichiometric ratio of 2 : 1 during the whole course of the catalytic reaction or past the induction period of some of the photocatalysts under light irradiation. In sacrificial hydrogen production, evolved hydrogen must be greater in quantity than the molar quantity of hydrogen (if any) present in the chemical structure of the photocatalyst. Otherwise, it represents the self-decomposition of the photocatalyst with or without proton reduction. In sacrificial oxygen evolution, it is recommended to use the oxygen isotope (i.e., ^{18}O-labelled water, for example) to confirm that oxygen is evolved solely through water oxidation and not from other oxygen-containing sources.

There is some confusion regarding the reporting of AQE or STH. In sacrificial hydrogen evolution, for example, AQE should represent the efficiency of the hydrogen evolution photocatalyst. However, STH values should report the measure of the efficiency of overall water-splitting. It is because the calculation of STH requires use of the value of the Gibb's free energy as one of the parameters. Gibb's free energy represents the amount of energy required to decompose the H_2O into H_2 and O_2 in a stoichiometric ratio. It means that if O_2 is not generated as the product of H_2O oxidation, which is true for sacrificial hydrogen evolution, the Gibb's free energy should not be used. In the calculation of the Gibb's free energy, the reaction temperature and pressure should be taken into account. To be compatible with universally standard practice, the STH value should be obtained under one sun (one sun is commonly used to report solar cell efficiency).

12.2 Design of modular photocatalyst system

Particulate photocatalysts suspended in aqueous solution are commonly used for water splitting. However, using laboratory-scale particle suspension systems limits the scalability of water splitting. Its large-scale deployment in industrial settings is a big problem. In particular, dispersing a large amount of particulate photocatalysts in a large amount of water and keeping it near homogenously suspended to avoid precipitation is a grand challenge. The added problem is the separation and collection of the photocatalyst powder from the suspension for further use, and tracking the movement of the sun in practical application. Therefore, design of a modular photocatalyst is urgently necessary for scaling up. One approach might be to deposit photocatalyst powders onto a specific substrate of specific size and dimension. As such, shallow horizontal pools or beds consisting of reactant solution and a panel-type photocatalyst would be a potential reactor for large-scale water splitting.

13. Conclusions and future perspective

In this contribution, we have reviewed the latest progress in metal-free photocatalysts for hydrogen production from water. For convenience, we have categorized the various metal-free photocatalysts into four types: elemental, binary compounds, ternary compounds and organic photocatalysts.

It is evident from current research that among the metal-free photocatalysts, carbon nitride is the most celebrated photocatalyst with AQE values greater than 60%. Carbon nitride therefore holds true promise as a next generation photocatalyst in terms of scalability, stability and selectivity. In contrast, development of elemental and organic photocatalysts is still in a nascent stage. Intensive research needs to be carried out to optimize their bulk and interfacial charge separation and transport, and electrochemical redox reactions for enhanced quantum efficiency with stable operation for long period of time.

Tuning crystal morphologies and structural features at the nanometer level would endow beneficial physicochemical properties for enhanced photocatalytic performance of nanostructured photocatalysts. Because of readily accessible and interconnected porous networks and high specific surface areas, nanostructured photocatalysts facilitate efficient light harvesting and kinetics of charge transport, adsorption of reactants, and transport of guest species to the active sites. These synergetic effects lead to significant enhancement of the photocatalytic performance. Although a great deal of research has invested in studying different nanostructures of carbon nitride, more intense research need to be warranted for other genre of metal-free photocatalysts to pin-point the structure-property relationship and their confluence on catalytic performance.

Of particular interest is organic photocatalysts for which little is known about the underlying photophysics and surface processes when immersed in an aqueous medium with or without sacrificial agents. Additionally, a well-founded and detailed understanding of the mechanism of exciton dissociation and its dependence on material parameters is still missing for polymeric photocatalysts. To promote exciton dissociation, incorporating a donor-acceptor (D-A) system may be employed.[389] The liberated excess energy during the transfer of the excited donor electron to the acceptor aids in complete dissociation of the excitons.[333] Exciton delocalization, as well as

interfacial dipoles may also be conducive to exciton dissociation.[390, 391]

The widely used selling point of porous conjugate polymers is their large surface area with permanent porosity (in some cases). Although, a reliable relationship between surface area and hydrogen evolution is yet to be established. Importantly, reported surface areas (in BET techniques) are measured in vacuum, while networks with low or even no apparent surface area can swell in solution. The question is how important is it to have a permanent surface area for high photocatalytic performance. It is time to ponder and ask the question- why a network whose surface area was measured in vacuum should give a reliable conclusion regarding the accessible sites in the liquid-swollen state. Answering this question seems a must when several linear, planarized, non-crosslinked and non-porous conjugated polymers have been shown better or at least comparable photocatalytic performance with microporous polymer photocatalysts.

Photocatalytic solar fuel production involves a complex series of photophysical and electrocatalytic processes. The processes involved in photocatalytic reactions can be divided into the following six components: photon absorption, exciton separation, carrier diffusion, carrier transport, catalytic efficiency, mass transfer of reactants and products. These six parameters have multiple impacts on the fundamental efficiencies. All of these parameters, despite happening at different time scales and spatial resolution, should therefore be optimized to achieve high values for the AQE.

There is no standard to judge and compare the different reported efficiencies of photocatalysts. The overall amount of hydrogen produced per unit time depends on the sample mass, reactor setup, light source and applied filters and many other parameters. Therefore, the same material can produce different values when tested in different labs. In the authors' opinion, this problem becomes more exacerbated when the rate of hydrogen is reported in units per time and mass catalyst (mol h^{-1} g^{-1}), because, hydrogen production and catalyst mass do not follow a linear relation. Reporting of the AQE values bears the same problem, and is often not measured with a reliable protocol.[309]

To produce hydrogen at scale, an Australian hydrogen taskforce has arisen following six questions that are believed to also be of a global concern:[392] (i) what scale is needed to achieve scale efficiencies and overcome cost barriers? (ii) what approaches could most effectively leverage existing infrastructure, share risks and benefits and overcome scale-up development issues? (iii) what arrangements should be put in place to prepare for and help manage expected transitional issues as they occur, including with respect to transitioning and upskilling the workforce? How do we ensure the availability of a skilled and mobile construction workforce and other resources to support scale-up as needed? (iv) what lessons can be learned from the experience of scaling up supply chains in other industries? (v) when should the various activities needed to prepare for hydrogen industry scale-up be completed by? (vi) what measures and incentives are needed to achieve these timings?

Solar fuel production brings opportunities to avert dangerous climate change. To take stock of solar fuel initiatives, it is imperative to know— what works and why? Getting a lucid answer requires, first of all, putting our collective experience together for a comprehensive global assessment of energy-innovation programs to establish the best practices.

Acknowledgements

The authors acknowledge the Robert A. Welch Foundation (Grant no. F-1436) and the United States Department of Energy, Basic Energy Sciences (Grant no. DE-FG02-09ER16119) for their generous support.

References

1. N. S. Lewis and D. G. Nocera, *Proc. Nat. Acad. Sci.*, 2006, **103**, 15729-15735.
2. N. Armaroli and V. Balzani, *Chem. Eur. J.*, 2016, **22**, 32-57.
3. W. Wang, J. C. Yu, D. Xia, P. K. Wong and Y. Li, *Environ. Sci. Technol.*, 2013, **47**, 8724-8732.
4. J. Markard, *Nat. Energy*, 2018, **3**, 628–633.
5. K. Maeda, *J. Photochem. Photobiol. C Photochem. Rev.*, 2011, **12**, 237-268.
6. Z. Li, B. Li, S. Peng, D. Li, S. Yang and Y. Fang, *RSC Adv.*, 2014, **4**, 35144-35148.
7. X.-S. Zhang, J.-Y. Hu and H. Jiang, *Chem. Eng. J. (Amsterdam, Neth.)*, 2014, **256**, 230-237.
8. A. Kudo and Y. Miseki, *Chem. Soc. Rev.*, 2009, **38**, 253-278.
9. W.-J. Ong, L.-L. Tan, Y. H. Ng, S.-T. Yong and S.-P. Chai, *Chem. Rev.*, 2016, **116**, 7159-7329.
10. J. Wen, J. Xie, X. Chen and X. Li, *Appl. Surface Sci.*, 2017, **391**, 72-123.
11. F. K. Kessler, Y. Zheng, D. Schwarz, C. Merschjann, W. Schnick, X. Wang and M. J. Bojdys, *Nat. Rev. Mater.*, 2017, **2**, 17030.
12. M. Z. Rahman, K. Davey and C. B. Mullins, *Adv. Sci.*, 2018, **5**, 1800820.
13. Y. Wang, A. Vogel, M. Sachs, R. S. Sprick, L. Wilbraham, S. J. A. Moniz, R. Godin, M. A. Zwijnenburg, J. R. Durrant, A. I. Cooper and J. Tang, *Nat. Energy*, 2019, **4**, 746–760.
14. G. Liu, P. Niu and H.-M. Cheng, *ChemPhysChem*, 2013, **14**, 885-892.
15. M. Z. Rahman, K. Davey and S.-Z. Qiao, *J. Mater. Chem. A*, 2018, **6**, 1305-1322.
16. M. G. Kibria, J. P. Edwards, C. M. Gabardo, C. T. Dinh, A. Seifitokaldani, D. Sinton and E. H. Sargent, *Adv. Mater.*, 2019, **32**, 1807166.
17. M. Z. Rahman and T. Edvinsson, *Joule*, 2019, **3**, 2290-2293.
18. M. Z. Rahman and T. Edvinsson, *Matter*, 2019, **3**, 562-564.
19. J. P. Pender, J. V. Guerrera, B. R. Wygant, J. A. Weeks, R. A. Ciufo, J. N. Burrow, M. F. Walk, M. Z. Rahman, A. Heller and C. B. Mullins, *ACS Nano*, 2019, **13**, 9279-9291.
20. G. Ciamician, *Science*, 1912, **36**, 385-394.
21. Plotnikov, *Algemeine Photochemie*, Walter De Gruyter, Berlin, 1936.
22. H. Kisch, *Angew. Chem. Int. Ed.* , 2013, **52**, 812-847.
23. A. Fujishima and K. Honda, *Nature*, 1972, **238**, 37-38.

24. D. Ravelli, D. Dondi, M. Fagnoni and A. Albini, *Chem. Soc. Rev.*, 2009, **38**, 1999-2011.
25. M. Fagnoni, D. Dondi, D. Ravelli and A. Albini, *Chem. Rev.*, 2007, **107**, 2725-2756.
26. B. Ohtani, *J. Photochem. Photobiol. C Photochem. Rev.*, 2010, **11**, 157-178.
27. M. G. Walter, E. L. Warren, J. R. McKone, S. W. Boettcher, Q. Mi, E. A. Santori and N. S. Lewis, *Chem. Rev.*, 2010, **110**, 6446-6473.
28. M. Z. Rahman, C. W. Kwong, K. Davey and S. Z. Qiao, *Energy Environ. Sci.*, 2016, **9**, 709-728.
29. S. Chen, T. Takata and K. Domen, *Nat. Rev. Mater.*, 2017, **2**, 17050.
30. M. Z. Rahman, *Renewable Sustainable Energy Rev.*, 2014, **30**, 734-742.
31. M. Z. Rahman and S. I. Khan, *Mater. Renew. Sust. Energy*, 2012, **1**.
32. M. Z. Rahman, Y. Tang and P. Kwong, *Appl. Phys. Lett.*, 2018, **112**, 253902.
33. M. Z. Rahman and C. B. Mullins, *Acc. Chem. Res.*, 2018, **52**, 248-257.
34. T. Hisatomi, K. Takanabe and K. Domen, *Catal Lett*, 2014, **145**, 95-108.
35. J. E. Kroeze, T. J. Savenije and J. M. Warman, *J. Am. Chem. Soc.*, 2004, **126**, 7608-7618.
36. B. Enright and D. Fitzmaurice, *J. Phys. Chem.*, 1996, **100**, 1027-1035.
37. J. Bisquert, *Phys. Chem. Chem. Phys.*, 2008, **10**, 3175-3194.
38. M. A. Henderson, *Surface Sci. Rep.*, 2011, **66**, 185-297.
39. A. Kubacka, M. Fernandez-Garcia and G. Colon, *Chem. Rev.*, 2011, **112**, 1555-1614.
40. A. Fujishima, X. Zhang and D. Tryk, *Surface Sci. Rep.*, 2008, **63**, 515-582.
41. Y. Tamaki, A. Furube, M. Murai, K. Hara, R. Katoh and M. Tachiya, *J. Am. Chem. Soc.*, 2006, **128**, 416-417.
42. K. Maeda, *ACS Catal.*, 2013, **3**, 1486-1503.
43. A. J. Bard, *Science*, 1980, **207**, 139.
44. N. Serpone and A. V. Emeline, *J. Phys. Chem. Lett.*, 2012, **3**, 673-677.
45. J. Sato, N. Saito, Y. Yamada, K. Maeda, T. Takata, J. N. Kondo, M. Hara, H. Kobayashi, K. Domen and Y. Inoue, *J. Am. Chem. Soc.*, 2005, **127**, 4150-4151.
46. K. Maeda, K. Teramura, D. Lu, T. Takata, N. Saito, Y. Inoue and K. Domen, *Nature*, 2006, **440**, 295-295.
47. N. Arai, N. Saito, H. Nishiyama, Y. Inoue, K. Domen and K. Sato, *Chem. Lett.*, 2006, **35**, 796-797.
48. C. A. Gueymard, *Solar Energy*, 2004, **76**, 423-453.
49. R. Niishiro, H. Kato and A. Kudo, *Phys. Chem. Chem. Phys.*, 2005, **7**, 2241-2245.
50. Y. Sakata, Y. Matsuda, T. Yanagida, K. Hirata, H. Imamura and K. Teramura, *Catal. Lett.*, 2008, **125**, 22-26.
51. R. Asahi, T. Morikawa, T. Ohwaki, K. Aoki and Y. Taga, *Science*, 2001, **293**, 269-271.
52. M. Yashima, Y. Lee and K. Domen, *Chem. Mater.*, 2007, **19**, 588-593.
53. X. Li, N. Kikugawa and J. Ye, *Adv. Mater.*, 2008, **20**, 3816-3819.
54. T. Nakahira, Y. Inoue, K. Iwasaki, H. Tanigawa, Y. Kouda, S. Iwabuchi, K. Kojima and M. Grätzel, *Makromol. Chem., Rapid Commun.*, 1988, **9**, 13-17.
55. J. Fang, S.-W. Cao, Z. Wang, M. M. Shahjamali, S. C. J. Loo, J. Barber and C. Xue, *Int. J. Hydrogen Energy*, 2012, **37**, 17853-17861.
56. E. Kowalska, O. O. Mahaney, R. Abe and B. Ohtani, *Phys. Chem. Chem. Phys.*, 2010, **12**, 2344-2355.
57. M. G. Méndez-Medrano, E. Kowalska, A. Lehoux, A. Herissan, B. Ohtani, S. Rau, C. Colbeau-Justin, J. L. Rodríguez-López and H. Remita, *J. Phys. Chem. C*, 2016, **120**, 25010-25022.
58. E. Bae, W. Choi, J. Park, H. S. Shin, S. B. Kim and J. S. Lee, *J. Phys. Chem. B*, 2004, **108**, 14093-14101.
59. J. R. Darwent and A. Mills, *J. Chem. Soc., Faraday Trans. 2: Mol. Chem. Phys.*, 1982, **78**, 359-367.
60. W. Erbs, J. Desilvestro, E. Borgarello and M. Graetzel, *J. Phys. Chem.*, 1984, **88**, 4001-4006.
61. Z. Zou, J. Ye, K. Sayama and H. Arakawa, *Nature*, 2001, **414**, 625-627.
62. Z. Zou, J. Ye and H. Arakawa, *J. Phys. Chem. B*, 2002, **106**, 13098-13101.
63. H. Liu, J. Yuan, W. Shangguan and Y. Teraoka, *J. Phys. Chem. C*, 2008, **112**, 8521-8523.
64. D. E. Scaife, *Solar Energy*, 1980, **25**, 41-54.
65. H. Kato and A. Kudo, *J. Phys. Chem. B*, 2002, **106**, 5029-5034.
66. R. Niishiro, R. Konta, H. Kato, W.-J. Chun, K. Asakura and A. Kudo, *J. Phys. Chem. C*, 2007, **111**, 17420-17426.
67. H. G. Kim, D. W. Hwang and J. S. Lee, *J J. Am. Chem. Soc.*, 2004, **126**, 8912-8913.
68. H. G. Kim, O. S. Becker, J. S. Jang, S. M. Ji, P. H. Borse and J. S. Lee, *J. Solid State Chem.*, 2006, **179**, 1214-1218.
69. J. Yu and A. Kudo, *Adv. Funct. Mater.*, 2006, **16**, 2163-2169.
70. H. Liu, R. Nakamura and Y. Nakato, *ChemPhysChem*, 2005, **6**, 2499-2502.
71. Y. Hosogi, Y. Shimodaira, H. Kato, H. Kobayashi and A. Kudo, *Chem. Mater.*, 2008, **20**, 1299-1307.
72. R. Abe, K. Sayama and H. Arakawa, *Chem. Phys. Lett.*, 2003, **379**, 230-235.
73. R. Abe, K. Sayama and H. Arakawa, *J. Photochem. Photobiol. A Chem.*, 2004, **166**, 115-122.
74. Q. Simon, D. Barreca, D. Bekermann, A. Gasparotto, C. Maccato, E. Comini, V. Gombac, P. Fornasiero, O. I. Lebedev, S. Turner, A. Devi, R. A. Fischer and G. Van Tendeloo, *Int. J. Hydrogen Energy*, 2011, **36**, 15527-15537.
75. D. Barreca, P. Fornasiero, A. Gasparotto, V. Gombac, C. Maccato, A. Pozza and E. Tondello, *Chem. Vap. Deposition*, 2010, **16**, 296-300.
76. A. Gasparotto, D. Barreca, D. Bekermann, A. Devi, R. A. Fischer, P. Fornasiero, V. Gombac, O. I. Lebedev, C. Maccato, T. Montini, G. Van Tendeloo and E. Tondello, *J. Am. Chem. Soc.*, 2011, **133**, 19362-19365.
77. Q. Simon, D. Barreca, A. Gasparotto, C. Maccato, T. Montini, V. Gombac, P. Fornasiero, O. I. Lebedev, S. Turner and G. Van Tendeloo, *J. Mater. Chem.* , 2012, **22**.
78. M. Cargnello, A. Gasparotto, V. Gombac, T. Montini, D. Barreca and P. Fornasiero, *Eur. J. Inorg. Chem.*, 2011, **2011**, 4309-4323.
79. C. Maccato, D. Barreca, G. Carraro, A. Gasparotto, V. Gombac and P. Fornasiero, *Surface Coat. Technol.*, 2013, **230**, 219-227.
80. M. Matsumura, Y. Saho and H. Tsubomura, *J. Phys. Chem.*, 1983, **87**, 3807-3808.

81. C. Xing, Y. Zhang, W. Yan and L. Guo, *Int. J. Hydrogen Energy*, 2006, **31**, 2018-2024.
82. K. Kobayakawa, A. Teranishi, T. Tsurumaki, Y. Sato and A. Fujishima, *Electrochim. Acta*, 1992, **37**, 465-467.
83. D. Chen and J. Ye, *J. Phys. Chem. Solid.*, 2007, **68**, 2317-2320.
84. N. Zheng, X. Bu, H. Vu and P. Feng, *Angewa. Chem. Int. Ed.*, 2005, **44**, 5299-5303.
85. N. Zheng, X. Bu and P. Feng, *J. Am. Chem. Soc.*, 2005, **127**, 5286-5287.
86. I. Tsuji, H. Kato, H. Kobayashi and A. Kudo, *J. Am. Chem. Soc.*, 2004, **126**, 13406-13413.
87. I. Tsuji, H. Kato and A. Kudo, *Angewa. Chem. Int. Ed.*, 2005, **44**, 3565-3568.
88. J. S. Jang, P. H. Borse, J. S. Lee, S. H. Choi and H. G. Kim, *J. Chem. Phys.*, 2008, **128**, 154717.
89. C. Acar, I. Dincer and C. Zamfirescu, *Int. Energy Res.*, 2014, **38**, 1903-1920.
90. N. Kakuta, K. H. Park, M. F. Finlayson, A. Ueno, A. J. Bard, A. Campion, M. A. Fox, S. E. Webber and J. M. White, *J. Phys. Chem.*, 1985, **89**, 732-734.
91. A. Kudo and M. Sekizawa, *Catal Lett*, 1999, **58**, 241-243.
92. I. Tsuji, H. Kato and A. Kudo, *Chem. Mater.*, 2006, **18**, 1969-1975.
93. W. Shangguan and A. Yoshida, *J. Phys. Chem. B*, 2002, **106**, 12227-12230.
94. S. Shen and L. Guo, *J. Solid State Chem.*, 2006, **179**, 2629-2635.
95. K. Maeda, K. Teramura, N. Saito, Y. Inoue and K. Domen, *J. Catal.*, 2006, **243**, 303-308.
96. G. Hitoki, T. Takata, J. N. Kondo, M. Hara, H. Kobayashi and K. Domen, *Chem. Commun.*, 2002, 1698-1699.
97. A. Kasahara, K. Nukumizu, G. Hitoki, T. Takata, J. N. Kondo, M. Hara, H. Kobayashi and K. Domen, *J. Phys. Chem. A*, 2002, **106**, 6750-6753.
98. A. Kasahara, K. Nukumizu, T. Takata, J. N. Kondo, M. Hara, H. Kobayashi and K. Domen, *J. Phys. Chem. B*, 2002, **107**, 791-797.
99. K. Nukumizu, J. Nunoshige, T. Takata, J. N. Kondo, M. Hara, H. Kobayashi and K. Domen, *Chem. Lett.*, 2003, **32**, 196-197.
100. K. Maeda, Y. Shimodaira, B. Lee, K. Teramura, D. Lu, H. Kobayashi and K. Domen, *J. Phys. Chem. C*, 2007, **111**, 18264-18270.
101. K. Maeda, B. Lee, D. Lu and K. Domen, *Chem. Mater.*, 2009, **21**, 2286-2291.
102. B. Siritanaratkul, K. Maeda, T. Hisatomi and K. Domen, *ChemSusChem*, 2011, **4**, 74-78.
103. A. Ishikawa, T. Takata, J. N. Kondo, M. Hara, H. Kobayashi and K. Domen, *J. Am. Chem. Soc.*, 2002, **124**, 13547-13553.
104. A. Ishikawa, Y. Yamada, T. Takata, J. N. Kondo, M. Hara, H. Kobayashi and K. Domen, *Chem. Mater.*, 2003, **15**, 4442-4446.
105. A. Ishikawa, T. Takata, T. Matsumura, J. N. Kondo, M. Hara, H. Kobayashi and K. Domen, *J. Phys. Chem. B*, 2004, **108**, 2637-2642.
106. M. Jansen and H. P. Letschert, *Nature*, 2000, **404**, 980-982.
107. R. Abe, M. Higashi and K. Domen, *J. Am. Chem. Soc.*, 2010, **132**, 11828-11829.
108. M. Hara, T. Takata, J. N. Kondo and K. Domen, *Catal. Today*, 2004, **90**, 313-317.
109. X. Wang, K. Maeda, A. Thomas, K. Takanabe, G. Xin, J. M. Carlsson, K. Domen and M. Antonietti, *Nat. Mater.*, 2009, **8**, 76-80.
110. J. Zhang, X. Chen , K. Takanabe, K. Maeda, K. Domen, J. D. Epping, X. Fu, M. Antonietti and X. Wang *Angewa. Chem. Int. Ed.*, 2010, **49**, 441-444.
111. C. Peng, J. Gao, S. Wang, X. Zhang, X. Zhang and X. Sun, *J. Phys. Chem. C*, 2011, **115**, 3866-3871.
112. F. Wang, W. K. H. Ng, J. C. Yu, H. Zhu, C. Li, L. Zhang, Z. Liu and Q. Li, *Appl. Catal. B Environ.*, 2012, **111-112**, 409-414.
113. G. Liu, P. Niu, L. Yin and H.-M. Cheng, *J. Am. Chem. Soc.*, 2012, **134**, 9070-9073.
114. Y.-D. Chiou and Y.-J. Hsu, *Appl. Catal. B Environ.l*, 2011, **105**, 211-219.
115. Y. Wang, A. Vogel, M. Sachs, R. S. Sprick, L. Wilbraham, S. J. A. Moniz, R. Godin, M. A. Zwijnenburg, J. R. Durrant, A. I. Cooper and J. Tang, *Nat. Energy*, 2019, **4**, 746-760.
116. S. Ghosh, N. A. Kouamé, L. Ramos, S. Remita, A. Dazzi, A. Deniset-Besseau, P. Beaunier, F. Goubard, P.-H. Aubert and H. Remita, *Nat. Mater.*, 2015, **14**, 505-511.
117. S. Ghosh, N. A. Kouame, S. Remita, L. Ramos, F. Goubard, P. H. Aubert, A. Dazzi, A. Deniset-Besseau and H. Remita, *Sci. Rep.*, 2015, **5**, 18002.
118. X. Yuan, D. Dragoe, P. Beaunier, D. B. Uribe, L. Ramos, M. G. Méndez-Medrano and H. Remita, *J. Mater. Chem. A*, 2020, **8**, 268-277.
119. G. Liu, L. C. Yin, P. Niu, W. Jiao and H. M. Cheng, *Angew. Chem. Int. Ed.* , 2013, **52**, 6242-6245.
120. G. A. M. Hutton, B. C. M. Martindale and E. Reisner, *Chem. Soc. Rev.*, 2017, **46**, 6111-6123.
121. P. Yang, J. Zhao, J. Wang, H. Cui, L. Li and Z. Zhu, *RSC Adv.*, 2015, **5**, 21332-21335.
122. B. C. M. Martindale, G. A. M. Hutton, C. A. Caputo, S. Prantl, R. Godin, J. R. Durrant and E. Reisner, *Angew. Chem. Int. Ed.* , 2017, **56**, 6459-6463.
123. G. Xie, K. Zhang, B. Guo, Q. Liu, L. Fang and J. R. Gong, *Adv Mater*, 2013, **25**, 3820-3839.
124. M. Latorre-Sánchez, A. Primo and H. García, *Angew. Chem. Int. Ed.*, 2013, **52**, 11813-11816.
125. C. Lavorato, A. Primo, R. Molinari and H. Garcia, *Chem. Eur. J.*, 2014, **20**, 187-194.
126. N. Zhang, Y. Zhang and Y.-J. Xu, *Nanoscale*, 2012, **4**.
127. Z. Hu, L. Yuan, Z. Liu, Z. Shen and J. C. Yu, *Angew Chem Int Ed Engl*, 2016, **55**, 9580-9585.
128. H. Liu, A. T. Neal, Z. Zhu, Z. Luo, X. Xu, D. Tománek and P. D. Ye, *ACS Nano*, 2014, **8**, 4033-4041.
129. X. Wang, A. M. Jones, K. L. Seyler, V. Tran, Y. Jia, H. Zhao, H. Wang, L. Yang, X. Xu and F. Xia, *Nat. Nanotechnol.*, 2015, **10**, 517-521.
130. L. Li, Y. Yu, G. J. Ye, Q. Ge, X. Ou, H. Wu, D. Feng, X. H. Chen and Y. Zhang, *Nat. Nanotechnol.*, 2014, **9**, 372-377.
131. X. Zhu, T. Zhang, Z. Sun, H. Chen, J. Guan, X. Chen, H. Ji, P. Du and S. Yang, *Adv. Mater.*, 2017, **29**, 1605776.
132. W. Hu, L. Lin, R. Zhang, C. Yang and J. Yang, *J. Am. Chem. Soc.*, 2017, **139**, 15429-15436.
133. B. Tian, B. Tian, B. Smith, M. C. Scott, Q. Lei, R. Hua, Y. Tian and Y. Liu, *Proc. Natl. Acad. Sci.*, 2018, **115**, 4345-4350.
134. M. Z. Rahman, M. Batmunkh, M. Bat-Erdene, J. G. Shapter and C. B. Mullins, *J. Mater. Chem. A*, 2018, **6**, 18403-18408.
135. Z. Hu, Z. Shen and J. C. Yu, *Green Chem.*, 2017, **19**, 588-613.
136. A. B. Smith, *Chem. Eng. News Archive*, 2003, **81**, 60.
137. B. Meyer, *Chem. Rev.*, 1976, **76**, 367-388.

138. B. Meyer, *Chem. Rev.*, 1964, **64**, 429-451.
139. A. K. Abass and N. H. Ahmad, *J. Phys. Chem. Solid.*, 1986, **47**, 143-145.
140. G. Liu, P. Niu, L. Yin and H. M. Cheng, *J. Am. Chem. Soc.*, 2012, **134**, 9070-9073.
141. D. Liu, J. Ma, R. Long, C. Gao and Y. Xiong, *Nano Today*, 2017, **17**, 96-116.
142. J. Kouvetakis, R. B. Kaner, M. L. Sattler and N. Bartlett, *Chem. Commun.*, 1986,1758-1759.
143. H. Yanagisawa, T. Tanaka, Y. Ishida, M. Matsue, E. Rokuta, S. Otani and C. Oshima, *Phys. Rev. Lett.*, 2004, **93**, 177003.
144. H. Tanaka, Y. Kawamata, H. Simizu, T. Fujita, H. Yanagisawa, S. Otani and C. Oshima, *Solid State Commun.*, 2005, **136**, 22-25.
145. H. Zhang, Y. Liao, G. Yang and X. Zhou, *ACS Omega*, 2018, **3**, 10517-10525.
146. H. Werheit, *J. Phys. Condens. Matter.*, 2006, **18**, 10655-10662.
147. H. Werheit, T. Au, R. Schmechel, S. O. Shalamberidze, G. I. Kalandadze and A. M. Eristavi, *J. Solid State Chem.*, 2000, **154**, 79-86.
148. K. A. Schwetz and P. Karduck, presented in part at the AIP Conf. Proc., 1991.
149. R. Schmechel and H. Werheit, *J. Phys. Condens. Matter.*, 1999, **11**, 6803-6813.
150. R. Schmechel and H. Werheit, *J. Solid State Chem.*, 2000, **154**, 61-67.
151. R. Schmechel, H. Werheit, T. U. Kampen and W. Mönch, *J. Solid State Chem.*, 2004, **177**, 566-568.
152. J. Liu, S. Wen, Y. Hou, F. Zuo, G. J. Beran and P. Feng, *Angew. Chem. Int. Ed.*, 2013, **52**, 3241-3245.
153. H. Hubert, B. Devouard, L. A. J. Garvie, M. O'Keeffe, P. R. Buseck, W. T. Petuskey and P. F. McMillan, *Nature*, 1998, **391**, 376-378.
154. D. Yan, P. Liu, Q. Tao, P. Zhu, J. Liu and H. a. Luo, *Solar RRL*, 2019, **3**, 1900014.
155. P. Popper and T. A. Ingles, *Nature*, 1957, **179**, 1075-1075.
156. F. V. Williams and R. A. Ruehrwein, *J. Am. Chem. Soc.*, 1960, **82**, 1330-1332.
157. L. Shi, P. Li, W. Zhou, T. Wang, K. Chang, H. Zhang, T. Kako, G. Liu and J. Ye, *Nano Energy*, 2016, **28**, 158-163.
158. T. Takenaka, M. Takigawa and K. Shohno, *J. Electrochem. Soc.*, 1978, **125**, 633-637.
159. L. Ju-seong, F. Akira, H. Kenichi and K. Yukinobu, *Bull. Chem. Soc. Jap.*, 1985, **58**, 2634-2637.
160. G. Zhao, A. Wang, W. He, Y. Xing and X. Xu, *Adv. Mater. Interfaces*, 2019, **6**, 1900062.
161. J. LIEBIG, *Ann. Pharm.*, 1834, **10**, 1-47.
162. B. V. Lotsch, M. Doblinger, J. Sehnert, L. Seyfarth, J. Senker, O. Oeckler and W. Schnick, *Chem. Eur. J.*, 2007, **13**, 4969-4980.
163. M. Doblinger, B. V. Lotsch, J. Wack, J. Thun, J. Senker and W. Schnick, *Chem. Commun.*, 2009, 1541-1543.
164. F. K. Kessler and W. Schnick, *Zeit. anorg. allgem. Chemi.*, 2019, **645**, 857-862.
165. M. J. Bojdys, J. O. Muller, M. Antonietti and A. Thomas, *Chem. Eur. J.*, 2008, **14**, 8177-8182.
166. M. Z. Rahman, J. Ran, Y. Tang, M. Jaroniec and S. Z. Qiao, *J. Mater. Chem. A*, 2016, **4**, 2445-2452.
167. Y. Kang, Y. Yang, L. C. Yin, X. Kang, G. Liu and H. M. Cheng, *Adv. Mater.*, 2015, **27**, 4572-4577.
168. M. Z. Rahman, P. C. Tapping, T. W. Kee, R. Smernik, N. Spooner, J. Moffatt, Y. Tang, K. Davey and S.-Z. Qiao, *Adv. Funct. Mater.*, 2017, **27**, 1702384.
169. M. Rahman, K. Davey and S. Z. Qiao, *Small*, 2017, **13**, 1700376.
170. L. Jiang, X. Yuan, Y. Pan, J. Liang, G. Zeng, Z. Wu and H. Wang, *Appl. Catal. B Environ.*, 2017, **217**, 388-406.
171. P. Yang, R. Wang, M. Zhou and X. Wang, *Angew. Chem. Int. Ed.* , 2018, **57**, 8674-8677.
172. G. Zhang, G. Li, Z. A. Lan, L. Lin, A. Savateev, T. Heil, S. Zafeiratos, X. Wang and M. Antonietti, *Angew. Chem. Int. Ed.*, 2017, **56**, 13445-13449.
173. H. Ou, P. Yang, L. Lin, M. Anpo and X. Wang, *Angew. Chem. Int. Ed.*, 2017, **56**, 10905-10910.
174. P. Yang, H. Ou, Y. Fang and X. Wang, *Angew. Chem. Int. Ed.* , 2017, **56**, 3992-3996.
175. L. Lin, H. Ou, Y. Zhang and X. Wang, *ACS Catal.*, 2016, **6**, 3921-3931.
176. D. Zheng, X. N. Cao and X. Wang, *Angew. Chem. Int. Ed.*, 2016, **55**, 11512-11516.
177. J. Zhang, G. Zhang, X. Chen, S. Lin, L. Mohlmann, G. Dolega, G. Lipner, M. Antonietti, S. Blechert and X. Wang, *Angew. Chem. Int. Ed.* , 2012, **51**, 3183-3187.
178. J. Zhang, M. Zhang, R. Q. Sun and X. Wang, *Angew. Chem. Int. Ed.* , 2012, **51**, 10145-10149.
179. J. Zhang, X. Chen, K. Takanabe, K. Maeda, K. Domen, J. D. Epping, X. Fu, M. Antonietti and X. Wang, *Angew. Chem. Int. Ed.* , 2010, **49**, 441-444.
180. K. Maeda, X. Wang, Y. Nishihara, D. Lu, M. Antonietti and K. Domen, *J. Phys. Chem. C*, 2009, **113**, 4940-4947.
181. J. Mahmood, E. K. Lee, M. Jung, D. Shin, H. J. Choi, J. M. Seo, S. M. Jung, D. Kim, F. Li, M. S. Lah, N. Park, H. J. Shin, J. H. Oh and J. B. Baek, *Proc. Natl. Acad. Sci.* , 2016, **113**, 7414-7419.
182. J. Mahmood, E. K. Lee, M. Jung, D. Shin, I. Y. Jeon, S. M. Jung, H. J. Choi, J. M. Seo, S. Y. Bae, S. D. Sohn, N. Park, J. H. Oh, H. J. Shin and J. B. Baek, *Nat .Commun.*, 2015, **6**, 6486.
183. N. Fechler, N. P. Zussblatt, R. Rothe, R. Schlogl, M. G. Willinger, B. F. Chmelka and M. Antonietti, *Adv. Mater.*, 2016, **28**, 1287-1294.
184. S. N. Talapaneni, G. P. Mane, D.-H. Park, K. S. Lakhi, K. Ramadass, S. Joseph, W. M. Skinner, U. Ravon, K. Al-Bahily and A. Vinu, *J. Mater. Chem. A*, 2017, **5**, 18183-18192.
185. G. P. Mane, S. N. Talapaneni, K. S. Lakhi, H. Ilbeygi, U. Ravon, K. Al-Bahily, T. Mori, D. H. Park and A. Vinu, *Angew. Chem. Int. Ed.*, 2017, **56**, 8481-8485.
186. J. Mahmood, F. Li, S. M. Jung, M. S. Okyay, I. Ahmad, S. J. Kim, N. Park, H. Y. Jeong and J. B. Baek, *Nat. Nanotechnol.*, 2017, **12**, 441-446.
187. J. Mahmood, S.-M. Jung, S.-J. Kim, J. Park, J.-W. Yoo and J.-B. Baek, *Chem. Mater.*, 2015, **27**, 4860-4864.
188. P. Kumar, E. Vahidzadeh, U. K. Thakur, P. Kar, K. M. Alam, A. Goswami, N. Mahdi, K. Cui, G. M. Bernard, V. K. Michaelis and K. Shankar, *J. Am. Chem. Soc.*, 2019, **141**, 5415−5436.
189. M. Z. Rahman, J. Moffatt and N. Spooner, *Mater. Horiz.*, 2018, **5**, 553-559.
190. M. Rahman and K. Davey, *Phys. Rev. Mater.*, 2018, **2**, 125402.
191. J. Fu, J. Yu, C. Jiang and B. Cheng, *Adv. Energy Mater.*, 2018, **8**.

192. Z. Zhang and J. T. Yates, Jr., *Chem. Rev.*, 2012, **112**, 5520-5551.
193. L. Zhang, H. H. Mohamed, R. Dillert and D. Bahnemann, *J. Photochem. Photobiol. C: Photochem. Rev.*, 2012, **13**, 263-276.
194. C. Merschjann, T. Tyborski, S. Orthmann, F. Yang, K. Schwarzburg, M. Lublow, M. C. Lux-Steiner and T. Schedel-Niedrig, *Phys. Rev. B*, 2013, **87**, 205204.
195. T. M. Clarke and J. R. Durrant, *Chem. Rev.*, 2010, **110**, 6736-6767.
196. K. L. Corp and C. W. Schlenker, *J. Am. Chem. Soc.*, 2017, **139**, 7904-7912.
197. C. Merschjann, S. Tschierlei, T. Tyborski, K. Kailasam, S. Orthmann, D. Hollmann, T. Schedel-Niedrig, A. Thomas and S. Lochbrunner, *Adv. Mater.*, 2015, **27**, 7993-7999.
198. R. Godin, Y. Wang, M. A. Zwijnenburg, J. Tang and J. R. Durrant, *J. Am. Chem. Soc.*, 2017, **139**, 5216-5224.
199. V. E. Ferry, A. Polman and H. A. Atwater, *ACS Nano*, 2011, **5**, 10055-10064.
200. T. Tyborski, C. Merschjann, S. Orthmann, F. Yang, M. C. Lux-Steiner and T. Schedel-Niedrig, *J. Phys. Condens. Matter.*, 2012, **24**, 162201.
201. H. Zhang, Y. Chen, R. Lu, R. Li and A. Yu, *Phys. Chem. Chem. Phys.*, 2016, **18**, 14904-14910.
202. G. Zhou, Y. Shan, Y. Hu, X. Xu, L. Long, J. Zhang, J. Dai, J. Guo, J. Shen, S. Li, L. Liu and X. Wu, *Nat. Commun.*, 2018, **9**, 3366.
203. J. H. Park, E. Vescovo, H. J. Kim, C. Kwon, R. Ramesh and T. Venkatesan, *Nature*, 1998, **392**, 794.
204. H. Ma, J. Feng, F. Jin, M. Wei, C. Liu and Y. Ma, *Nanoscale*, 2018, **10**, 15624-15631.
205. Z. Chen, Q. Zhang and Y. Luo, *Angew. Chem. Int. Ed.* , 2018, **57**, 5320-5324.
206. G. Zhang, L. Lin, G. Li, Y. Zhang, A. Savateev, X. Wang and M. Antonietti, *Angew. Chem. Int. Ed.*, 2018, **57**, 9372 – 9376.
207. Y. Chen, J. Li, Z. Hong, B. Shen, B. Lin and B. Gao, *Phys. Chem. Chem. Phys.*, 2014, **16**, 8106-8113.
208. Z. Wu, H. Gao, S. Yan and Z. Zou, *Dalton Trans.*, 2014, **43**, 12013-12017.
209. Q. Xiang, J. Yu and M. Jaroniec, *J. Phys. Chem. C*, 2011, **115**, 7355-7363.
210. L. Yang, X. Li, G. Zhang, P. Cui, X. Wang, X. Jiang, J. Zhao, Y. Luo and J. Jiang, *Nat. Commun.*, 2017, **8**, 16049.
211. Q. Liu, T. Chen, Y. Guo, Z. Zhang and X. Fang, *Appl. Catal. B Environ.*, 2016, **193**, 248-258.
212. Q. Han, B. Wang, J. Gao and L. Qu, *Angew. Chem. Int. Ed.*, 2016, **55**, 10849-10853.
213. X. Zhang, B. Peng, S. Zhang and T. Peng, *ACS Sust. Chem. Eng.*, 2015, **3**, 1501-1509.
214. L. Song, T. Li and S. Zhang, *J. Phys. Chem. C*, 2017, **121**, 293-299.
215. A. Jin, Y. Jia, C. Chen, X. Liu, J. Jiang, X. Chen and F. Zhang, *J. Phys. Chem. C*, 2017, **121**, 21497-21509.
216. M. Zhou, Z. Hou, L. Zhang, Y. Liu, Q. Gao and X. Chen, *Sust. Energy Fuels*, 2017, **1**, 317-323.
217. M. Zhu, S. Kim, L. Mao, M. Fujitsuka, J. Zhang, X. Wang and T. Majima, *J. Am. Chem. Soc.*, 2017, **139**, 13234-13242.
218. Y.-P. Yuan, S.-W. Cao, Y.-S. Liao, L.-S. Yin and C. Xue, *Appl. Catal. B Environ.*, 2013, **140-141**, 164-168.
219. R. Godin, A. Kafizas and J. R. Durrant, *Curr. Op. Electrochem.*, 2017, **2**, 136-143.
220. L. Jing, R. Zhu, D. L. Phillips and J. C. Yu, *Adv. Funct. Mater.*, 2017, 29, 1703484.
221. G. Liu, G. Zhao, W. Zhou, Y. Liu, H. Pang, H. Zhang, D. Hao, X. Meng, P. Li, T. Kako and J. Ye, *Adv. Funct. Mater.*, 2016, 28, 1602779.
222. J. Chen, C.-L. Dong, D. Zhao, Y.-C. Huang, X. Wang, L. Samad, L. Dang, M. Shearer, S. Shen and L. Guo, *Adv. Mater.*, 2017, 29, 1606198.
223. J. Liu, Y. Liu, N. Liu, Y. Han, X. Zhang, H. Huang, Y. Lifshitz, S.-T. Lee, J. Zhong and Z. Kang, *Science*, 2015, **347**, 970-974.
224. W. Che, W. Cheng, T. Yao, F. Tang, W. Liu, H. Su, Y. Huang, Q. Liu, J. Liu, F. Hu, Z. Pan, Z. Sun and S. Wei, *J. Am. Chem. Soc.*, 2017, **139**, 3021-3026.
225. S. Wang, L. Zhang, Z. Xia, A. Roy, D. W. Chang, J.-B. Baek and L. Dai, *Angew. Chem. Int. Ed.*, 2012, **51**, 4209-4212.
226. C. N. R. Rao and M. Chhetri, *Adv. Mater.*, 2019, **31**, e1803668.
227. L. Chen and X. Wang, *Chem. Commun.*, 2017, **53**, 11988-11991.
228. Z. Luo, Y. Fang, M. Zhou and X. Wang, *Angew. Chem. Int. Ed.*, 2019, **58**, 6033-6037.
229. L. Song, *Adv. Mater.*, 2012, **24**, 4878-4895.
230. A. Pakdel, Y. Bando and D. Golberg, *Chem. Soc. Rev.*, 2014, **43**, 934-959.
231. A. Pakdel, X. Wang, C. Zhi, Y. Bando, K. Watanabe, T. Sekiguchi, T. Nakayama and D. Golberg, *J. Mater. Chem.*, 2012, **22**, 4818-4824.
232. R. Nascimento, J. d. R. Martins, R. J. C. Batista and H. Chacham, *J. Phys. Chem. C*, 2015, **119**, 5055-5061.
233. Y. Lin and J. W. Connell, *Nanoscale*, 2012, **4**, 6908-6939.
234. L. Ci, *Nat. Mater.*, 2010, **9**, 430-435.
235. R. Zhao, J. Wang, M. Yang, Z. Liu and Z. Liu, *J. Phys. Chem. C*, 2012, **116**, 21098-21103.
236. P. Karamanis, N. Otero and C. Pouchan, *J. Phys. Chem. C*, 2015, **119**, 11872-11885.
237. C. Huang, C. Chen, M. Zhang, L. Lin, X. Ye, S. Lin, M. Antonietti and X. Wang, *Nat. Commun.*, 2015, **6**.
238. X. Li, J. Zhao and J. Yang, *Sci. Rep.*, 2013, **3**, 1858.
239. N. kumar, K. Moses, K. Pramoda, S. N. Shirodkar, A. K. Mishra, U. V. Waghmare, A. Sundaresan and C. N. R. Rao, *J. Mater. Chem. A*, 2013, **1**, 5806.
240. R. Sen, B. C. Satishkumar, A. Govindaraj, K. R. Harikumar, G. Raina, J.-P. Zhang, A. K. Cheetham and C. N. R. Rao, *Chem. Phys. Lett.*, 1998, **287**, 671-676.
241. S. Y. Kim, J. Park, H. C. Choi, J. P. Ahn, J. Q. Hou and H. S. Kang, *J. Am. Chem. Soc.*, 2007, **129**, 1705-1716.
242. K. Raidongia, K. P. S. S. Hembram, Umesh V. Waghmare, M. Eswaramoorthy and C. N. R. Rao, *Z. Anorg. Allg. Chem.*, 2010, **636**, 30-35.
243. A. J. Cowan and J. R. Durrant, *Chem. Soc. Rev.*, 2013, **42**, 2281-2293.
244. G. Liu, K. Du, S. Haussener and K. Wang, *ChemSusChem*, 2016, **9**, 2878-2904.
245. I. Roger, M. A. Shipman and M. D. Symes, *Nat. Rev. Chem.*, 2017, **1**, 0003.
246. Y. Yang, J. Gu, J. L. Young, E. M. Miller, J. A. Turner, N. R. Neale and M. C. Beard, *Science*, 2015, **350**, 1061-1065.
247. K. Appavoo, M. Liu, C. T. Black and M. Y. Sfeir, *Nano Lett.*, 2015, **15**, 1076-1082.
248. M. Z. Rahman, J. Zhang, Y. Tang, K. Davey and S.-Z. Qiao, *Mater. Chem. Front.*, 2017, **1**, 562-571.

249. Y. Bai, H. Huang, C. Wang, R. Long and Y. Xiong, *Mater. Chem. Front.*, 2017, **1**, 1951-1964.
250. S. Bai and Y. Xiong, *Chem. Commun.*, 2015, **51**, 10261-10271.
251. G. Zhang, Z. A. Lan and X. Wang, *Angew. Chem. Int. Ed.*, 2016, **55**, 15712-15727.
252. V. S. Vyas, V. W.-h. Lau and B. V. Lotsch, *Chem. Mater.*, 2016, **28**, 5191-5204.
253. S. Yanagida, A. Kabumoto, K. Mizumoto, C. Pac and K. Yoshino, *J. Chem. Soc., Chem. Commun.*, 1985, 474-475.
254. J. Mahmood, M. A. R. Anjum and J. B. Baek, *Adv. Mater.*, 2018, **31**, 1805062.
255. A. Schwarzer, T. Saplinova and E. Kroke, *Coord. Chem. Rev.*, 2013, **257**, 2032-2062.
256. D. Schwarz, Y. Noda, J. Klouda, K. Schwarzova-Peckova, J. Tarabek, J. Rybacek, J. Janousek, F. Simon, M. V. Opanasenko, J. Cejka, A. Acharjya, J. Schmidt, S. Selve, V. Reiter-Scherer, N. Severin, J. P. Rabe, P. Ecorchard, J. He, M. Polozij, P. Nachtigall and M. J. Bojdys, *Adv. Mater.*, 2017, **29**, 1703399.
257. D. Schwarz, Y. S. Kochergin, A. Acharjya, A. Ichangi, M. V. Opanasenko, J. Cejka, U. Lappan, P. Arki, J. He, J. Schmidt, P. Nachtigall, A. Thomas, J. Tarabek and M. J. Bojdys, *Chem. Eur. J.*, 2017, **23**, 13023-13027.
258. S. Kuecken, A. Acharjya, L. Zhi, M. Schwarze, R. Schomacker and A. Thomas, *Chem. Commun.* , 2017, **53**, 5854-5857.
259. P. Pachfule, A. Acharjya, J. Roeser, T. Langenhahn, M. Schwarze, R. Schomacker, A. Thomas and J. Schmidt, *J. Am. Chem. Soc.*, 2018, **140**, 1423-1427.
260. D. Schwarz, A. Acharjya, A. Ichangi, Y. S. Kochergin, P. Lyu, M. V. Opanasenko, J. Tarabek, J. Vacek Chocholousova, J. Vacek, J. Schmidt, J. Cejka, P. Nachtigall, A. Thomas and M. J. Bojdys, *ChemSusChem*, 2019, **12**, 194-199.
261. J. Huang, J. Tarabek, R. Kulkarni, C. Wang, M. Dracinsky, G. J. Smales, Y. Tian, S. Ren, B. R. Pauw, U. Resch-Genger and M. J. Bojdys, *Chem. Eur. J.*, 2019, **53**, 12342-12348.
262. J. Roeser, D. Prill, M. J. Bojdys, P. Fayon, A. Trewin, A. N. Fitch, M. U. Schmidt and A. Thomas, *Nat. Chem.*, 2017, **9**, 977-982.
263. R. S. Sprick, J. X. Jiang, B. Bonillo, S. Ren, T. Ratvijitvech, P. Guiglion, M. A. Zwijnenburg, D. J. Adams and A. I. Cooper, *J. Am. Chem. Soc.*, 2015, **137**, 3265-3270.
264. R. S. Sprick, B. Bonillo, R. Clowes, P. Guiglion, N. J. Brownbill, B. J. Slater, F. Blanc, M. A. Zwijnenburg, D. J. Adams and A. I. Cooper, *Angew. Chem. Int. Ed.*, 2016, **55**, 1792-1796.
265. R. S. Sprick, B. Bonillo, M. Sachs, R. Clowes, J. R. Durrant, D. J. Adams and A. I. Cooper, *Chem. Commun.*, 2016, **52**, 10008-10011.
266. D. J. Woods, R. S. Sprick, C. L. Smith, A. J. Cowan and A. I. Cooper, *Adv. Energy Mater.*, 2017, **7**, 1700479.
267. R. S. Sprick, Y. Bai, A. A. Y. Guilbert, M. Zbiri, C. M. Aitchison, L. Wilbraham, Y. Yan, D. J. Woods, M. A. Zwijnenburg and A. I. Cooper, *Chem. Mater.*, 2018, **31**, 305-313.
268. X. Wang, L. Chen, S. Y. Chong, M. A. Little, Y. Wu, W. H. Zhu, R. Clowes, Y. Yan, M. A. Zwijnenburg, R. S. Sprick and A. I. Cooper, *Nat. Chem.*, 2018, **10**, 1180-1189.
269. Y. Bai, L. Wilbraham, B. J. Slater, M. A. Zwijnenburg, R. S. Sprick and A. I. Cooper, *J. Am. Chem. Soc.*, 2019, **141**, 9063-9071.
270. Catherine M. Aitchison, R. S. Sprick and A. I. Cooper, *J. Mater. Chem. A*, 2019, **7**, 2490-2496.
271. A. Vogel, M. Forster, L. Wilbraham, C. L. Smith, A. J. Cowan, M. A. Zwijnenburg, R. S. Sprick and A. I. Cooper, *Faraday Discuss.*, 2019, **215**, 84-97.
272. C. S. Diercks and O. M. Yaghi, *Science*, 2017, **355**, eaal1585.
273. A. P. Côté, A. I. Benin, N. W. Ockwig, M. Keeffe, A. J. Matzger and O. M. Yaghi, *Science*, 2005, **310**, 1166.
274. N. Huang, P. Wang and D. Jiang, *Nat. Rev. Mater.*, 2016, **1**, 16068.
275. T. Banerjee, K. Gottschling, G. Savasci, C. Ochsenfeld and B. V. Lotsch, *ACS Energy Lett.*, 2018, **3**, 400-409.
276. Y. Jin, Q. Wang, P. Taynton and W. Zhang, *Acc. Chem. Res.*, 2014, **47**, 1575-1586.
277. S. J. Rowan, S. J. Cantrill, G. R. L. Cousins, J. K. M. Sanders and J. F. Stoddart, *Angew. Chem. Int. Ed.*, 2002, **41**, 898-952.
278. S. Kandambeth, K. Dey and R. Banerjee, *J. Am. Chem. Soc.*, 2019, **141**, 1807-1822.
279. M. S. Lohse and T. Bein, *Adv. Funct. Mater.*, 2018, **28**, 1705553.
280. S. Kandambeth, A. Mallick, B. Lukose, M. V. Mane, T. Heine and R. Banerjee, *J. Am. Chem. Soc.*, 2012, **134**, 19524-19527.
281. S. Kandambeth, D. B. Shinde, M. K. Panda, B. Lukose, T. Heine and R. Banerjee, *Angew. Chem. Int. Ed.*, 2013, **52**, 13052-13056.
282. L. Stegbauer, K. Schwinghammer and B. V. Lotsch, *Chem. Sci.*, 2014, **5**, 2789-2793.
283. V. S. Vyas, F. Haase, L. Stegbauer, G. Savasci, F. Podjaski, C. Ochsenfeld and B. V. Lotsch, *Nat. Commun.*, 2015, **6**, 8508.
284. L. Stegbauer, S. Zech, G. Savasci, T. Banerjee, F. Podjaski, K. Schwinghammer, C. Ochsenfeld and B. V. Lotsch, *Adv. Energy Mater.*, 2018, **8**, 1703278.
285. T. Banerjee, F. Haase, G. Savasci, K. Gottschling, C. Ochsenfeld and B. V. Lotsch, *J. Am. Chem. Soc.*, 2017, **139**, 16228-16234.
286. F. Haase, T. Banerjee, G. Savasci, C. Ochsenfeld and B. V. Lotsch, *Faraday Discuss.*, 2017, **201**, 247-264.
287. B. P. Biswal, H. A. Vignolo-Gonzalez, T. Banerjee, L. Grunenberg, G. Savasci, K. Gottschling, J. Nuss, C. Ochsenfeld and B. V. Lotsch, *J. Am. Chem. Soc.*, 2019, **141**, 11082-11092.
288. E. Jin, Z. Lan, Q. Jiang, K. Geng, G. Li, X. Wang and D. Jiang, *Chem*, 2019, **5**, 1632-1647.
289. M. Sachs, R. S. Sprick, D. Pearce, S. A. J. Hillman, A. Monti, A. A. Y. Guilbert, N. J. Brownbill, S. Dimitrov, X. Shi, F. Blanc, M. A. Zwijnenburg, J. Nelson, J. R. Durrant and A. I. Cooper, *Nat. Commun.*, 2018, **9**, 4968.
290. P. Guiglion, A. Monti and M. A. Zwijnenburg, *J. Phys. Chem. C*, 2017, **121**, 1498-1506.
291. M. J. Bojdys, J. Jeromenok, A. Thomas and M. Antonietti, *Adv. Mater.*, 2010, **22**, 2202-2205.
292. G. Algara-Siller, N. Severin, S. Y. Chong, T. Bjorkman, R. G. Palgrave, A. Laybourn, M. Antonietti, Y. Z. Khimyak, A. V. Krasheninnikov, J. P. Rabe, U. Kaiser, A. I. Cooper, A. Thomas and M. J. Bojdys, *Angew. Chem. Int. Ed.* , 2014, **53**, 7450-7455.
293. N. E. Braml, L. Stegbauer, B. V. Lotsch and W. Schnick, *Chem. Eur. J.*, 2015, **21**, 7866-7873.
294. S. Ren, M. J. Bojdys, R. Dawson, A. Laybourn, Y. Z. Khimyak, D. J. Adams and A. I. Cooper, *Adv. Mater.*, 2012, **24**, 2357-2361.

295. M. Liu, L. Guo, S. Jin and B. Tan, *J. Mater. Chem. A*, 2019, **7**, 5153-5172.
296. K. Schwinghammer, B. Tuffy, M. B. Mesch, E. Wirnhier, C. Martineau, F. Taulelle, W. Schnick, J. Senker and B. V. Lotsch, *Angew. Chem. Int. Ed.*, 2013, **52**, 2435-2439.
297. J. Bi, W. Fang, L. Li, J. Wang, S. Liang, Y. He, M. Liu and L. Wu, *Macromol. Rapid. Commun.*, 2015, **36**, 1799-1805.
298. K. Schwinghammer, S. Hug, M. B. Mesch, J. Senker and B. V. Lotsch, *Energy Environ. Sci.*, 2015, **8**, 3345-3353.
299. K. Wang, L.-M. Yang, X. Wang, L. Guo, G. Cheng, C. Zhang, S. Jin, B. Tan and A. Cooper, *Angew. Chem. Int. Ed.*, 2017, **56**, 14149-14153.
300. L. Guo, Y. Niu, H. Xu, Q. Li, S. Razzaque, Q. Huang, S. Jin and B. Tan, *J. Mater. Chem. A*, 2018, **6**, 19775-19781.
301. C. B. Meier, R. S. Sprick, A. Monti, P. Guiglion, J.-S. M. Lee, M. A. Zwijnenburg and A. I. Cooper, *Polymer*, 2017, **126**, 283-290.
302. W. Huang, Q. He, Y. Hu and Y. Li, *Angew. Chem.*, 2019, **131**, 8768-8772.
303. L. Li, W. Fang, P. Zhang, J. Bi, Y. He, J. Wang and W. Su, *J. Mater. Chem. A*, 2016, **4**, 12402-12406.
304. M. Liu, Q. Huang, S. Wang, Z. Li, B. Li, S. Jin and B. Tan, *Angew. Chem. Int. Ed.*, 2018, **57**, 11968-11972.
305. N. Wang, G. Cheng, L. Guo, B. Tan and S. Jin, *Adv. Funct. Mater.*, 2019, **29**, 1904781.
306. J. Xie, S. A. Shevlin, Q. Ruan, S. J. A. Moniz, Y. Liu, X. Liu, Y. Li, C. C. Lau, Z. X. Guo and J. Tang, *Energy Environ. Sci.*, 2018, **11**, 1617-1624.
307. K. S. W. Sing, *pac*, 1985, **57**, 603.
308. A. Thomas, *Angew. Chem. Int. Ed.*, 2010, **49**, 8328-8344.
309. N. Chaoui, M. Trunk, R. Dawson, J. Schmidt and A. Thomas, *Chem. Soc. Rev.*, 2017, **46**, 3302-3321.
310. Y. Xu, S. Jin, H. Xu, A. Nagai and D. Jiang, *Chem. Soc. Rev.*, 2013, **42**, 8012-8031.
311. T. Ben, H. Ren, S. Ma, D. Cao, J. Lan, X. Jing, W. Wang, J. Xu, F. Deng, J. M. Simmons, S. Qiu and G. Zhu, *Angew. Chem. Int. Ed.* , 2009, **48**, 9457-9460.
312. R. Dawson, A. I. Cooper and D. J. Adams, *Prog. Poly.Sci.*, 2012, **37**, 530-563.
313. J. X. Jiang, F. Su, A. Trewin, C. D. Wood, N. L. Campbell, H. Niu, C. Dickinson, A. Y. Ganin, M. J. Rosseinsky, Y. Z. Khimyak and A. I. Cooper, *Angew. Chem. Int. Ed.*, 2007, **46**, 8574-8578.
314. V. S. Vyas and B. V. Lotsch, *Nature*, 2015, **521**, 41.
315. T. Banerjee and B. V. Lotsch, *Nat. Chem.*, 2018, **10**, 1175-1177.
316. T. Banerjee, T. Bennett, K. Butler, T. L. Easun, M. Eddaoudi, R. Forgan, L. Gagliardi, C. Hendon, M. Jorge, C. Lamberti, J. M. Lee, K. Leus, J. Li, W. Lin, M. Ranocchiari, N. Rosi, J. G. Santaclara, S. Shevlin, K. Svane, V. Ting, M. van der Veen, P. Van Der Voort, A. Walsh, D. Woods, O. M. Yaghi and G. Zhu, *Faraday Discuss.*, 2017, **201**, 87-99.
317. L. Li, Z. Cai, Q. Wu, W. Y. Lo, N. Zhang, L. X. Chen and L. Yu, *J. Am. Chem. Soc.*, 2016, **138**, 7681-7686.
318. X. Yang, Z. Hu, Q. Yin, C. Shu, X. F. Jiang, J. Zhang, X. Wang, J. X. Jiang, F. Huang and Y. Cao, *Adv. Funct. Mater.*, 2019, **29**, 1808156.
319. C. Yang, B. C. Ma, L. Zhang, S. Lin, S. Ghasimi, K. Landfester, K. A. Zhang and X. Wang, *Angew. Chem. Int. Ed.*, 2016, **55**, 9202-9206.
320. Y. Xiang, X. Wang, L. Rao, P. Wang, D. Huang, X. Ding, X. Zhang, S. Wang, H. Chen and Y. Zhu, *ACS Energy Lett.*, 2018, **3**, 2544-2549.
321. Y. Xu, N. Mao, S. Feng, C. Zhang, F. Wang, Y. Chen, J. Zeng and J.-X. Jiang, *Macromol. Chem. Phys.*, 2017, **218**, 1700049.
322. Y. Liu, Z. Liao, X. Ma and Z. Xiang, *ACS Appl. Mater. Interfaces*, 2018, **10**, 30698-30705.
323. C. Dai, S. Xu, W. Liu, X. Gong, M. Panahandeh-Fard, Z. Liu, D. Zhang, C. Xue, K. P. Loh and B. Liu, *Small*, 2018, **14**, e1801839.
324. Z. Wang, X. Yang, T. Yang, Y. Zhao, F. Wang, Y. Chen, J. H. Zeng, C. Yan, F. Huang and J.-X. Jiang, *ACS Catal.*, 2018, **8**, 8590-8596.
325. Z. Chen, J. Wang, S. Zhang, Y. Zhang, J. Zhang, R. Li and T. Peng, *ACS Appl. Energy Mater.*, 2019, **2**, 5665-5676.
326. Y. Zhao, W. Ma, Y. Xu, C. Zhang, Q. Wang, T. Yang, X. Gao, F. Wang, C. Yan and J.-X. Jiang, *Macromolecules*, 2018, **51**, 9502-9508.
327. S. Bi, Z.-A. Lan, S. Paasch, W. Zhang, Y. He, C. Zhang, F. Liu, D. Wu, X. Zhuang, E. Brunner, X. Wang and F. Zhang, *Adv. Functional Mater.*, 2017, **27,** 1703146.
328. G. Märkl, *Angew. Chem. Int. Ed.*, 1966, **5**, 846-847.
329. P. Tokarz and P. M. Zagórski, *Chem. Heterocycl. Comp.*, 2017, **53**, 858-860.
330. P. Le Floch, in *Phosphorus-Carbon Heterocyclic Chemistry*, ed. F. Mathey, Elsevier Science Ltd, Oxford, 2001, pp. 485-533.
331. K. Dimroth, Berlin, Heidelberg, 1973.
332. C. Schwarz, H. Bassler, I. Bauer, J. M. Koenen, E. Preis, U. Scherf and A. Kohler, *Adv. Mater.*, 2012, **24**, 922-925.
333. C. Schwarz, S. Tscheuschner, J. Frisch, S. Winkler, N. Koch, H. Bässler and A. Köhler, *Phys. Rev. B*, 2013, **87**, 155205.
334. P. Guiglion, C. Butchosa and M. A. Zwijnenburg, *Macromol. Chem. Phys.*, 2016, **217**, 344-353.
335. R. S. Sprick, Catherine M. Aitchison, E. Berardo, L. Turcani, L. Wilbraham, B. M. Alston, K. E. Jelfs, M. A. Zwijnenburg and A. I. Cooper, *J. Mater. Chem. A*, 2018, **6**, 11994-12003.
336. X. Zong, X. Miao, S. Hua, L. An, X. Gao, W. Jiang, D. Qu, Z. Zhou, X. Liu and Z. Sun, *Appl. Catal. B Environ.*, 2017, **211**, 98-105.
337. R. S. Sprick, L. Wilbraham, Y. Bai, P. Guiglion, A. Monti, R. Clowes, A. I. Cooper and M. A. Zwijnenburg, *Chem. Mater.*, 2018, **30**, 5733-5742.
338. L. Guo, J. Ge and P. Wang, *Photochem. Photobiol.*, 2018, **94**, 916-934.
339. L. Feng, C. Zhu, H. Yuan, L. Liu, F. Lv and S. Wang, *Chem. Soc. Rev.*, 2013, **42**, 6620-6633.
340. J. Yu, Y. Rong, C. T. Kuo, X. H. Zhou and D. T. Chiu, *Anal. Chem.*, 2017, **89**, 42-56.
341. K. Li and B. Liu, *Chem. Soc. Rev.*, 2014, **43**, 6570-6597.
342. X. Chen, R. Li, Z. Liu, K. Sun, Z. Sun, D. Chen, G. Xu, P. Xi, C. Wu and Y. Sun, *Adv. Mater.*, 2017, **29**, 1604850.
343. Y. Jiang and J. McNeill, *Chem. Rev.*, 2017, **117**, 838-859.
344. K. Pu, A. J. Shuhendler, J. V. Jokerst, J. Mei, S. S. Gambhir, Z. Bao and J. Rao, *Nat. Nanotechnol.*, 2014, **9**, 233-239.
345. P. Zhao, L. Wang, Y. Wu, T. Yang, Y. Ding, H. G. Yang and A. Hu, *Macromolecules*, 2019, **52**, 4376-4384.
346. P.-J. Tseng, C.-L. Chang, Y.-H. Chan, L.-Y. Ting, P.-Y. Chen, C.-H. Liao, M.-L. Tsai and H.-H. Chou, *ACS Cataly.*, 2018, **8**, 7766-7772.

347. L. Wang, R. Fernandez-Teran, L. Zhang, D. L. Fernandes, L. Tian, H. Chen and H. Tian, *Angew. Chem. Int. Ed.*, 2016, **55**, 12306-12310.
348. P. B. Pati, G. Damas, L. Tian, D. L. A. Fernandes, L. Zhang, I. B. Pehlivan, T. Edvinsson, C. M. Araujo and H. Tian, *Energy Environ. Sci.*, 2017, **10**, 1372-1376.
349. N. Kaeffer, A. Morozan and V. Artero, *J. Phys. Chem. B*, 2015, **119**, 13707-13713.
350. L. Wang, Y. Zhang, L. Chen, H. Xu and Y. Xiong, *Adv. Mater.*, 2018, **30**, 1801955.
351. X. Gao, H. Liu, D. Wang and J. Zhang, *Chem. Soc. Rev.*, 2019, **48**, 908-936.
352. A. A. Zakhidov, R. H. Baughman, Z. Iqbal, C. Cui, I. Khayrullin, S. O. Dantas, J. Marti and V. G. Ralchenko, *Science*, 1998, **282**, 897-901.
353. R. H. Baughman, H. Eckhardt and M. Kertesz, *J. Chem. Phys.*, 1987, **87**, 6687-6699.
354. G. Li, Y. Li, H. Liu, Y. Guo, Y. Li and D. Zhu, *Chem. Commun.* , 2010, **46**, 3256-3258.
355. R. S. Weatherup, B. Dlubak and S. Hofmann, *ACS Nano*, 2012, **6**, 9996-10003.
356. Z. Wang, C. Li and K. Domen, *Chem. Soc. Rev.*, 2019, **48**, 2109-2125.
357. L. Wang, X. Zheng, L. Chen, Y. Xiong and H. Xu, *Angew. Chem. Int. Ed.*, 2018, **57**, 3454-3458.
358. L. Wang, Y. Wan, Y. Ding, S. Wu, Y. Zhang, X. Zhang, G. Zhang, Y. Xiong, X. Wu, J. Yang and H. Xu, *Adv. Mater.*, 2017, **29**, 1702428.
359. F. Wang, J. Mielby, F. H. Richter, G. Wang, G. Prieto, T. Kasama, C. Weidenthaler, H. J. Bongard, S. Kegnaes, A. Furstner and F. Schuth, *Angew. Chem. Int. Ed.*, 2014, **53**, 8645-8648.
360. F. C. Krebs, R. B. Nyberg and M. Jørgensen, *Chem. Mater.*, 2004, **16**, 1313-1318.
361. D. Pun, T. Diao and S. S. Stahl, *J. Am. Chem. Soc.*, 2013, **135**, 8213-8221.
362. T. Xue, Z. Lin, C.-Y. Chiu, Y. Li, L. Ruan, G. Wang, Z. Zhao, C. Lee, X. Duan and Y. Huang, *Sci. Adv.*, 2017, **3**, e1600615.
363. Y. Zheng, Y. Jiao, M. Jaroniec and S. Z. Qiao, *Angew. Chem. Int. Ed.*, 2015, **54**, 52-65.
364. J. Zheng, W. Sheng, Z. Zhuang, B. Xu and Y. Yan, *Sci. Adv.*, 2016, **2**, e1501602.
365. Y. Shiraishi, Y. Kofuji, S. Kanazawa, H. Sakamoto, S. Ichikawa, S. Tanaka and T. Hirai, *Chem. Commun.*, 2014, **50**, 15255-15258.
366. J. Kosco, M. Sachs, R. Godin, M. Kirkus, L. Francas, M. Bidwell, M. Qureshi, D. Anjum, J. R. Durrant and I. McCulloch, *Adv. Energy Mater.*, 2018, **8**, 1802181.
367. T. Shibata, A. Kabumoto, T. Shiragami, O. Ishitani, C. Pac and S. Yanagida, *J. Phys. Chem.*, 1990, **94**, 2068-2076.
368. S. Matsuoka, H. Fujii, T. Yamada, C. Pac, A. Ishida, S. Takamuku, M. Kusaba, N. Nakashima and S. Yanagida, *J. Phys. Chem.*, 1991, **95**, 5802-5808.
369. A. A. Bakulin, A. Rao, V. G. Pavelyev, P. H. M. van Loosdrecht, M. S. Pshenichnikov, D. Niedzialek, J. Cornil, D. Beljonne and R. H. Friend, *Science*, 2012, **335**, 1340-1344.
370. M. B. Smith and J. Michl, *Annu. Rev. Phys. Chem.*, 2013, **64**, 361-386.
371. T. N. Singh-Rachford and F. N. Castellano, *Coord. Chem. Rev.*, 2010, **254**, 2560-2573.
372. W. Shockley and H. J. Queisser, *J. Appl. Phys.*, 1961, **32**, 510-519.
373. M. B. Smith and J. Michl, *Chem. Rev.*, 2010, **110**, 6891-6936.
374. M. B. J. Roeffaers, B. F. Sels, H. Uji-i, F. C. De Schryver, P. A. Jacobs, D. E. De Vos and J. Hofkens, *Nature*, 2006, **439**, 572.
375. B. M. Weckhuysen, *Nature*, 2006, **439**, 548.
376. D. R. Gamelin, *Nat. Chem.*, 2012, **4**, 965-967.
377. J. B. Sambur, T.-Y. Chen, E. Choudhary, G. Chen, E. J. Nissen, E. M. Thomas, N. Zou and P. Chen, *Nature*, 2016, **530**, 77-80.
378. Y. Jiao, Y. Zheng, K. Davey and S.-Z. Qiao, *Nat. Energy*, 2016, **1**, 16130.
379. Y. Jiao, Y. Zheng, M. Jaroniec and S. Z. Qiao, *Chem. Soc. Rev.*, 2015, **44**, 2060-2086.
380. T. Y. Ma, S. Dai, M. Jaroniec and S. Z. Qiao, *Angew. Chem. Int. Ed.*, 2014, **53**, 7281-7285.
381. Y. Zheng, Y. Jiao, Y. Zhu, L. H. Li, Y. Han, Y. Chen, A. Du, M. Jaroniec and S. Z. Qiao, *Nat. Commun.*, 2014, **5**, 3783.
382. R. Parsons, *Trans. Faraday Soc.*, 1958, **54**, 1053-1063.
383. M. R. Shaner, H. A. Atwater, N. S. Lewis and E. W. McFarland, *Energy Environ. Sci.*, 2016, **9**, 2354-2371.
384. L. C. Seitz, Z. Chen, A. J. Forman, B. A. Pinaud, J. D. Benck and T. F. Jaramillo, *ChemSusChem*, 2014, **7**, 1372-1385.
385. B. A. Pinaud, J. D. Benck, L. C. Seitz, A. J. Forman, Z. Chen, T. G. Deutsch, B. D. James, K. N. Baum, G. N. Baum, S. Ardo, H. Wang, E. Miller and T. F. Jaramillo, *Energy Environ. Sci.*, 2013, **6**, 1983.
386. M. Qureshi and K. Takanabe, *Chem. Mater.*, 2016, **29**, 158-167.
387. K. Takanabe, *J. Catal.*, 2019, **370**, 480-484.
388. H. Kisch, *Angew. Chem. Int. Ed.* , 2010, **49**, 9588-9589; author reply 9590-9581.
389. D. Schwarz, A. Acharja, A. Ichangi, P. Lyu, M. V. Opanasenko, F. R. Gossler, T. A. F. Konig, J. Cejka, P. Nachtigall, A. Thomas and M. J. Bojdys, *Chem. Eur. J.*, 2018, **24**, 11916-11921.
390. V. I. Arkhipov, P. Heremans and H. Bässler, *Appl. Phys. Lett.*, 2003, **82**, 4605-4607.
391. A. V. Nenashev, S. D. Baranovskii, M. Wiemer, F. Jansson, R. Österbacka, A. V. Dvurechenskii and F. Gebhard, *Phy. Rev. B*, 2011, **84**, 035210.
392. National Hydrogen Strategy, 2019.

TOC

Title: Metal-Free Photocatalysts for Hydrogen Evolution
Authors: Mohammad Z Rahman, Md Golam Kibria, and Charles Buddie Mullins

TOC Text: This article provides a comprehensive review of the latest progress, challenges and recommended future research related to metal-free photocatalysts for hydrogen production via water-splitting.

TOC graphic: